Suspension-Colloidal Transport in Porous Media: Basic Equations, Analytical Model and Nonlinear Physics Effects

---

Hao Zhang, B.Sc. (Honours)

A thesis submitted for the degree of

Master of Philosophy (M.Phil.)

Australian School of Petroleum

Faculty of Engineering, Computer & Mathematical Sciences

The University of Adelaide

November 2018

To my grandmother,

Kelan Zhang,

the person who loved me most,

She passed away in January.

It is my great regret that I cannot accompany with her at her last moments.

I will miss her forever.

Table of Contents

Abstract

Hereby I present a Master of philosophy thesis by publications. The thesis includes two peer-reviewed journal papers. One has been published in *International Journal of Non-linear Mechanics*. The other has been submitted to *Transport in Porous Media* and is currently under review.

Flow of colloidal-suspensions and nanofluids in porous media is encountered in numerous processes of the natural subsurface environment and industrial relevant fields. The physical and chemical mechanisms of particle transport and subsequent retention are of great significance in study of current filtration theory.

This thesis focuses on one-dimensional non-linear advection-dispersion problems for suspensions flow through porous media. It accounts for monodisperse colloids flow with simultaneous multiple capture mechanisms, chemical flow with multiple reactions, and co-transport phenomena of natural clays and nanoparticles. Mathematical models are proposed for the above problems, and analytical solutions or numerical solutions are derived for quasi-linear or non-linear governing systems. These can be applied to wider range of reaction-advection-diffusion particulate flow problems, and supplemented to classical colloids filtration theory. A summary for publications is as follows.

The first paper Two main particle capture mechanisms, i.e., straining (size-exclusion) and attachment, are widely recognised and used in suspension colloidal flow. From the observation of the laboratory tests, a typical breakthrough curve (BTC) of two capture mechanisms has been found, describing that outlet particle concentration first increases then reaches a stabilisation within a few pore volumes injected after the breakthrough moment. During steady state, the suspended concentration remains constant, which is always lower than the injected concentration. The two-capture model, in terms of novel filtration functions, is developed both for the general and approximated cases. Modelling results match laboratory data with a high

accuracy, and dependencies of the model coefficients with respect to salinity and jamming ratio agree with Derjaguin–Landau–Verwey–Overbeek (DLVO) theory.

The second paper Engineered nanoparticles injection into subsurface formation is widely applied in many engineering fields at present. The phenomenon of nanoparticle transport with attachment is significantly affected by the presence of the natural clay fines. A mathematical model is proposed with the assumption that one population of particles holds similar kinetics coefficients, due to the same electrostatic interactions between grains and particles, in presence of another population, Therefore, the two-capture model can be extended for co-transport of two particle populations with the introduction of two independent filtration coefficients. The model matches the co-transport experimental data with close agreement. However, the non-monotonic tendency of kaolinite fines coefficients with different salinities draws us back to the theoretic study. The aggregation between kaolinite and kaolinite may occur under the experiment conditions due to the analysis of DLVO calculations, which is not accounted for in the model.

Declaration

I certify that this work contains no material which has been accepted for the award of any other degree or diploma in my name, in any university or other tertiary institution and, to the best of my knowledge and belief, contains no material previously published or written by another person, except where due reference has been made in the text. In addition, I certify that no part of this work will, in the future, be used in a submission in my name, for any other degree or diploma in any university or other tertiary institution without the prior approval of the University of Adelaide and where applicable, any partner institution responsible for the joint-award of this degree.

I acknowledge that copyright of published works contained within this thesis resides with the copyright holder(s) of those works.

I also give permission for the digital version of my thesis to be made available on the web, via the University's digital research repository, the Library Search and also through web search engines, unless permission has been granted by the University to restrict access for a period of time.

Acknowledgement

I would never be capable of finishing my master thesis without support and help from my supervisors, colleagues from research group and my family.

Frist of all, my sincere gratitude to my principal supervisor Prof. Pavel Bedrikovetsky. It is his moderate care, adequate supervision and strict requirements that manages me to submit my thesis for Master of Philosophy within about one and half years. The most important and profound influence he made on me was that he not only taught me methodology for research but also the way to think about problems in mathematics and science. He inspired and encouraged me to continue on research which gave me more confidence to candidature of Ph.D. in the future.

Next, I would like to express my great thanks and appreciation to co-supervisor Dr. Zhenjiang You, who had spent a lot time in helping me solve problems and improve my research abilities in all respects. He is an experienced and knowledgeable scholar. Many suggestions from him is greatly beneficial to me. It is my honour to meet him and have him as my co-supervisor.

Sincere thanks towards to my research partner and friend Mr. Gabriel de Veiga Cabral Malgaresi. He contributed a lot in all the publications in this thesis. It is his great cooperation and carefully discussions that make our research work modified and published.

Many thanks to Dr. Sara Borazjani, who had taught me about basic knowledge in mathematical modelling with her great patience. I have made great and fast progress in applied mathematics with her help in the first few months. Best wish to her and her child. May happiness and health with them forever.

Last but not least, I would like to thank my family for their financial and moral support. I hope that our thoughts would not be limited by the results of the thesis, and I sincerely hope that the first half sentence would not be merely a hope. Thanks again to all who contributed to the work of this thesis.

Thesis by Publication

Published Journal Paper

Zhang, H., Malgaresi, G.V.C. and Bedrikovetsky, P., 2018. Exact solutions for suspension-colloidal transport with multiple capture mechanisms. *International Journal of Non-Linear Mechanics*, 105, pp.27-42.

Submitted Journal Papers

Malgaresi, G.V.C., Zhang, H., Chrysikopoulos, C.V., Bedrikovetsky, P.: Cotransport of suspended colloids and nanoparticles in porous media. Submitted to *Transport in Porous Media*.

1 Contextual Statement

Significance of the project

The trend of petroleum industry towards enhanced oil recovery (EOR) and cost reduction have been not changed during last a few decades. A large number of new technologies have been developed to maintain productivity and profitability in production wells, such as low salinity water flooding, low salinity polymer flooding and polymer microsphere injection for water shutoff (Borazjani, Bedrikovetsky, & Farajzadeh, 2016; Farajzadeh, Bedrikovetsky, Lotfollahi, & Lake, 2016; Sorbie, 2013). The technologies are highly related to deep bed filtration (or depth filtration), fines mobilization, migration and deposition, which are essential processes in the subsurface petroleum-bearing formation. Moreover, reservoir formation damage are mainly associated with those porous media transport phenomena (Civan, 2015). For example, seawater or produced water injection to reservoirs during waterflooding results in chemical incompatible or reaction between fluid and clays on the surface of rock; Invasion of mud fluid into formations during well drilling brings about internal cake and the occurrence of a damaged zone near the wellbore (Civan, 2011; Kalantariasl, Farajzadeh, You, & Bedrikovetsky, 2015; Khilar & Fogler, 1998; Khilar, Vaidya, & Fogler, 1990; Yang et al., 2018; Zeinijahromi, Lemon, & Bedrikovetsky, 2011).

Fundamental colloidal-suspension transport theory is commonly used in the above problems. Experimental investigation with mathematical modelling is the common method in the study of colloidal suspension flow. Laboratory tests, such as core flooding and visualisation experiment, are main approaches to investigate physical and chemical effects on transport processes. The development of mathematical model helps to explain phenomena of experiments, and it makes predictions about the fate of particle or its transport and retention behaviours. Furthermore, analytical solutions can provide a faster calculation for qualitative interpretation of the laboratory results, and analysis of the model parameters gives an insight

into capture mechanisms of transport particle and their dependency of chemistry properties among rock, particles and carried fluid. It also helps to develop streamline and front tracking techniques for three dimensional (3D) reservoir simulation (Borazjani & Bedrikovetsky, 2017).

State of the art

Mathematical modelling is a fundamental approach to help in the development of technologies for colloidal suspension transport in porous media. One dimensional (1D) particle transport problem is commonly described in a well-defined governing system, which presents quantitative formulations of transport with capture kinetic equation.

The governing system is composed of mass balance equation for suspended and retained particles and kinetic equation for particle capture (Bedrikovetsky, 2008; Zhenjiang You, Osipov, Bedrikovetsky, & Kuzmina, 2014),

$$\frac{\partial}{\partial t}\left(\phi c+\sigma\right)+U\frac{\partial c}{\partial x}=\frac{\partial}{\partial x}\left(D\frac{\partial c}{\partial x}\right) \tag{1.1}$$

$$\frac{\partial \sigma}{\partial t}=\lambda\left(\sigma\right)cU \tag{1.2}$$

where c is suspended particle concentration, L^{-3}; σ is retained particle concentration, L^{-3}; ϕ is porosity; x is transport distance, L; t is time, T; λ is filtration coefficient, L^{-1}; D is dispersion coefficient, L^2T^{-1}; and U is flow velocity, LT^{-1}.

This is so-called classical filtration model. It is assumed that particle capture rate is proportional to the particle flux. If dispersion is negligible in the system, a first order quasi-linear hyperbolic equation is obtained by substitution of kinetics into mass balance equation.

$$\frac{\partial}{\partial t}\left(\phi c+\sigma\right)+U\frac{\partial c}{\partial x}=0 \tag{1.3}$$

$$\frac{\partial \sigma}{\partial t}=\lambda\left(\sigma\right)cU \tag{1.4}$$

Deep bed filtration (DBF) or depth filtration problem describes that constant concentration particles inject into a clean bed. The problem has the following initial and boundary conditions,

$$t = 0 : c = \sigma = 0 \tag{1.5}$$

$$x = 0 : c = c^0 \tag{1.6}$$

where c^0 is initial suspended particle concentration, L^{-3}.

Fines migration problem describes that retained particles keep lifting from rock surface due to some disturbances (such as low-salinity water flooding). It has the following initial and boundary conditions,

$$t = 0 : c = c^0, \sigma = 0 \tag{1.7}$$

$$x = 0 : c = 0 \tag{1.8}$$

The first-order hyperbolic system (1.3-1.6) or (1.3, 1.4, 1.7, 1.8) allows for exact solutions to suspended concertation c and retained concentration σ. Although several limitations exist in the classical model, it helps to provide a fundamental approach to solve one dimensional (1D) particle transport problem.

Scope of the work The main achievements of the thesis include:

- Non-linear 1D problem of suspension-colloidal transport in porous media deviated from classical filtration theory
- The non-linear transformation technique potential and “aggregation” procedure that degenerates n-capture system into a single-capture system.
- Mathematical models for 1D suspension-colloidal with multiple particle capture mechanisms.
- Exaction solutions for 1D suspension-colloidal flow with two capture mechanisms: for approximated and aggregated filtration function.
- Exaction solution for chemical reactive flow with multiple reactions.
- Numerical solution for co-transport of two particle populations.

- Numerical solution for multiple capture mechanisms with the suspended function.

1.1 Thesis structure

This is a publication format thesis for Master of Philosophy degree. Two journal papers are included in the thesis, of which one paper has been published in *International Journal of Non-linear Mechanics* and another has been submitted to peer-review journals, *Transport in Porous media*. The body of the thesis is composed of six chapters and described as follows.

The first chapter is contextual statement. It provides an overview of research significance in petroleum industry, state of the art and main achievements of the thesis. Moreover, the relation between journal articles and thesis is discussed in the sub-section 1.2.

The second chapter is literature review. It presents in detail basic knowledge and methodology of the colloidal suspension transport in porous media, the existing problems and possible causes of problems for mathematical model in the current literature. It contains colloidal suspension transport phenomena and behaviours, current filtration theory and mathematical models in 1D particulate flow problem.

The third, and fourth chapters present the papers titled “Exact solutions for suspension-colloidal transport with multiple capture mechanisms”, and “Cotransport of suspended colloids and nanoparticles in porous media”. The last chapter draws conclusions and finalises the thesis. It discusses the overall significance of thesis to this subject, the contribution to the current filtration theory, existing problems and further directions of research development.

Paper	Chapter	Title	status
1	Chapter 3	Exact solutions for suspension-colloidal transport with multiple capture mechanisms	Published
2	Chapter 4	Cotransport of suspended colloids and nanoparticles in porous media	Submitted for publication

1.2 How the publications are related to the thesis

The classical filtration model allows for exact solution. Considering a constant filtration coefficient, the solution presents a constant breakthrough concertation after the breakthrough moment, at or before 1 pore volume injected (PVI), and an exponential form of decreasing particle retained concertation along the transport distance. However, a large number of laboratory tests for colloidal suspensions flow in cores showed that the breakthrough curves along with retention profiles cannot be matched by tuning the filtration coefficient of the classical filtration model. Explanations of the deviation have been presented in several publications, such as heterogeneity of surface charges, pore size distribution, tortuosity. However, clear theoretic interpretations that can resolve the deviation are not available in the current literature.

The first paper "Exact solutions for suspension-colloidal transport with multiple capture mechanisms" developed analytical models accounting for multiple particle capture mechanisms. The work derived exact solutions for the first order non-linear hyperbolic systems in 1D colloidal suspension flow problems. The deviation process includes two procedures. First, the "aggregation" technique degenerates the multiple capture $(n+1)\times(n+1)$ system with *n* kinetics to a single capture 2×2 system with one kinetics equation that contains the aggregated filtration function. Then, the non-linear transformation "potential" allows for reduction of the system to one scalar quasi-linear hyperbolic PDE that allows for exact solution. The piece-wise filtration function that is an approximation form of the aggregated filtration, also allows for exact solution. The solutions matched BTCs in which suspended concentration monotonically increases during several PVIs then reaches the stabilisation that is less than injected concentration ($c<c^0$). The high accuracy of matching allows for validating the model and giving reasonable interpretation of experimental phenomenon, both with aggregated and piece-wise

linear (approximated) filtration function. The proposed model solved the defect of the classical filtration model that cannot match the BTCs with the stabilisation.

The second paper "Co-transport of suspended colloids and nanoparticles in porous media" presented a novel model for co-transport of two population colloids, in which kaolinite and nanoparticles co-injection experiments has been used to validate the proposed model. The model for mono-dispersion particle is extended from the first paper, which describes a typical form of BTCs with a stabilisation. The co-transport model is based on the assumption that electrostatic interaction for the particle and the rock surface and the fraction of the rock surface available to attachment by a particle are the same (or similar) for individual transport and for simultaneous co-transport of two populations, which can be interpreted by DLVO calculation. The proposed models matched the laboratory data with a close agreement, only left an unexpected behaviour of kaolinite fines due to kaolinite-kaolinite particle aggregation that was not considered in the model. The proposed models from the second paper continued the work from the first one, in which the co-transport model has been derived based on the piece-wise linear filtration function.

The work derived several exact solutions and numerical solutions for 1D non-linear colloidal suspension transport problems, which can be used to interpret the experimental phenomena for breakthrough curves and retained profiles and provide experience for wider range of non-linear particulate flow problems.

Reference

Bedrikovetsky, P. (2008). Upscaling of stochastic micro model for suspension transport in porous media. *Transport in Porous Media, 75*(3), 335-369.

Borazjani, S., & Bedrikovetsky, P. (2017). Exact solutions for two-phase colloidal-suspension transport in porous media. *Applied mathematical modelling, 44*, 296-320.

Borazjani, S., Bedrikovetsky, P., & Farajzadeh, R. (2016). Analytical solutions of oil displacement by a polymer slug with varying salinity. *Journal of Petroleum Science and Engineering*, *140*, 28-40.

Civan, F. (2011). *Porous media transport phenomena*: John Wiley & Sons.

Civan, F. (2015). *Reservoir formation damage*: Gulf Professional Publishing.

Farajzadeh, R., Bedrikovetsky, P., Lotfollahi, M., & Lake, L. (2016). Simultaneous sorption and mechanical entrapment during polymer flow through porous media. *Water Resources Research*, *52*(3), 2279-2298.

Kalantariasl, A., Farajzadeh, R., You, Z., & Bedrikovetsky, P. (2015). Nonuniform external filter cake in long injection wells. *Industrial & Engineering Chemistry Research*, *54*(11), 3051-3061.

Khilar, K. C., & Fogler, H. S. (1998). *Migrations of fines in porous media* (Vol. 12): Springer Science & Business Media.

Khilar, K. C., Vaidya, R. N., & Fogler, H. S. (1990). Colloidally-induced fines release in porous media.

Sorbie, K. S. (2013). *Polymer-improved oil recovery*: Springer Science & Business Media.

Yang, Y., Siqueira, F., Vaz, A., Badalyan, A., You, Z., Zeinijahromi, A., . . . Bedrikovetsky, P. (2018). Fines Migration in Aquifers and Oilfields: Laboratory and Mathematical Modelling. *Flow and Transport in Subsurface Environment*, 3-67.

Zeinijahromi, A., Lemon, P., & Bedrikovetsky, P. (2011). Effects of induced fines migration on water cut during waterflooding. *Journal of Petroleum Science and Engineering*, *78*(3-4), 609-617.

2 Literature Review

2.1 Introduction

Transport of suspension-colloidal in porous media is generally encountered in various processes of natural environment and industrial relevant felids. To understand the behaviours of colloid transport and fate has a great significance in the environmental, chemical and petroleum engineering (Bedrikovetsky, You, Badalyan, Osipov, & Kuzmina, 2017; Z You, Bedrikovetsky, & Kuzmina, 2013). For example, it helps to control the propagation of contaminants in aquifers, to improve the quality of potable water supplies, and to dispose industrial wastes in water treatment process (Bradford, Simunek, Bettahar, van Genuchten, & Yates, 2003; Bradford, Yates, Bettahar, & Simunek, 2002; Elimelech, Gregory, & Jia, 2013; Shannon et al., 2010). In petroleum industry, it is commonly described as deep bed filtration or fines migration in the subsurface hydrocarbon-bearing formations. Particle transport and capture by rock induces formation damage that leads to permeability impairment, such as poor-quality water injection or produced water re-injection, invasion of drilling mud fluid into oil-bearing formations. However, it also can be used to develop new technologies to enhance oil recovery, such as applications of low-salinity waterflooding (Lager, Webb, Black, Singleton, & Sorbie, 2008), low-salinity polymer flooding (Sorbie, 2013), polymer microspheres injection (Yao et al., 2017), and fixing natural movable fines in reservoirs by Nano fluid (Yuan & Moghanloo, 2018; Yuan, Moghanloo, & Zheng, 2016).

The structure of literature review is as follows. Section 2.2 focuses on particle transport behaviours and various capture mechanisms in porous media, in which the torque balance of forces and the extended DLVO theory are reviewed in detail. Section 2.3 presents mathematical models of 1D particulate flow problem in porous media; it also reviews exact solutions to the models and introduces inverse problem.

2.2 Colloidal suspensions transport behaviours and capture mechanisms

A wide range of colloidal suspensions exist in the natural subsurface systems, such as clays, mineral precipitates, metal oxides, viruses and bacteria (Bradford et al., 2003; Civan, 2011; Elimelech et al., 2013). Kaolinite, chlorite and illite are the most common natural clays in the petroleum-bearing formation(Civan, 2015; Khilar & Fogler, 1998). The rock surface is initially coated by fines; and detachment of those fines slightly influences the porosity but highly affects the permeability of rock, especially in blocking small pore throats by detached fines.

Particle capture mechanisms

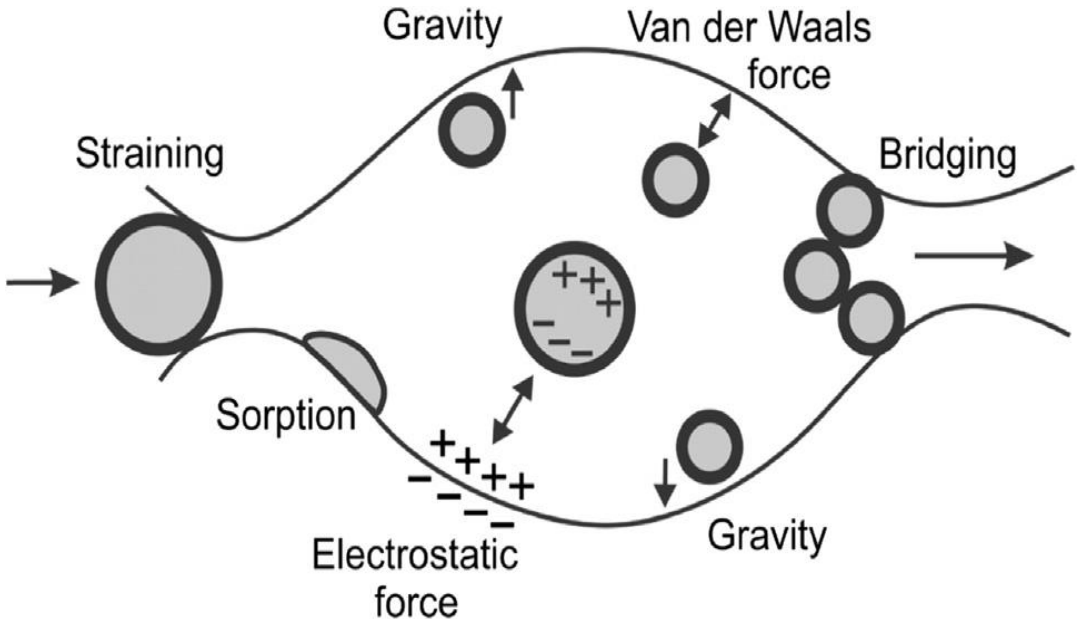

Figure 2.1 Schematic of various capture mechanism in a single pore (Guedes, 2009)

There are a number of capture mechanisms due to different physical effects and forces: size exclusion, straining, bridging, attachment (electrostatic attraction), gravity segregation and diffusion into dead-end pores and stagnant flow zones, as shown in figure 2.1(Guedes, Al-Abduwani, Bedrikovetsky, & Currie, 2009).

Size exclusion occurs at the narrow pore inlet, particles blocked the pore throat, when the particle radii larger than the pore radii (Bedrikovetsky, 2008; Chalk, Gooding, Hutten, You, &

Bedrikovetsky, 2011; Z You et al., 2013). Straining describes that particles retain at the junction of grains or grain surface due to surface roughness and electrostatic attraction. Bridging is a small pore throat blocked by several particles. Attachment is a state of equilibrium for attraction and repulsion, which can be explained by the torque balance.

The torque balance of forces

Particle attachment-detachment is generally described in the mechanical equilibrium of a particle attached to the rock surface. Analysis of torque balance of forces acting on the particle helps to understand the process of particles release or detachment. Particles attached to the rock surface are mainly due to electrostatic and gravitational forces, while the drag and lifting forces act as release (or removal) force to detach particles. The torque balance of forces exerting on a particle is discussed in detail by Bedrikovetsky, Zeinijahromi, Siqueira, Furtado, and de Souza (2012) and Bradford, Torkzaban, and Shapiro (2013) as shown in figure 2.2,

$$F_d l_d = \left(F_e - F_l + F_g\right) l_n \tag{2.1}$$

where F_d, F_e, F_L, and F_g are drag, electrostatic, lifting, and gravitational forces, MLT^{-2}; and l_d and l_n are the tangential and normal lever arms, respectively, L.

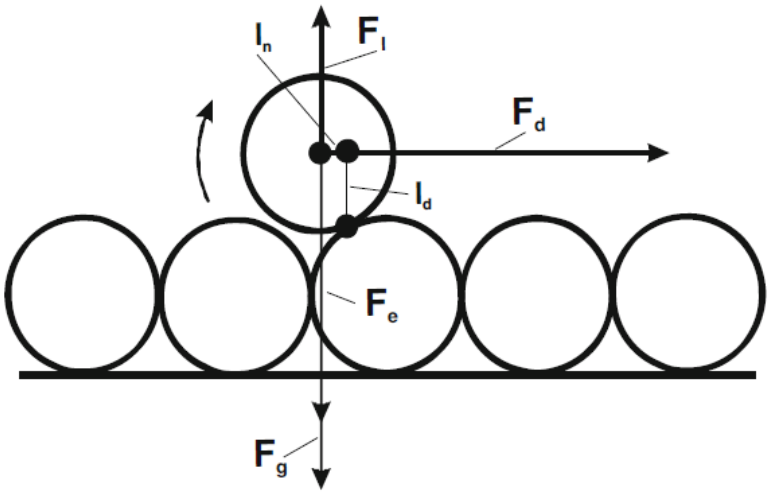

Figure 2.2 Torque balance of forces exerting on a single particle (Bedrikovetsky, 2011)

The drag and lifting forces exerting on a particle are velocity-dependent. (Altmann & Ripperger, 1997; Bergendahl & Grasso, 2003):

$$F_d = \frac{\omega \pi \mu r_s^2 u}{r_p} \tag{2.2}$$

$$F_l = \chi r_s^3 \sqrt{\frac{\rho \mu u^3}{r_p}} \tag{2.3}$$

where ω and χ are the drag coefficient and the lift coefficient, which is usually calculated from computational fluid dynamics modelling (CFD); μ is the viscosity of fluid, $ML^{-1}T^{-1}$; r_p is the particle radius, L; r_s is the pore radius, L; and ρ is the density of fluid, ML^{-3}.

The gravitational force (buoyance) for a spherical particle is,

$$F_g = \frac{4}{3} \pi r_s^3 \Delta \rho g \tag{2.4}$$

where $\Delta\rho$ is the density difference between particles and fluid, ML^{-3}; g is the gravitational acceleration, MT^{-2}.

The extended DLVO theory

The total electrostatic force is generally calculated from the total energy. The extended Derjaguin-Landau-Verwey-Overbeek (DLVO) theory is used to calculate the interaction energies between the particles and the grain surface. The total potential energy is consist of London Van der Waals attraction, electrical double layer and born repulsive potentials (Derjaguin & Landau, 1941; Gregory, 1981; Hogg, Healy, & Fuerstenau, 1966; Verwey, Overbeek, & Overbeek, 1999),

$$V = V_{LVW} + V_{EDL} + V_{BR} \tag{2.5}$$

where V, V_{LVW} , V_{EDL} and V_{BR} are the total energy potential, the London-Van der Waals, electrical double layer and born repulsive potential, respectively, ML^2T^{-2}.

The London-Van der Waals potential is the electrical attraction between two close macroscopic bodies. The attraction exerts between the particle surface and the grain surface in a porous medium. The London-Van der Waals interaction is the integration of all the relevant intermolecular interactions between polar molecules. The London-Van der Waals energy between sphere-plate is expressed as follows (Gregory, 1981):

$$V_{LVW} = -\frac{A_{132} r_s}{6h}\left[1 - \frac{5.32h}{\lambda_w}\ln\left(1 + \frac{\lambda_w}{5.32h}\right)\right] \tag{2.6}$$

where A_{132} is the Hamaker constant (Israelachvili, 2011); λ_w is the characteristic wavelength of interaction, L; and h is the surface-to-surface separation distance, L; r_s is the mean particle size, L.

The electrical double layer energy usually acts as repulsion between the particles and the rock surface due to the similar charges, but it can be attractive if the two interacting objects have the opposite charges.

The net charge on the particle surface affects the ion distribution in the neighbourhood of interfacial region, creating an electrical double layer around the surface. The overlap of two electrical double layers gives rise to an interaction between the particles and rock surface. Considering a spherical particle and a plate surface for grain, the electrical double layer potential energy is proposed by (Gregory, 1975),

$$V_{EDL} = -\frac{128\pi r_s n_\infty k_b T}{\kappa^2}\psi_s \psi_b e^{-kh} \tag{2.3}$$

$$\kappa = \sqrt{\frac{e^2 \sum \mathrm{n}_{i0}\, \mathrm{z}_i^{\,2}}{\varepsilon_0 \varepsilon_3 k_b T}} \tag{2.4}$$

$$\psi_s = \tanh\left(\frac{ez\zeta_s}{4k_b T}\right) \tag{2.5}$$

$$\psi_g = \tanh\left(\frac{ez\zeta_g}{4k_b T}\right) \tag{2.6}$$

where κ is the inverse Debye screening length; k_b is Boltzmann constant; n_∞ is the bulk number density of ions; e is the elementary electric charge; n_{i0} is the number concentration of ions i in bulk solution, z is the valence of symmetrical electrolyte solution; ε_0 is the dielectric permittivity of vacuum; ε_3 is the dielectric constant of the fluid; ψ_s and ψ_g are the reduced zeta potentials for particle and grain, and ζ_s and ζ_g are the zeta potentials for the particle and grain, respectively.

A number of different forms for electrical double layer energy potential are well formulated by Elimelech et al. (2013).

The born repulsive potential acts at a short-range. It results from the strong repulsive forces between the atoms as their electron clouds approach and overlap each other. An expression for the born repulsion potential between a sphere and a plate was formulated by Ruckenstein and Prieve (1976),

$$V_{BR} = \frac{A_{132s}}{6h}\left(\frac{\sigma_{LJ}}{r_s}\right)^6\left[\frac{8+R}{(2+R)^2}+\frac{6-R}{Z^7}\right]; R = \frac{h}{r_s} \tag{2.7}$$

where σ_{LJ} is the atomic collision diameter taken from Bhattacharjee, Ko, and Elimelech (1998).

The total potential energy is commonly presented in the energy profile with respect to separated distance between the particles and the rock surface. There are two energy maximum and minimum in typical curves of the total energy profile as shown in Fig. 2.3 (Russell, Chequer, et al., 2018),

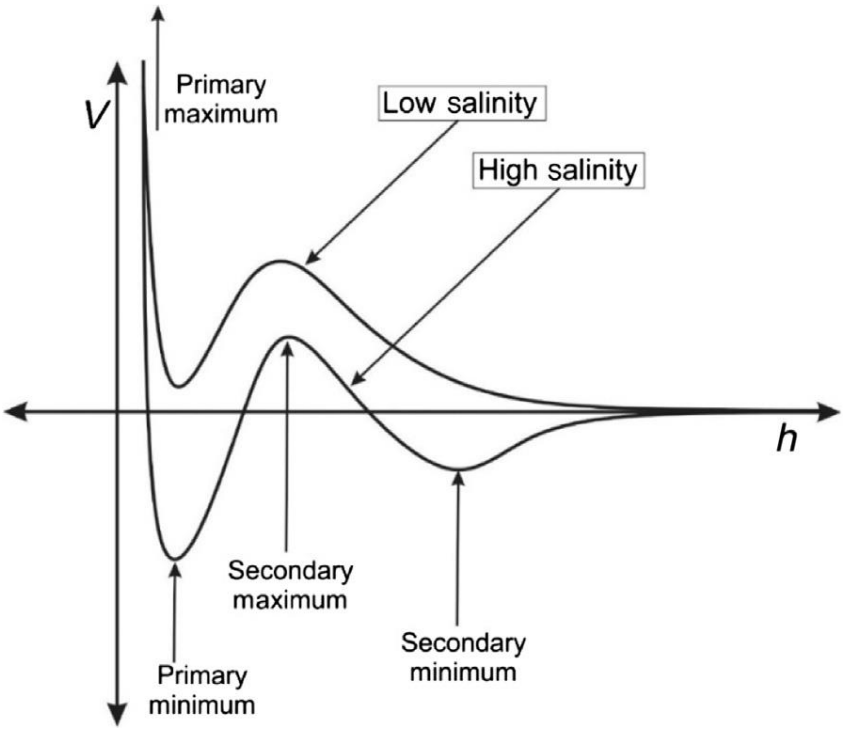

Figure 2.3 Typical curves of the total potential energy profile accounting for high and low salinity effects (Russell et al., 2018)

Differentiating the total potential energy allows for converting the total potential energy into the total electrostatic force (Bradford et al., 2013; Elimelech et al., 2013),

$$F = -\frac{\partial V}{\partial h} \tag{2.8}$$

where F is the total electrostatic force, MLT^{-2}.

2.3 Mathematical models for suspension-colloidal flow in porous media

Mathematical models of particle transport problem revolve around a continuity equation with respect to particle concentration. The equation is described in detail as follows (Russell, Chequer, et al., 2018):

(*Particle accumulation rate = Divergence of particle advective and dispersion flux – Particle capture rate*)

$$\frac{\partial(\phi c)}{\partial t} = -U\frac{\partial c}{\partial x} + D\frac{\partial^2 c}{\partial x^2} - \frac{\partial \sigma}{\partial t} \tag{2.9}$$

It is called mass balance equation for suspended particle and retained particle (derived in 1D), which is usually expressed as (Herzig, Leclerc, & Goff, 1970; Payatakes, Rajagopalan, & Tien, 1974),

$$\frac{\partial}{\partial t}\left(\phi c+\sigma\right)+U\frac{\partial c}{\partial x}=\frac{\partial}{\partial x}\left(D\frac{\partial c}{\partial x}\right) \tag{2.10}$$

It should be noted here that suspended particle concentration *c* is defined as the number of suspended particles per pore volume, while retained particle concentration σ is defined as the number of retained particles per bulk rock volume.

Particle dispersion

Peclet number, defined as the ratio between particle advection and dispersive fluxes, can be used to describe the effects of dispersion. In small scale, the typical core length is small, assuming 10cm, so the Peclet number is also commonly small that dispersion cannot be negligible. In large scale, dispersion of particle can be neglected with respect to reservoir length because Peclet number is significantly larger than one (if assumed reservoir length *L* is larger than 100 meter).

$$\frac{U}{D}L\gg 1 \tag{2.11}$$

However, dispersion of particle is remarkable in a heterogeneous porous medium even if it is considered in small scale (Lake, Johns, Rossen, & Pope, 2014); the model accounting for dispersion in capture kinetic is proposed and the exact solution is derived by (Altoe, Bedrikovetski, Siqueira, de Souza, & Shecaira, 2006; Bedrikovetsky, Siqueira, de Souza, & Shecaira, 2006).

Particle capture kinetic equation is commonly used to formulate particle capture rate by an empirical (material) filtration λ (σ). It is assumed that particle capture rate is proportional to particle advective flux (hydrodynamic dispersion is negligible here) (Elimelech et al., 2013; Sharma & Yortsos, 1987; Vaz, Bedrikovetsky, Fernandes, Badalyan, & Carageorgos, 2017).

$$\frac{\partial \sigma}{\partial t} = \lambda(\sigma) cU \tag{2.12}$$

Interpretation of filtration function

The filtration function (coefficient) has a clear physical interpretation in statistics, which is the probability for a particle capture by rock per unitary length of the transport trajectory. It can be formulated as follows (Vaz et al., 2017),

$$\frac{\Delta \sigma}{\Delta t} = \frac{pcU\Delta tA}{lA\Delta t} = \frac{p}{l} cU = \lambda cU \tag{2.13}$$

If the probability of a particle capture by (or pass through) a sieve is p (or 1-p), the number of particles crossing sieve, of which section area is A, during time interval Δt is $cUA\Delta t$, and l is the transport distant during Δt, so that particle capture takes place in the volume Al. Therefore, the number of particle capture per unit of volume in the interval Δt is equal to pcU/l, where cU is particle flux, and p/l is defined as the filtration coefficient.

The traditional attachment-detachment model

The attachment filtration coefficient λ_a from the classical colloid theory is proportional to the collision efficiency and sticking efficiency (Borazjani et al., 2016; Bradford, Torkzaban, & Walker, 2007; Bradford et al., 2002; Elimelech et al., 2013)

$$\lambda_a = \frac{k_a \phi}{U} = \frac{3}{2} \frac{(1-\phi)}{d_c} \alpha \eta_0 \phi \tag{2.14}$$

where k_a is the first order attachment coefficient, T^{-1}; d_c is the median grain diameter, L; α is the colloid attachment (sticking) efficiency that is the probability of a particle attaches to the grain surface; η_0 is the single collector contact (collision) efficiency that is the probability for the particle flowing towards the grain to strike the grain.

The kinetics equation for traditional particle attachment-detachment model is (Bradford et al., 2003; Bradford et al., 2002; Tufenkji, 2007),

$$\frac{\partial \sigma_a}{\partial t} = \lambda_a c U - k_{\det} \sigma_a \tag{2.15}$$

where k_{det} is the first order detachment coefficient, T^{-1}.

Eq. (2.15) describes attachment and detachment occur simultaneously, which is the equation only for non-equilibrium. However, it does not reflect the mechanical equilibrium condition by torque balance of a particle attached to the rock surface. Moreover, the model exhibits a delay response to any abrupt, while the most common experiments exhibit an instant response (Russell, Wong, Zeinijahromi, & Bedrikovetsky, 2018). The detachment coefficient is empirical or phenomenology that does not contains clear interpretations by physics (Russell, Chequer, et al., 2018).

The modified attachment-detachment model

Considering torque balance for the mechanical equilibrium condition, the modified detachment model is derived, in which the maximum retention function is introduced (Bedrikovetsky, Siqueira, Furtado, & Souza, 2011; Bedrikovetsky et al., 2012; Chequer, Vaz, & Bedrikovetsky, 2018)

$$\frac{\partial \sigma_a}{\partial t} = \lambda_a c U, \sigma_a < \sigma_{cr}(U, \gamma) \tag{2.16}$$

$$\sigma_a = \sigma_{cr}(U, \gamma) \tag{2.17}$$

where σ_a is attached particle concentration L^{-3}, σ_{cr} is the critical attached particle concentration L^{-3}, and γ is ionic strength (salinity).

The maximum retention function reflects the critical value of retained particle concertation in a porous medium which is affected by velocity, ionic strength, pH and temperature.

The typical forms of filtration function or coefficient, such as the constant filtration coefficient and the Langmuir filtration function for monolayer attachment, have been review

in the Introduce of the paper “Exact solution for suspension-colloidal transport with multiple capture mechanisms” (*Chapter Three*).

Exact solutions and inverse problems

The governing system (2.10, 2.12) allows for deriving exact solutions for the suspended concentration and retained concentration. During laboratory tests, the outlet (effluents) suspended concentration is usually measured. The breakthrough concertation taken from BTCs allows to determine the filtration function directly, which is so-call the direct problem (Bolster, Hornberger, Mills, & Wilson, 1998; Foppen, Mporokoso, & Schijven, 2005). The problem has the inverse problem to the exact solution, in which the filtration coefficient is unknown and suspended concentration and retained concentration are taken from laboratory tests.

The inverse problem to the solution has been solved by Alvarez et al. 2006, in which it is described as the unique and stable solution if compared with small perturbations of experiment data. The filtration function (or coefficient) calculated from the solution of the direct problem can be applied to predicting the retention profiles, which relates the RPs with BTCs. Another inverse is associated with the calculation of permeability reduction with respect to the pressure drop of the core(A. Alvarez et al., 2005; A. C. Alvarez, Hime, Marchesin, & Bedrikovetsky, 2007).

Reference

Altmann, J., & Ripperger, S. (1997). Particle deposition and layer formation at the crossflow microfiltration. *Journal of Membrane Science, 124*(1), 119-128.

Altoe, F., Bedrikovetski, P., Siqueira, A., de Souza, A., & Shecaira, F. (2006). Correction of Basic Equations for Deep Bed Filtration with Dispersion.

Alvarez, A., Bedrikovetsky, P., Hime, G., Marchesin, A., Marchesin, D., & Rodrigues, J. (2005). A fast inverse solver for the filtration function for flow of water with particles in porous media. *Inverse problems, 22*(1), 69.

Alvarez, A. C., Hime, G., Marchesin, D., & Bedrikovetsky, P. G. (2007). The inverse problem of determining the filtration function and permeability reduction in flow of water with particles in porous media. *Transport in Porous Media, 70*(1), 43-62.

Bedrikovetsky, P. (2008). Upscaling of stochastic micro model for suspension transport in porous media. *Transport in Porous Media, 75*(3), 335-369.

Bedrikovetsky, P., Siqueira, A., de Souza, A., & Shecaira, F. (2006). Correction of basic equations for deep bed filtration with dispersion. *Journal of Petroleum Science and Engineering, 51*(1-2), 68-84.

Bedrikovetsky, P., Siqueira, F. D., Furtado, C. A., & Souza, A. L. S. (2011). Modified particle detachment model for colloidal transport in porous media. *Transport in Porous Media, 86*(2), 353-383.

Bedrikovetsky, P., You, Z., Badalyan, A., Osipov, Y., & Kuzmina, L. (2017). Analytical model for straining-dominant large-retention depth filtration. *Chemical Engineering Journal, 330*, 1148-1159.

Bedrikovetsky, P., Zeinijahromi, A., Siqueira, F. D., Furtado, C. A., & de Souza, A. L. S. (2012). Particle detachment under velocity alternation during suspension transport in porous media. *Transport in Porous Media, 91*(1), 173-197.

Bergendahl, J. A., & Grasso, D. (2003). Mechanistic basis for particle detachment from granular media. *Environmental science & technology, 37*(10), 2317-2322.

Bhattacharjee, S., Ko, C.-H., & Elimelech, M. (1998). DLVO interaction between rough surfaces. *Langmuir, 14*(12), 3365-3375.

Bolster, C. H., Hornberger, G. M., Mills, A. L., & Wilson, J. L. (1998). A method for calculating bacterial deposition coefficients using the fraction of bacteria recovered from laboratory columns. *Environmental science & technology, 32*(9), 1329-1332.

Borazjani, S., & Bedrikovetsky, P. (2017). Exact solutions for two-phase colloidal-suspension transport in porous media. *Applied mathematical modelling, 44*, 296-320.

Borazjani, S., Bedrikovetsky, P., & Farajzadeh, R. (2016). Analytical solutions of oil displacement by a polymer slug with varying salinity. *Journal of Petroleum Science and Engineering, 140*, 28-40.

Bradford, S. A., Simunek, J., Bettahar, M., van Genuchten, M. T., & Yates, S. R. (2003). Modeling colloid attachment, straining, and exclusion in saturated porous media. *Environmental science & technology, 37*(10), 2242-2250.

Bradford, S. A., Torkzaban, S., & Shapiro, A. (2013). A theoretical analysis of colloid attachment and straining in chemically heterogeneous porous media. *Langmuir, 29*(23), 6944-6952.

Bradford, S. A., Torkzaban, S., & Walker, S. L. (2007). Coupling of physical and chemical mechanisms of colloid straining in saturated porous media. *Water Research, 41*(13), 3012-3024.

Bradford, S. A., Yates, S. R., Bettahar, M., & Simunek, J. (2002). Physical factors affecting the transport and fate of colloids in saturated porous media. *Water Resources Research, 38*(12).

Chalk, P., Gooding, N., Hutten, S. J., You, Z., & Bedrikovetsky, P. G. (2011). *Laboratory and theoretical investigation of size exclusion suspension flow in rocks.* Paper presented at the SPE European Formation Damage Conference.

Chequer, L., Vaz, A., & Bedrikovetsky, P. (2018). Injectivity decline during low-salinity waterflooding due to fines migration. *Journal of Petroleum Science and Engineering, 165*, 1054-1072.

Civan, F. (2011). *Porous media transport phenomena*: John Wiley & Sons.

Civan, F. (2015). *Reservoir formation damage*: Gulf Professional Publishing.

Derjaguin, B., & Landau, L. (1941). The theory of stability of highly charged lyophobic sols and coalescence of highly charged particles in electrolyte solutions. *Acta Physicochim. URSS, 14*(633-52), 58.

Elimelech, M., Gregory, J., & Jia, X. (2013). *Particle deposition and aggregation: measurement, modelling and simulation*: Butterworth-Heinemann.

Farajzadeh, R., Bedrikovetsky, P., Lotfollahi, M., & Lake, L. (2016). Simultaneous sorption and mechanical entrapment during polymer flow through porous media. *Water Resources Research, 52*(3), 2279-2298.

Foppen, J., Mporokoso, A., & Schijven, J. (2005). Determining straining of Escherichia coli from breakthrough curves. *Journal of contaminant hydrology, 76*(3-4), 191-210.

Gregory, J. (1975). Interaction of unequal double layers at constant charge. *Journal of Colloid and Interface Science, 51*(1), 44-51.

Gregory, J. (1981). Approximate expressions for retarded van der Waals interaction. *Journal of Colloid and Interface Science, 83*(1), 138-145.

Guedes, R. G., Al-Abduwani, F. A., Bedrikovetsky, P., & Currie, P. K. (2009). Deep-bed filtration under multiple particle-capture mechanisms. *SPE Journal, 14*(03), 477-487.

Herzig, J., Leclerc, D., & Goff, P. L. (1970). Flow of suspensions through porous media—application to deep filtration. *Industrial & Engineering Chemistry, 62*(5), 8-35.

Hogg, R., Healy, T. W., & Fuerstenau, D. (1966). Mutual coagulation of colloidal dispersions. *Transactions of the Faraday Society, 62*, 1638-1651.

Israelachvili, J. N. (2011). *Intermolecular and surface forces*: Academic press.

Kalantariasl, A., Farajzadeh, R., You, Z., & Bedrikovetsky, P. (2015). Nonuniform external filter cake in long injection wells. *Industrial & Engineering Chemistry Research, 54*(11), 3051-3061.

Khilar, K. C., & Fogler, H. S. (1998). *Migrations of fines in porous media* (Vol. 12): Springer Science & Business Media.

Khilar, K. C., Vaidya, R. N., & Fogler, H. S. (1990). Colloidally-induced fines release in porous media.

Lager, A., Webb, K. J., Black, C., Singleton, M., & Sorbie, K. S. (2008). Low salinity oil recovery-an experimental investigation1. *Petrophysics, 49*(01).

Lake, L. W., Johns, R. T., Rossen, W. R., & Pope, G. A. (2014). Fundamentals of enhanced oil recovery.

Payatakes, A. C., Rajagopalan, R., & Tien, C. (1974). Application of porous media models to the study of deep bed filtration. *The canadian journal of chemical engineering, 52*(6), 722-731.

Ruckenstein, E., & Prieve, D. C. (1976). Adsorption and desorption of particles and their chromatographic separation. *AIChE Journal, 22*(2), 276-283.

Russell, T., Chequer, L., Borazjani, S., You, Z., Zeinijahromi, A., & Bedrikovetsky, P. (2018). Formation Damage by Fines Migration: Mathematical and Laboratory Modeling, Field Cases. In *Formation Damage During Improved Oil Recovery* (pp. 69-175): Elsevier.

Russell, T., Wong, K., Zeinijahromi, A., & Bedrikovetsky, P. (2018). Effects of delayed particle detachment on injectivity decline due to fines migration. *Journal of Hydrology, 564*, 1099-1109.

Shannon, M. A., Bohn, P. W., Elimelech, M., Georgiadis, J. G., Marinas, B. J., & Mayes, A. M. (2010). Science and technology for water purification in the coming decades. In *Nanoscience And Technology: A Collection of Reviews from Nature Journals* (pp. 337-346): World Scientific.

Sharma, M., & Yortsos, Y. (1987). Transport of particulate suspensions in porous media: model formulation. *AIChE Journal, 33*(10), 1636-1643.

Sorbie, K. S. (2013). *Polymer-improved oil recovery*: Springer Science & Business Media.

Tufenkji, N. (2007). Colloid and microbe migration in granular environments: a discussion of modelling methods. In *Colloidal transport in porous media* (pp. 119-142): Springer.

Vaz, A., Bedrikovetsky, P., Fernandes, P., Badalyan, A., & Carageorgos, T. (2017). Determining model parameters for non-linear deep-bed filtration using laboratory pressure measurements. *Journal of Petroleum Science and Engineering, 151*, 421-433.

Verwey, E. J. W., Overbeek, J. T. G., & Overbeek, J. T. G. (1999). *Theory of the stability of lyophobic colloids*: Courier Corporation.

Yang, Y., Siqueira, F., Vaz, A., Badalyan, A., You, Z., Zeinijahromi, A., . . . Bedrikovetsky, P. (2018). Fines Migration in Aquifers and Oilfields: Laboratory and Mathematical Modelling. *Flow and Transport in Subsurface Environment*, 3-67.

Yao, C., Wang, D., Wang, J., Hou, J., Lei, G., & Steenhuis, T. S. (2017). Effect of ionic strength on the transport and retention of polyacrylamide microspheres in reservoir water shutoff treatment. *Industrial & Engineering Chemistry Research, 56*(28), 8158-8168.

You, Z., Bedrikovetsky, P., & Kuzmina, L. (2013). *Exact solution for long-term size exclusion suspension-colloidal transport in porous media.* Paper presented at the Abstract and Applied Analysis.

You, Z., Osipov, Y., Bedrikovetsky, P., & Kuzmina, L. (2014). Asymptotic model for deep bed filtration. *Chemical Engineering Journal, 258*, 374-385.

Yuan, B., & Moghanloo, R. G. (2018). Nanofluid pre-treatment, an effective strategy to improve the performance of low-salinity waterflooding. *Journal of Petroleum Science and Engineering, 165*, 978-991.

Yuan, B., Moghanloo, R. G., & Zheng, D. (2016). *Analytical modeling of nanofluid injection to improve the performance of low salinity water flooding.* Paper presented at the Offshore Technology Conference Asia.

Zeinijahromi, A., Lemon, P., & Bedrikovetsky, P. (2011). Effects of induced fines migration on water cut during waterflooding. *Journal of Petroleum Science and Engineering, 78*(3-4), 609-617.

3 Exact Solutions for Suspension-Colloidal Transport with Multiple Capture Mechanisms

H. Zhang, G. Malgaresi, P. Bedrikovetsky

Statement of Authorship

Title of Paper	Exact solutions for suspension-colloidal transport with multiple capture mechanisms
Publication Status	☑ Published ☐ Accepted for Publication ☐ Submitted for Publication ☐ Unpublished and Unsubmitted w ork w ritten in manuscript style
Publication Details	Zhang, H., Malgaresi, G.V.C. and Bedrikovetsky, P., 2018. Exact solutions for suspension-colloidal transport with multiple capture mechanisms. International Journal of Non-Linear Mechanics, 105, pp.27-42.

Principal Author

Name of Principal Author (Candidate)	Hao Zhang		
Contribution to the Paper	Derived mathematical model and exact and numerical solutions, analysed and matched lab data, interpreted results		
Overall percentage (%)	80 %		
Certification:	This paper reports on original research I conducted during the period of my Higher Degree by Research candidature and is not subject to any obligations or contractual agreements with a third party that would constrain its inclusion in this thesis. I am the primary author of this paper.		
Signature		Date	22/10/2018

Co-Author Contributions

Name of Co-Author	Gabriel Malgaresi		
Contribution to the Paper	Helped in interpretation of lab data, and calculation of DLVO theory.		
Signature		Date	23/10/2018.

Name of Co-Author	Pavel Bedrikovetsky		
Contribution to the Paper	Supervised development of the whole work.		
Signature		Date	23/10/2018

International Journal of Non-Linear Mechanics 105 (2018) 27–42

Contents lists available at ScienceDirect

International Journal of Non-Linear Mechanics

journal homepage: www.elsevier.com/locate/nlm

Exact solutions for suspension-colloidal transport with multiple capture mechanisms

H. Zhang, G.V.C. Malgaresi, P. Bedrikovetsky *

Australian School of Petroleum, University of Adelaide, Australia

A B S T R A C T

We discuss one-dimensional (1D) non-linear problems of suspension-colloidal transport in porous media with two simultaneous particle capture mechanisms. The first mechanism corresponds to low retention concentration and constant filtration function. The second mechanism corresponds to large retention concentration with blocking (Langmuir) filtration function. The 1D flow problems are non-linear; however, they allow for exact solutions. The exact solutions are obtained for the general two-capture case, and also for piecewise-linear approximation of the filtration function. The proposed filtration function describes the breakthrough curves (BTCs) that monotonically increase with time and stabilise at some value lower than the injected concentration; those BTCs are observed for numerous suspension-colloidal flows. The tuning method for determining the model coefficients is developed. Close agreement between the laboratory and modelling data validates the proposed form of filtration function.

1. Introduction

Colloidal-suspension flows in porous media occur in different processes of environmental, chemical, civil and petroleum engineering, and also in energy sector and geology [1–3]. Mathematical modelling is an essential part of design and planning of various technological processes in those areas, like industrial waste management in aquifers, injection of cold water and hot water/steam production from geothermal reservoirs, industrial filtering, management of potable water resources, water injection in oil fields for pressure maintenance, etc. [3–6].

Particle capture by the rock during suspension-colloidal flows occurs by size exclusion, straining, attachment, segregation, diffusion into dead-end pores, etc. [1,4,7–12], (Fig. 1). The effects of particle retention are decreasing suspension concentration and permeability. The suspension concentration decline due to retention is important for industrial waste disposal and aquifer contamination, while the permeability decline yields production and injection well impairment.

Governing equations for deep bed filtration (DBF) in porous media contain mass balance for suspended and retained particles, particle capture rate that is proportional to the particle advective flux, and Darcy's law accounting for permeability decline due to particle retention [7,13–16]:

$$\frac{\partial}{\partial t}(\phi c+\sigma)+U\frac{\partial c}{\partial x}=\frac{\partial}{\partial x}\left(D\frac{\partial c}{\partial x}\right) \tag{1}$$

$$\frac{\partial \sigma}{\partial t}=\lambda(\sigma)\,cU \tag{2}$$

$$U=-\frac{k(\sigma)}{\mu(c)}\frac{\partial p}{\partial x} \tag{3}$$

where x is the linear coordinate in the flow direction, t is the time, c and σ are the suspended and attached concentrations, ϕ is the porosity, U is the fluid velocity, D is the dispersion (diffusion) coefficient, λ is the filtration coefficient, k is the permeability, μ is the viscosity, and p is the pressure. The suspension concentration c is determined as the number of suspended particles in unitary volume of carrier fluid, while the retained concentration σ is defined as the number of attached particles in unitary volume of the rock.

Constant-concentration injection into clean bed corresponds to the following initial and boundary conditions:

$$t=0:\ c=\sigma=0 \tag{4}$$

$$x=0:\ c=c^0 \tag{5}$$

The initial condition (4) for concentration c holds as x tends to infinity.

Another form of the retention rate equation is its proportionality of the rate to overall particle flux q, which is the total of advective and diffusive fluxes [8,13,17]:

$$\frac{\partial \sigma}{\partial t}=\lambda(\sigma)\,q,\quad q=cU-D\frac{\partial c}{\partial x} \tag{6}$$

Fig. 2 shows the difference in capture scenarios by models given by Eqs. (2) and (6). The capture occurs at a site shown as a sieve-screen. The overall particle displacement by the flux q is decomposed into those by the advective and diffusive fluxes. Eq. (2) corresponds to the case where the capture occurs during the advective move (Fig. 2a). Eq. (6) corresponds to diffusive move (Fig. 2b).

* Corresponding author.
E-mail address: pavel@asp.adelaide.edu.au (P. Bedrikovetsky).

https://doi.org/10.1016/j.ijnonlinmec.2018.07.007
Received 3 June 2018; Received in revised form 10 July 2018; Accepted 15 July 2018
Available online 27 July 2018
0020-7462/© 2018 Elsevier Ltd. All rights reserved.

Index

c	Suspended particle concentration [L^{-3}]
c^0	Injected particle concentration [L^{-3}]
C	Dimensionless suspended particle concentration [-]
D	Dispersion (diffusion) coefficient [$L^2\ T^{-1}$]
j	Jamming ratio [-]
L	Length of the core [L]
p	Pressure [$M\ L^{-1}\ T^{-2}$]
q	Total flux [$L^{-2}\ T^{-1}$]
r	Radius [L]
r_p	Mean pore radius [L]
r_s	Particle radius [L]
S	Dimensionless total retained particle concentration [-]
S_1	Dimensionless attached particle concentration for 1st mechanism [-]
S_2	Dimensionless strained particle concentration for 2nd mechanism [-]
S_m	Dimensionless maximum retained particle concentration [-]
t	Time [T]
T	Dimensionless time [PVI]
T_{inj}	Dimensionless injection time [PVI]
T_m	Dimensionless stabilisation time at the inlet [PVI]
U	Flow velocity [$L\ T^{-1}$]
x	Axial coordinate [L]
X	Dimensionless axial coordinate [-]

Greek letters

γ	Salinity [mM]
ε	Small filtration coefficient variable [-]
σ	Retained particle concentration [L^{-3}]
σ_1	Attached particle concentration [L^{-3}]
σ_2	Strained particle concentration [L^{-3}]
σ_m	Maximum attached particle concentration [L^{-3}]
ϕ	Porosity [-]
λ	Filtration coefficient [L^{-1}]
λ_0	Attachment filtration coefficient at no retention [L^{-1}]
λ_1	Straining filtration coefficient [L^{-1}]
Λ	Dimensionless filtration [-]
Λ_0	Dimensionless initial attachment filtration coefficient [-]
Λ_1	Dimensionless straining filtration coefficient [-]
ρ	Density [$M\ L^{-3}$]
μ	Viscosity [$M\ L^{-1}\ T^{-1}$]

Superscripts

0	Initial value

Subscripts

inj	Injection
m	Maximum (for retained concentration and time)
p	Pore
s	Suspension

Abbreviations

BTC	Breakthrough curve
DBF	Deep bed filtration
ODE	Ordinary differential equation
PDE	Partial differential equation
CFD	Computational fluid dynamics

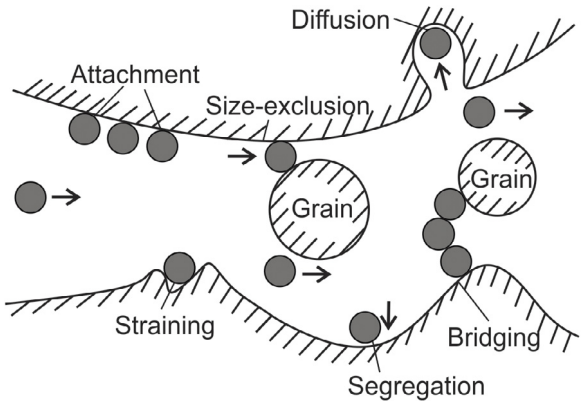

Fig. 1. Various particle capture mechanisms in a single pore.

The Peclet number is the ratio between the advective and dispersive fluxes. In large scale (reservoir) approximation, where the typical boundary size exceeds 100m, Peclet number significantly exceeds one, $UL/D >> 1$, and the dispersive/diffusion terms are neglected in both Eqs. (2) and (6). During laboratory corefloods, where the typical core length is 0.1 m, Peclet number can be lower than one, and the diffusion is important.

The assumptions of monolayer Langmuir's attachment where one attached particle occupies one vacancy, and vice versa, yield the "active-mass" law for the particle–vacancy "reaction" [18–20]:

$$\lambda(\sigma) = \begin{cases} \lambda_0 \left(1 - \dfrac{\sigma}{\sigma_m}\right), & \sigma < \sigma_m \\ 0, & \sigma > \sigma_m \end{cases} \tag{7}$$

where σ_m is the maximum number of retention vacancies per unitary volume occupied by the attached particles. The Langmuir blocking filtration function, given by Eq. (7) is usually used for monolayer electrostatic attachment of particles on the rock surface, but is also applicable for straining and size exclusion [10,18,19]. Plot of the Langmuir filtration function corresponds to curve 2 in Fig. 3a. The exact solution of the 1D flow problem (1)–(5) corresponds to breakthrough curve 2 in Fig. 3b, which is zero before the breakthrough at the moment of injection of one pore volume, then jumps up to some value and tends to injected concentration when time tends to infinity [18].

For small retained concentration, where $\sigma << \sigma_m$, the filtration coefficient is assumed to be constant, $\lambda(\sigma) = \lambda_1$ (straight line 1 in Fig. 3a). For this case, the breakthrough concentration is equal zero before the breakthrough moment, then jumps up to some value and remains constant during the overall flow period (curve 1 in Fig. 3b) [18]. This type of the breakthrough behaviour was observed for various capture mechanisms [1,4–6,11,21]. To be specific, further in the text the term attachment corresponds to the Langmuir's blocking capture, while the low-retention mechanism is called size exclusion, or straining.

BTCs that equal zero before the breakthrough moment, jumping up to some value and then tending to a limit that is lower than the injected concentration as time tends to infinity, have been observed in numerous laboratory tests (curve 3 in Fig. 3b) [4,5,8–10,13,19,22,23]. However, this specific type of BTCs has not been interpreted by capture kinetics neither in terms of an analytical model; the filtration functions that yield this type of breakthrough curves, are not available.

Suspended-colloidal particles are subject to different capture mechanisms (Fig. 1). Each capture process depends on parameters that are stochastically distributed over the porous space, like surface charge, pore throat and particle sizes, roughness, tortuosity, etc. The stochastic models for suspension-colloidal-nano transport include random-walk equations [24,25], Boltzmann's model [25,26], network and 3D computational fluid dynamics (CFD) models [21], and randomly distributed filtration coefficients [10,25,27].

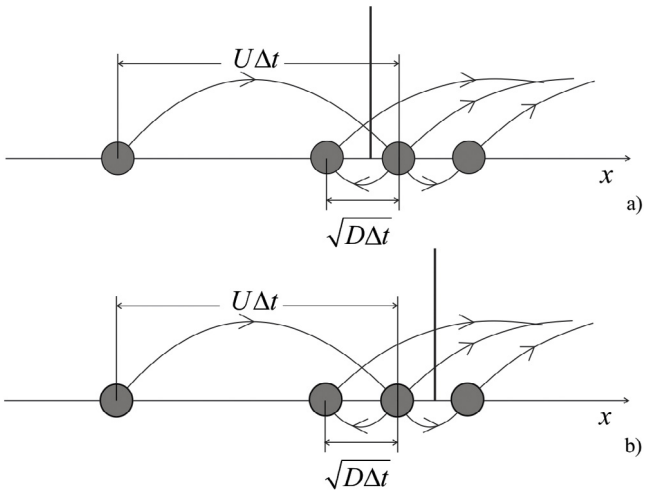

Fig. 2. Traditional and modified models for particle capture by the porous media, where the vertical bar corresponds to the capture site: (a) particle capture from the advective flux; (b) particle capture from the overall advective and diffusive flux.

The population balance models account for fine particle distribution in size, surface charge, shape, etc. [28,29] and for accessibility of different pores by different size particles due to geometric restrictions and the corresponding reduction of the overall particle flux [7,30]. For transport of homogeneous suspension, the population balance equations allow for exact averaging; the upscaled equations coincide with the traditional DBF system that accounts for accessibility and flux-reduction functions [7].

Exact solutions for DBF Eqs. (1)–(3) yield well-posed inverse problems. The filtration function in Eq. (2) is determined from BTC, and formation damage function in Eq. (3) is calculated from the pressure drop history across the core [31]. The filtration function can also be determined from the retention profile, claiming significantly lower data scattering than after BTC treatment [31].

Exact analytical solutions are also used for qualitative interpretation of the results of laboratory coreflooding and calculation of the model coefficients. The comparison of the concentration waves provided by the analytical models with those measured during corefloods or field tests yields a more profound understanding of the transport processes. The analytical models are also widely used in three-dimensional reservoir simulations using stream-line and front-tracking techniques. The above applications have motivated numerous studies on the exact solutions for 1D colloidal-suspended and reactive transport problems [15,16,20,23,32–37].

Two-capture mechanism models with size exclusion and attachment are widely used in suspension-colloidal studies [1,4,38,39]. An analytical model for deep bed filtration of a binary mixture of two distinct particle populations, where each specie is captured by its own separate capture mechanism is derived; high quality match using constant and Langmuir's filtration functions is achieved [22]. The asymptotic solutions for two-population and two-capture models have been obtained [40,41]. However, exact solutions for two simultaneous capture mechanisms of uniform particles are not available.

In the current paper, we discuss non-linear 1D problem for suspension-colloidal transport in porous media with two simultaneous particle capture mechanisms. We prove that any number of capture mechanisms can be aggregated into one mechanism following either of scenarios given by Eqs. (2) or (6). For dispersion-free case with two simultaneous particle capture mechanisms given by constant and blocking (Langmuir) filtration functions, we derive an exact solution. The solution exhibits BTC that monotonically grows after the breakthrough and tends to the limit that is lower than the injected concentration. The analytical model closely matches numerous laboratory tests, validating the interpretation of BTCs that stabilise below the injected concentration, by the two-capture model.

The structure of the paper is as follows. Section 2 and Appendices A and B present mathematical model for suspension-colloidal flows with multiple capture mechanisms, and show that it is equivalent to a single-capture system. Section 3 discusses two capture mechanisms with constant (straining) and Langmuir (attachment) filtration functions, including derivation of exact solution for 1D flow, and the exact and approximate formulae for aggregation. Section 4 derives the exact solution for binary (piecewise linear) filtration function with explicit formulae for BTCs. Section 5 presents sensitivity study of filtration functions and BTCs with respect to three model parameters. Section 6 compares the exact and numerical solutions. Section 7 matches two series of laboratory tests and exhibits the results of matching by the analytical model. Section 8 derives the aggregation procedure and exact solution for reactive flows with multiple chemical reactions. Section 9 discusses the results, the limitations of the model and some practical applications. Section 10 draws the conclusions and finalises the paper.

2. Suspension-colloidal flow system with multiple capture mechanisms

System of equations for DBF of particles with n capture mechanisms accounting for dispersion (diffusion) of particles, given by Eqs. (A.1)–(A.3) is presented in Appendix A. Here any combination of different particle capture mechanisms, presented in Fig. 1, is discussed. All capture rates are proportional to the particle advective flux [12,18].

Lemma 1. *System (A.1)– (A.3) for suspension-colloidal flow with n particle capture mechanisms $\lambda_i(\sigma_1, \sigma_2 \ldots \sigma_n)$ is equivalent to that with a single capture*

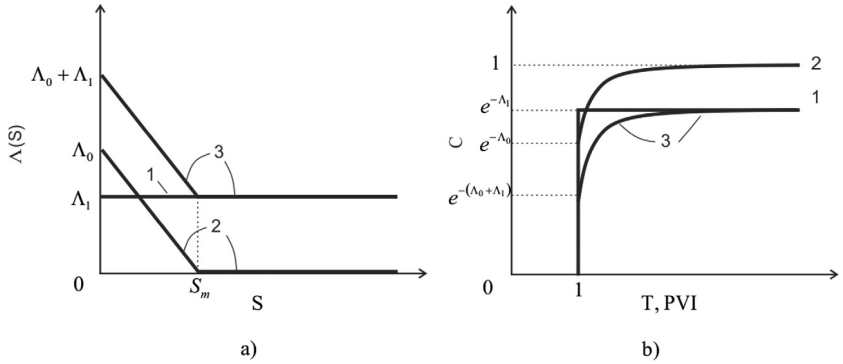

Fig. 3. Various forms of breakthrough curves for different forms of filtration function: (a) filtration functions; (b) breakthrough curves. Here 1 – constant filtration function, 2 – Langmuir (blocking) filtration function, and 3 is the binary filtration function.

mechanism (2), where the aggregated filtration function $\lambda(\sigma)$ is determined by Cauchy's problem for system of ordinary differential equations (ODE) (A.9).

The proof is presented in Appendix A.

Appendix B discusses the modified DBF system with dispersion, where the capture rate is proportional to the overall particle flux that includes advective and diffusive fluxes, given by Eqs. (1), (6) ([8,13,17]). Lemma 1 is also valid for system (A.1), (A.2), (B.1). The proof is presented in Appendix B.

Further we discuss the large-scale flows, where the dispersion is negligible.

Introduce the following dimensionless parameters and variables into dispersion-free systems (1), (2) and (4), (5):

$$T=\frac{Ut}{\phi L};\ X=\frac{x}{L};\ C=\frac{c}{c^0};\ \Lambda_0=\lambda_0 L;\ S_m=\frac{\sigma_m}{\phi c^0};\ S=\frac{\sigma}{\phi c^0};\ \Lambda_1=\lambda_1 L;$$
$$S_1=\frac{\sigma_1}{\phi c^0};\ S_2=\frac{\sigma_2}{\phi c^0} \tag{8}$$

The dimensionless system becomes:

$$\frac{\partial(C+S)}{\partial T}+\frac{\partial C}{\partial X}=0 \tag{9}$$

$$\frac{\partial S}{\partial T}=\Lambda(S)C \tag{10}$$

Initial and boundary conditions (4), (5) for dimensionless variables become

$$T=0:\ C=S=0 \tag{11}$$

$$X=0:\ C=1 \tag{12}$$

The exact solution for system (9), (10) subject to initial and boundary conditions (11), (12) is derived in the next section.

3. Suspension-colloidal flow system with two capture mechanisms

In the current section we derive the expression for filtration function that corresponds to two fines capture mechanisms (Section 3.1), develop the exact solution for the general case of aggregated filtration function (Section 3.2) and its particular case for two capture mechanisms (Section 3.3). Then, properties of the filtration function, which is the aggregation of Langmuir and constant filtration functions, are described (Section 3.4). The explicit asymptotic formulae for aggregated two-mechanism filtration functions with small rate by either mechanism are derived (Section 3.5)

3.1. Aggregation formula for overall filtration function

Consider the case $n=2$ of two capture mechanisms. One mechanism with low retention has constant filtration function. Another one has the Langmuir blocking filtration function, given by Eq. (7).

Changing T to S_2 as a free variable in ODE that corresponds to the capture rate for the first capture mechanism (A.3) at $X=$ const yields

$$\frac{dS_1}{dS_2}=\frac{dS_1}{dT}\Big/\frac{dS_2}{dT}=\frac{\Lambda_0}{\Lambda_1}\left(1-\frac{S_1}{S_m}\right) \tag{13}$$

Accounting for initial conditions (11), (12) and integrating Eq. (13) by separation of variables results in

$$S_2=-\frac{S_m\Lambda_1}{\Lambda_0}\ln\left(1-\frac{S_1}{S_m}\right) \tag{14}$$

The total retained concentration and overall filtration function become

$$S(S_1)=S_1+S_2=S_1-\frac{S_m\Lambda_1}{\Lambda_0}\ln\left(1-\frac{S_1}{S_m}\right) \tag{15}$$

$$\Lambda(S)=\Lambda_0\left(1-\frac{S_1(S)}{S_m}\right)+\Lambda_1 \tag{16}$$

respectively, where $S_1=S_1(S)$ is the inverse function to Eq. (15). So, the formula for the aggregated filtration function (16) contains transcendental Eq. (15).

Fig. 4a presents the continuous curve for the aggregated filtration function.

3.2. Exact solution for any aggregated filtration function $\Lambda(S)$

Following works [15–17], here we present the general schema for solution of Eqs. (9), (10) for any arbitrary filtration function. Introducing the potential $\Phi(S)$ from Eq. (10)

$$\Phi(S)=\int_0^S\frac{du}{\Lambda(u)} \tag{17}$$

transforms Eq. (10) into

$$C=\frac{\partial\Phi(S)}{\partial T} \tag{18}$$

Substituting expression (18) into Eq. (9) and changing order of differentiation in the third term yields:

$$\frac{\partial}{\partial T}\left(\frac{\partial\Phi(S)}{\partial T}+S\right)+\frac{\partial}{\partial T}\left(\frac{\partial\Phi(S)}{\partial X}\right)=0 \tag{19}$$

Integration of Eq. (19) in T accounting for initial conditions (11), (12) results in:

$$\frac{\partial\Phi(S)}{\partial T}+S+\frac{\partial\Phi(S)}{\partial X}=0 \tag{20}$$

Performing differentiation in (20) yields

$$\frac{\partial S}{\partial T}+\frac{\partial S}{\partial X}=-\Lambda(S)S \tag{21}$$

Representing Eq. (21) in characteristic form with T as a parameter along characteristics shows that $S=0$ at $T<X$ (Fig. 5a). Ahead of the concentration front $X=T$, $S=0$. Breakthrough in Fig. 5b occurs after the moment t_1, so the S-value in profile in Fig. 5c is zero.
The characteristic form at $T>X$ is:

$$\frac{dS}{dX}=-\Lambda(S)S,\ \frac{dT}{dX}=1 \tag{22}$$

Ordinate axes is a characteristic for quasi-linear hyperbolic system (9), (10), i.e. (11), (12) is a Goursat problem [12]. It allows determining $S(0, T)$ from Eq. (10) and boundary condition (12). Accounting for boundary condition (12) in Eq. (10) and integrating it by separation of variables yields

$$\int_0^{S(0,T)}\frac{du}{\Lambda(u)}=T \tag{23}$$

Integration of ODE (22) with initial condition (11) yields

$$\int_{S(0,T-X)}^{S(X,T)}\frac{du}{\Lambda(u)u}=-X \tag{24}$$

Here $S(0, T\text{-}X)$ is determined from transcendental Eq. (23). Then $S(X, T)$ is determined from transcendental Eq. (24).

The Riemann invariant for system (9), (10) that corresponds to unity eigen-value is C/S [15–17,42]:

$$\frac{C(X,T)}{S(X,T)}=\frac{1}{S(0,T-X)} \tag{25}$$

yielding the explicit expression for suspended concentration $C(X, T)$ versus $S(X, T)$.

3.3. Exact solution for 1D transport with two mechanism capture

In this section we derive the exact solution for aggregated function of two capture mechanisms, given by Eqs. (15) and (16).

The system for two-mechanism capture with Langmuir and constant filtration functions is:

$$\frac{\partial(C+S_1+S_2)}{\partial T}+\frac{\partial C}{\partial X}=0 \tag{26}$$

$$\frac{\partial S_1}{\partial T}=\Lambda^1(S_1)C,\quad \Lambda^1(S_1)=\begin{cases}\Lambda_0\left(1-\dfrac{S_1}{S_m}\right), & S_1<S_m\\ 0, & S_1>S_m\end{cases} \tag{27}$$

$$\frac{\partial S_2}{\partial T}=\Lambda_1 C \tag{28}$$

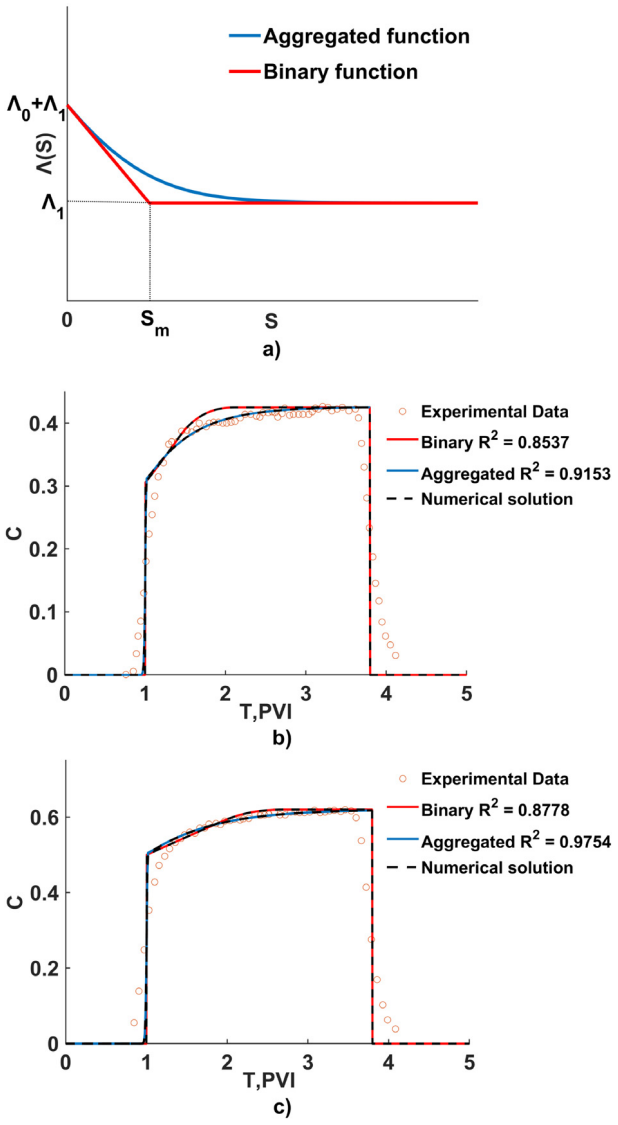

Fig. 4. Comparison between analytical and numerical solutions: (a) aggregated and binary filtration functions (blue and red curves, respectively); (b,c) breakthrough concentrations calculated by analytical models for aggregated and binary filtration functions (blue and red curves). Dashed black curves are obtained by numerical modelling. (For interpretation of the references to colour in this figure legend, the reader is referred to the web version of this article.)

Introducing potential from Eq. (27)

$$\Phi\left(S_1\right)=\int_0^{S_1}\frac{du}{\Lambda^1\left(u\right)} \tag{29}$$

transforms Eq. (27) into

$$C=\frac{\partial\Phi\left(S_1\right)}{\partial T} \tag{30}$$

Substituting Eqs. (14) and (30) into Eq. (26) yields

$$\frac{\partial}{\partial T}\left(\frac{\partial\Phi\left(S_1\right)}{\partial T}+S_1+S_2\left(S_1\right)\right)+\frac{\partial}{\partial X}\left(\frac{\partial\Phi\left(S_1\right)}{\partial T}\right)=0 \tag{31}$$

Changing order of derivatives in second differential term in Eq. (31), integrating the result in T accounting for initial condition (11), (12) yields

$$\frac{1}{\Lambda^1\left(S_1\right)}\frac{\partial S_1}{\partial T}+\frac{1}{\Lambda^1\left(S_1\right)}\frac{\partial S_1}{\partial X}=-S_1+\frac{S_m\Lambda_1}{\Lambda_0}\ln\left(1-\frac{S_1}{S_m}\right) \tag{32}$$

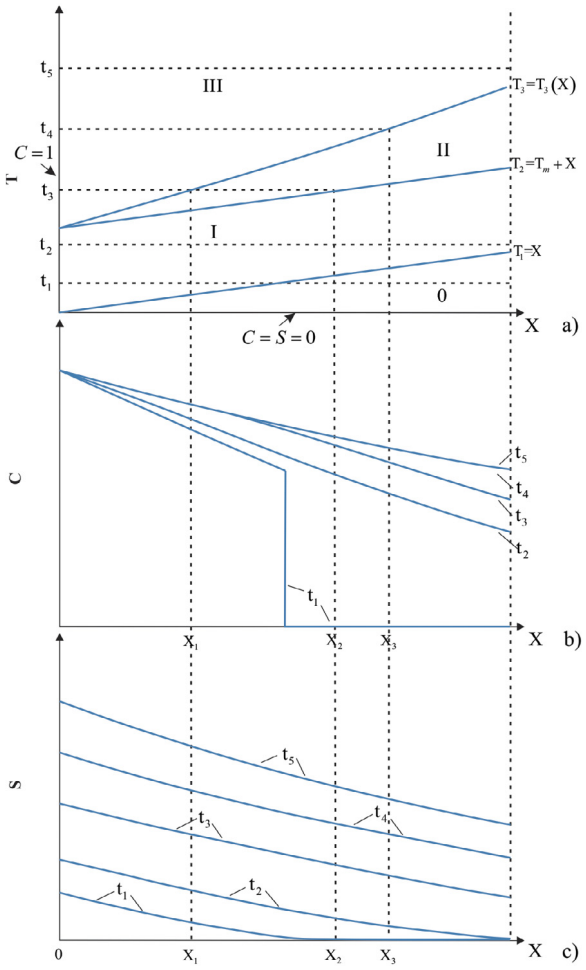

Fig. 5. Exact solution for 1D suspension-colloidal flow with piecewise-linear filtration function: (a) movement of concentration fronts (x, t)-plane; (b) suspended concentration profiles; (c) retained concentration profiles.

Representing Eq. (32) in characteristic form with T as a parameter along characteristics shows that $S_1=S_2=0$ at $T<X$ (Fig. 5a).

Characteristic form of Eq. (32) at $T>X$ is

$$\frac{dS_1}{dX}=\Lambda^1\left(S_1\right)\left[-S_1+\frac{S_m\Lambda_1}{\Lambda_0}\ln\left(1-\frac{S_1}{S_m}\right)\right],\ \frac{dT}{dX}=1 \tag{33}$$

At $T=0$, where $C=1$, separation of variables in Eq. (27) results in

$$S_1(0,T)=S_m\left[1-\exp(-\frac{\Lambda_0}{S_m}T)\right] \tag{34}$$

Integration of ODE (33) along the characteristic line results in

$$\int_{S_1(0,T-X)}^{S_1(X,T)}\frac{dS_1}{\Lambda_0(1-\frac{S_1}{S_m})\left[S_1-\frac{S_m\Lambda_1}{\Lambda_0}\ln(1-\frac{S_1}{S_m})\right]}=-X \tag{35}$$

Substitution of expression (34) into Eq. (35) determines S_1 in implicit form:

$$\int_{S_m\left[1-\exp\left[-\frac{\Lambda_0}{S_m}(T-X)\right]\right]}^{S_1(X,T)}\frac{dS_1}{\Lambda_0(1-\frac{S_1}{S_m})\left[S_1-\frac{S_m\Lambda_1}{\Lambda_0}\ln(1-\frac{S_1}{S_m})\right]}=-X \tag{36}$$

$S_2(0,T)$ is calculated from Eq. (28) with $C=1$:

$$S_2(0,T)=\Lambda_1 T \tag{37}$$

Using Riemann invariant C/S (25) of system (26)–(28) and Eqs. (14), (36) allows calculating suspended concentration $C(X, T)$:

$$\frac{C(X,T)}{S_1(X,T) - \frac{S_m \Lambda_1}{\Lambda_0} \ln\left[1 - \frac{S_1(X,T)}{S_m}\right]} = \frac{1}{S_m\left[1 - \exp\left[-\frac{\Lambda_0}{S_m}(T-X)\right]\right] + \Lambda_1 (T-X)} \tag{38}$$

Both retained concentrations are zero along the concentration front $T_1(X) = X$. The suspended concentration behind the front $C^-(T, T)$ is calculated from Eq. (26):

$$C^-(T,T) = \exp\left[-\left(\Lambda_0 + \Lambda_1\right) T\right] \tag{39}$$

The solution shows that initial data are held ahead of the concentration front $T_1(X) = X$ (Fig. 5a). Behind the concentration front, the exact solution for $S_1(X, T)$ is expressed implicitly by transcendental Eq. (36), allowing for explicit calculation of S_2 using formula (14) and explicit calculation of $C(X, T)$ using formula (38).

Fig. 4a shows forms of aggregated filtration function (blue curve) and binary filtration function (red curve). Fig. 4b shows breakthrough concentrations $C(1, T)$ as obtained from the least square fit [43] by using the binary model (red curve), which is obtained for $\Lambda_0 = 0.2151$, $\Lambda_1 = 0.4780$ and $S_m = 0.5614$. The tuning data for this laboratory test and the coefficient of determination are presented in eighth row of Table 2. The blue curve corresponds to aggregated model with $S_m = 0.1164$. BTCs at $T = 1$ and their stabilised values are the same, so the filtration coefficients Λ_0 and Λ_1 are the same for both models.

Fig. 4c also shows the comparison between matching the laboratory data by the binary and aggregated models. The filtration coefficients for both models are $\Lambda_0 = 0.3318$ and $\Lambda_1 = 0.8557$. Maximum retained concentrations are $S_m = 0.4331$ and $S_m = 0.1005$ for binary and aggregated models, respectively. The tuning data for this laboratory test and the coefficient of determination are presented in fifth row of Table 2.

3.4. Properties of aggregated function for two capture mechanisms

Eq. (39) shows that suspended concentration at the breakthrough time $T = 1$ is equal to

$$C(1,1) = \exp\left(-\Lambda_0 - \Lambda_1\right) \tag{40}$$

Eq. (38) shows that at $T \to \infty$, suspended concentration tends to

$$C(1,\infty) = \exp\left(-\Lambda_1\right) \tag{41}$$

Formulae (40) and (41) allow determining both filtration coefficients from the breakthrough curve

$$\Lambda_1 = -\ln\left[C(1,\infty)\right] \tag{42}$$

$$\Lambda_0 = \ln\left[\frac{C(1,\infty)}{C(1,1)}\right] \tag{43}$$

The parameter S_m is determined by matching the BTC at intermediate times $[1,\infty)$.

Now let us describe some properties of the aggregated filtration function.

At $S = 0$, as it follows from Eqs. (27), (28),

$$\Lambda(0) = \Lambda_0 + \Lambda_1 \tag{44}$$

For large retention concentrations,

$$\lim_{S\to\infty} \Lambda(S) = \Lambda_1 \tag{45}$$

Lemma 2. *The aggregated filtration function is convex, i.e. $\Lambda''(S)>0$.*

The derivative of $\Lambda = \Lambda(S)$ is calculated from Eq. (16)

$$\frac{d\Lambda(S)}{dS} = -\frac{\Lambda_0}{S_m}\frac{dS_1(S)}{dS} \tag{46}$$

where

$$\frac{dS_1(S)}{dS} = \left(1 - \frac{S_m \Lambda_1}{\Lambda_0 S_m - \Lambda_0 S_1 + S_m \Lambda_1}\right) \tag{47}$$

Substituting Eq. (47) into Eq. (46) yields

$$\frac{d\Lambda(S)}{dS} = -\frac{\Lambda_0}{S_m}\left(1 - \frac{S_m \Lambda_1}{\Lambda_0 S_m - \Lambda_0 S_1 + S_m \Lambda_1}\right) \tag{48}$$

The second derivative can be calculated from Eq.(48)

$$\frac{d^2\Lambda(S)}{dS^2} = \frac{\Lambda_1 \Lambda_0^2}{\left(\Lambda_0 S_m - \Lambda_0 S_1 + \Lambda_1 S_m\right)^2}\frac{dS_1(S)}{dS} > 0 \tag{49}$$

Taking derivative of Eq. (15) shows that $dS/dS_1>0$, which proves the lemma.

Now we introduce the binary filtration function as a total of linear and constant filtration coefficient, as given in Eq. below:

$$\Lambda(S) = \begin{cases} \Lambda_0\left(1 - \frac{S}{S_m}\right) + \Lambda_1 & , S \le S_m \\ \Lambda_1 & , S > S_m \end{cases} \tag{50}$$

Lemma 3. *Let the aggregated and binary filtration functions have the same values of coefficients Λ_0, S_m and Λ_1. The aggregated filtration function is higher than the corresponding binary filtration function.*

Derivative of the aggregated function (16) is obtained from Eq. (48)

$$\left.\frac{d\Lambda(S)}{dS}\right|_{S=0} = -\frac{{\Lambda_0}^2}{S_m\left(\Lambda_0 + \Lambda_1\right)} \tag{51}$$

Derivative of the binary function (50) is:

$$\left.\frac{d\Lambda(S)}{dS}\right|_{S=0} = -\frac{\Lambda_0}{S_m} \tag{52}$$

Slope (52) is lower than slope (51). Therefore, the curve is located above the straight line at some neighbourhood of $S = 0$. The curve $\Lambda(S)$ is convex, so for all $S > 0$, curve is located above the straight line. The curve is located above horizontal straight line, $\Lambda(S) = \Lambda_1$, which proves the lemma.

Blue curve in Fig. 4a possesses the above mentioned properties.

3.5. Asymptotic formulae for aggregated filtration function

Consider the case of small filtration coefficient of Langmuir blocking function. Substituting $\varepsilon\Lambda_0$ instead of Λ_0 in Eqs. (50) and keeping zero and first terms in Taylor series yields the explicit formula

$$\Lambda(S) = \Lambda_1 + \varepsilon\Lambda_0 \tag{53}$$

Green and black curves in Fig. 8a correspond to $\varepsilon = 0.1$ and $\varepsilon = 0.3$. The forms of both filtration curves correspond to dominant straining. The corresponding BTC curves in Fig. 8b exhibit variation that has order of magnitude ε. The higher is the filtration coefficient Λ_0, the lower is the BTC.

Now consider the case of small constant filtration coefficient Λ_1. Substituting $\varepsilon\Lambda_1$ instead of Λ_1 in Eqs. (50) and keeping zero and first terms in Taylor series yields the explicit formula

$$\Lambda(S) = \Lambda_0\left(1 - \frac{S}{S_m}\right) + \varepsilon\Lambda_1\left[1 - \ln\left(1 - \frac{S}{S_m}\right)\right] \tag{54}$$

Red and blue curves in Fig. 8a correspond to $\varepsilon = 0.1$ and $\varepsilon = 0.3$. The declined intervals of the filtration curves correspond to attachment, while the stabilised intervals correspond to straining. The forms of both filtration curves show that attachment capture mechanism dominates.

4. Exact solutions for binary filtration function

In this section we derive the explicit formulae for solution for the case of binary filtration function (50).

Ahead of concentration front $X > T$ in zone 0, $C = S = 0$ (Fig. 5a).

Table 1
Fitted parameters from binary analytical model.

Porous media	r_p (μm)	r_s (μm)	C^0 (L^{-1})	Λ_1	Λ_0	S_m	T_m	T_{inj}	T_3	R^2
Glass beads	20	0.225	4.24×10^{11}	0.4155	0.0788	0.4531	0.9986	2.8186	2.5603	0.9168
		0.5	3.86×10^{10}	1.6869	0.2793	1.6987	0.9319	3.2511	6.3653	0.9506
		1	4.85×10^{9}	1.8209	0.7048	2.5257	1.1725	3.4887	9.3540	0.9492
Sand 70110	11.5	0.225	4.24×10^{11}	0.3696	0.4744	0.5376	0.9357	1.9538	2.5862	0.9657
		0.5	3.86×10^{10}	0.5108	0.5390	1.5146	2.0242	1.8827	5.0008	0.9950
		1	4.85×10^{9}	2.8276	–	–	–	1.8467	–	–
Sand 3550	27.5	0.225	4.24×10^{11}	0.1863	0.1162	0.2719	1.1343	1.7662	2.4332	0.9510
		0.5	3.86×10^{10}	0.1393	0.0839	0.1851	1.0401	1.7767	2.2387	0.8757
		1	4.85×10^{9}	1.5344	–	–	–	1.7873	–	–
Sand 2030	54.5	0.225	4.24×10^{11}	0.1508	0.0849	0.1879	0.9883	1.5921	2.1911	0.9572
		0.5	3.86×10^{10}	0.1924	–	–	–	1.5241	–	–
		1	4.85×10^{9}	0.6349	0.3327	0.7675	0.9720	1.7583	3.0440	0.8542

Table 2
Fitted parameters from binary analytical model — Injection time: $T_{inj} = 2.8$ PVI.

Porous media	r_p (μm)	r_s (μm)	C^0 (L^{-1})	γ (mM)	Λ_1	Λ_0	S_m	T_m	T_3	R^2
Glass beads	25.4	0.0315	3.6×10^{12}	20	0.1221	0.1263	0.2695	1.5146	2.8012	0.8725
			2.2×10^{12}	30	0.6636	0.2039	0.6212	0.8164	2.6980	0.9579
			5.8×10^{11}	33	2.0402	0.3677	2.4572	1.1073	10.167	0.8624
		0.16	6.6×10^{10}	20	0.0513	0.1844	0.0963	0.7964	1.8953	0.9190
			2.8×10^{10}	30	0.4780	0.2151	0.5614	0.9697	2.6895	0.8778
			1.7×10^{10}	40	1.2040	0.2231	1.4718	1.1215	4.9739	0.9003
			1×10^{10}	30	0.4080	0.3260	0.1931	0.3561	1.6001	0.8440
		1.5	5×10^{9}	100	0.8557	0.3318	0.4331	0.4277	2.1125	0.8537
			5.1×10^{9}	300	1.8326	0.3747	0.4407	0.2188	2.4819	0.7542

The potential Φ is calculated explicitly:

$$\Phi(S) = \frac{\Lambda_0}{S_m} \ln\left[\frac{\Lambda_0 + \Lambda_1}{\Lambda_0\left(1 - \frac{S}{S_m}\right) + \Lambda_1}\right] \tag{55}$$

It allows calculating retention concentration at the inlet:

$$S(0,T) = \begin{cases} \dfrac{\Lambda_0 + \Lambda_1}{\Lambda_0} S_m \\ \quad \times\left(1 - \exp\left(-\frac{\Lambda_0}{S_m} T\right)\right), & T < T_m = -\dfrac{S_m}{\Lambda_0} \ln\left(\dfrac{\Lambda_1}{\Lambda_0 + \Lambda_1}\right) \\ \Lambda_1 (T - T_m) + S_m & T < T_m \end{cases} \tag{56}$$

where T_m is a moment when retained concentration at the inlet reaches the value S_m.

The explicit solution in zone I is calculated by formulae (24), (56):

$$S(X,T) = \frac{S_m \frac{(\Lambda_0 + \Lambda_1)}{\Lambda_0}\left(1 - \exp\left[-\frac{\Lambda_0}{S_m}(T - X)\right]\right)}{\left[1 - \exp\left[-\frac{\Lambda_0}{S_m}(T - X)\right]\right] + \exp\left[\left(\Lambda_0 + \Lambda_1\right) X - \frac{\Lambda_0}{S_m}(T - X)\right]\Big]} \tag{57}$$

Suspended concentration is calculated from Riemann invariant (38) as:

$$C(X,T) = \left[1 - \exp\left[-\frac{\Lambda_0}{S_m}(T - X)\right] + \exp\left[\left(\Lambda_0 + \Lambda_1\right) X - \frac{\Lambda_0}{S_m}(T - X)\right]\right]^{-1} \tag{58}$$

In zone III where $S > S_m$, the filtration function is constant and equal to Λ_1. The solution is determined from Eqs. (24), (38), (56):

$$C(X,T) = \exp\left(-\Lambda_1 X\right) \tag{59}$$

$$S(X,T) = \left[\Lambda_1\left(T - X - T_m\right) + S_m\right] \exp\left(-\Lambda_1 X\right) \tag{60}$$

The front boundary of zone III, where $S = S_m$, is calculated from Eq. (60):

$$T = \frac{S_m}{\Lambda_1}\left[\exp\left(\Lambda_1 X\right) - 1\right] + X + T_m \tag{61}$$

The solution in zone II is determined by Eqs. (24), (38) along the characteristic straight lines with boundary condition $S = S_m$ at the moving boundary (61): Eqs. (62) and (63) are given in Box I. Fig. 5b and c show suspended and retained concentration profiles at five different moments. Profile at the moment t_1 before the breakthrough encompasses zones 0 and I. At the moment t_2 after the breakthrough, the profile corresponds to zone I. Moment t_3 represents zones III, II and I. Moment t_4 represents zones III and II, at the moment t_5 only zone III remains in the profile. Fig. 5c shows monotonic increase of retained concentration during accumulation according to retention rate (10). Monotonically decreasing filtration function (50) yields monotonic increase of suspended concentration (Fig. 5b).

5. Sensitivity study

Fig. 6a shows the sensitivity of the aggregated and binary filtration functions for two commingled capture mechanisms with respect to Λ_0 and Λ_1. Fig. 6b shows the corresponding BTCs. Continuous curves correspond to aggregated filtration function, while the results for binary filtration function are shown by dashed curves. Increase in Λ_1 yields increase of both filtration functions. Points $S = 0$ and $S \to \infty$ in Fig. 6a shift up by the values of Λ_1. Increase in Λ_0 also yields the increase in filtration functions, but the asymptotic values remain the same. The higher is the filtration function, the lower is the breakthrough concentration, so BTCs move down with increase of either Λ_0 or Λ_1.

Fig. 7a shows the behaviour of both filtration functions given for different S_m. Points $S = 0$ and $S \to \infty$ with changing S_m in Fig. 7a and points $T = 0$ and $T \to \infty$ *in Fig. 7b remain the same. The larger is the* S_m *the slower is the stabilisation of the filtration function at the value* $\Lambda(S) = \Lambda_1$ (Fig. 7b).

Fig. 8a presents sensitivity study of aggregated filtration function with small blocking (green and black curves) and small straining (red and blue curves) as calculated by formulae (53) and (54). Fig. 8b shows the corresponding BTCs. The higher is the filtration function, the lower is the BTC.

6. Comparison between exact and numerical solutions

Fig. 4b and c show the comparison between the exact and numerical solutions. The black dashed curves correspond to numerical solutions for the same values of the model coefficients that are obtained in

$$S(X,T) = \frac{S_m(\Lambda_0+\Lambda_1)}{\Lambda_1 \exp\left[(\Lambda_0+\Lambda_1)\left(X - \frac{1}{\Lambda_1}\ln\left[\frac{\Lambda_1}{S_m}(T-X-T_m)+1\right]\right)\right]+\Lambda_0} \tag{62}$$

$$C(X,T) = \frac{S_m(\Lambda_0+\Lambda_1)}{\left[\Lambda_1(T-X-T_m)+S_m\right]\left\{\Lambda_1 \exp\left[(\Lambda_0+\Lambda_1)\left(X - \frac{1}{\Lambda_1}\ln\left[\frac{\Lambda_1}{S_m}(T-X-T_m)+1\right]\right)\right]+\Lambda_0\right\}} \tag{63}$$

Box I.

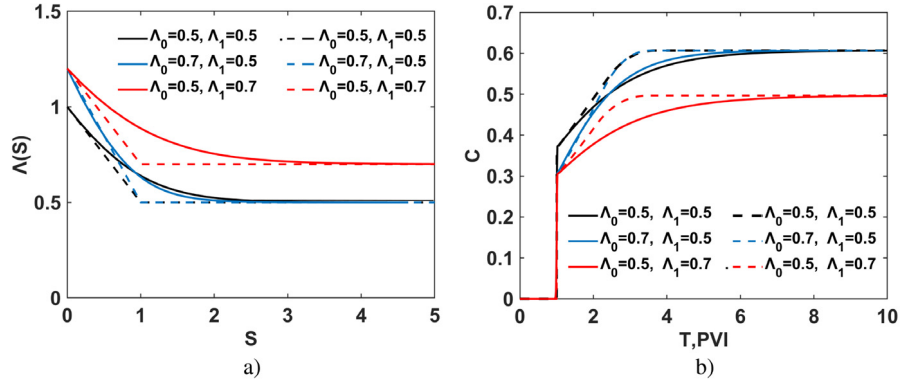

Fig. 6. Exact and approximate forms of filtration function for two simultaneous capture mechanisms and sensitivity analysis with respect to Λ_0, and Λ_1 where $S_m = 0.5$: (a) filtration functions; (b) breakthrough curves.

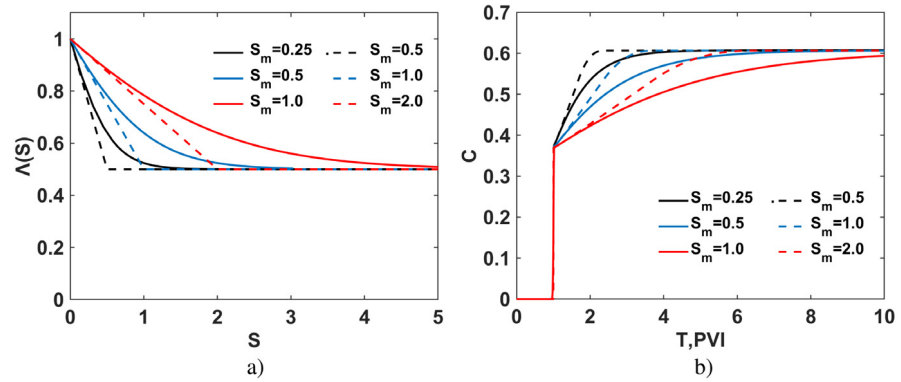

Fig. 7. Exact and approximate forms of filtration function for two simultaneous capture mechanisms and sensitivity analysis with respect to S_m where $\Lambda_0 = \Lambda_1 = 0.5$: (a) filtration functions; (b) breakthrough curves.

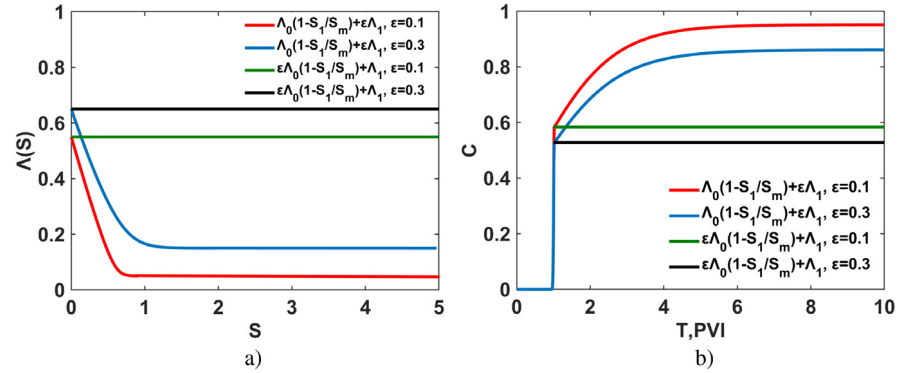

Fig. 8. Aggregated filtration function with small straining $\varepsilon\Lambda_1$ (red and blue curves for $\varepsilon = 0.1$ and $\varepsilon = 0.3$, respectively) and small attachment $\varepsilon\Lambda_0$ (green and black curves for $\varepsilon = 0.1$ and $\varepsilon = 0.3$, respectively) using asymptotic formulae for aggregation: (a) forms of filtration functions; (b) breakthrough curves. (For interpretation of the references to colour in this figure legend, the reader is referred to the web version of this article.)

Section 3.3 by matching the laboratory data using the binary and aggregated filtration functions.

The governing equations (26)–(28) subject to initial and boundary conditions (11), (12) were solved numerically using the Shampine's

software package [44,45]. The algorithm implements a two-step Lax–Friedrichs finite-difference method [45]. The Matlab computer program, and pertinent supporting information are available from http://faculty.smu.edu/shampine/current.html. The space and time steps employed in the finite-difference method are $\Delta X = 0.0001$, $\Delta T = 0.00009$. Numerical solutions for aggregated and binary filtration functions are given by black dashed curves.

The numerically and analytically calculated curves coincide.

7. Analysis of the results of laboratory data tuning

This section treats the laboratory data using the analytical model (57)–(63) for binary retention function. Calculations of electrostatic forces (using the DLVO theory, [10,19]) show that the particles are attracted to the rock surface.

The results of injection of particles with radii $r_s = 0.225$, 0.5, and 1.0 μm into porous media with pore radii $r_p = 20$, 11.5, 27.5, and 54.5 μm are shown in Fig. 9 [1]. Fig. 9a, d, g, and j present the results of injection of particles with radius $r_s = 0.225$ μm. Fig. 9b, e, h, and k present the results of injection of particles with radius $r_s = 0.5$ μm. Fig. 9c, f, i, and l present the results into pores with radius $r_s = 1$ μm. Table 1 presents the injected concentrations and the matching results using the analytical model for binary filtration function.

Fig. 10 shows the dependencies of three model parameters of jamming ratio

$$j = \frac{r_s}{r_p} \tag{64}$$

where r_s and r_p are the particle and pore radii, respectively.

Assume that Langmuir blocking function corresponds to monolayer attachment of particles, and the filtration coefficient Λ_1 is for straining. Fig. 10a, b, c, and d corresponds to four series of tests with different porous media. The larger are the particles, the stronger is the electrostatic particle–rock attachment, and the higher is the filtration coefficient Λ_0 [1,4,10]. The larger are the particles, the higher is the surface occupied by one particle, and the lower is the total concentration of attached particles that cover the overall rock surface. The larger are the particles, the higher is the jamming ratio, and the higher is the straining filtration coefficient Λ_1 [2,18,21].

Fig. 11 shows 9 tests with injection of particles with three different radii $r_s = 0.0315$ μm, $r_s = 0.16$ μm, and $r_s = 1.5$ μm in the same porous media with $r_p = 25.4$ μm [46]. Different salinities 20, 30, 33, 40, 100 and 300 are used. Fig. 12a, b and c corresponds to $r_s = 0.0315$ μm, $r_s = 0.16$ μm, and $r_s = 1.5$ μm, respectively.

The higher is the salinity the higher is the electrostatic grain-particle attraction, the higher is filtration coefficient Λ_1. The higher is the attraction, the more compact occupation of the rock surface occurs, and the higher is the S_m [1,4,46]. The same dependency of straining coefficient Λ_1 versus salinity takes place. It is explained by increasing attachment to pore throats with salinity increase, so the throats become thinner, jamming ratio decreases, and the filtration coefficient for straining increases [1,4,10,46].

The cases for $r_s = 0.16$ μm and $\gamma = 30$ mM, and $r_s = 1.5$ μm and $\gamma = 100$ mM have been treated by the aggregated model. Fig. 4b and c show the binary model by red curves, and blue curves correspond to aggregated model. The aggregated model presents more precise match than the binary model. The coefficient of determination R^2 is higher for the aggregated model for all the cases which have been calculated.

8. Chemical reactive flow with multiple reactions: aggregation, exact solution

The aggregation technique (Appendices A and B) and introduction of potential yielding an exact solution (Section 3.2) can be extended for the case of chemical reactive flow with multiple reactions between the fluid and multicomponent rock.

Mass balance for reacting fluid flowing through the multicomponent rock is

$$\phi \frac{\partial c}{\partial t} + U \frac{\partial c}{\partial x} = -\sum_k \frac{1}{n_k} \frac{\partial y_k}{\partial t} \tag{65}$$

where ϕ is the porosity, c is the molar concentration of reagent dissolved in the fluid, U is Darcy velocity, y_k is the molar concentration of kth component in the rock, n_k is the number of moles reacting with one molar of the fluid component (stoichiometric coefficient).

The reaction rate for kth component is

$$\frac{\partial y_k}{\partial t} = -K_{ak} c y_k^{n_k} \tag{66}$$

where K_{ak} is the kinetic coefficient.

Initial and boundary conditions corresponding to reacting fluid injection into porous media are:

$$t = 0 : y_k = y_{k0}, \quad c = 0 \tag{67}$$

$$x = 0 : c = c^0 \tag{68}$$

Adding Eq. (66) we obtain the expression for the total reaction rate

$$\frac{\partial y}{\partial t} = -c \sum_k K_{ak} y_k^{n_k} \tag{69}$$

For fixed x, Eq. (69) form system of n ODE for unknowns $y_k = y_k(t)$. Changing independent variable from t to y and performing chain differentiation in Eq. (69) yields a system of n ODE for unknowns $y_k = y_k(y)$

$$\frac{dy_k}{dy} = \frac{K_{ak} y_k^{n_k}}{\sum_k K_{ak} y_k^{n_k}} \tag{70}$$

As it follows from Eq. (67), initial conditions for system (70) are:

$$t = 0 : y_{k0}, \; y_0 = \sum_k y_{k0} \tag{71}$$

The solution of system (70) subject to initial conditions (71) is

$$y_k = y_k(y) \tag{72}$$

Calculations of mass balance follow from Eq. (65):

$$\phi \frac{\partial c}{\partial t} + U \frac{\partial c}{\partial x} = -\frac{\partial}{\partial t} \sum_k \frac{y_k(y)}{n_k} = -\frac{\partial G(y)}{\partial t}, \quad G(y) = \sum_k \frac{y_k(y)}{n_k} \tag{73}$$

Calculations of the total reactive rate follow from Eq. (69):

$$\frac{\partial y}{\partial t} = -c \sum_k K_{ak} y_k^{n_k}(y) = -c F(y), \quad F(y) = \sum_k K_{ak} y_k^{n_k}(y) \tag{74}$$

Finally, we obtain system of 2×2 partial differential equations

$$\phi \frac{\partial c}{\partial t} + U \frac{\partial c}{\partial x} = -\frac{\partial G(y)}{\partial t}, \frac{\partial y}{\partial t} = -c F(y) \tag{75}$$

with the following initial and boundary conditions

$$t = 0 : y_0 = \sum_k y_{k0}, \; c = 0$$
$$x = 1 : c = c^0 \tag{76}$$

The exact solution of the problem (75), (76) is obtained using the method of potential, presented in Section 3.2. Introduction of potential from Eq. (17), its substitution into Eq. (75) and integration in t reduces the system to one scalar hyperbolic equation. This equation is solved by method of characteristics, like in Section 3.2.

9. Summary and discussion

Nonlinear methods of aggregation and potential We derived exact solutions for several non-linear initial–boundary value problems corre-

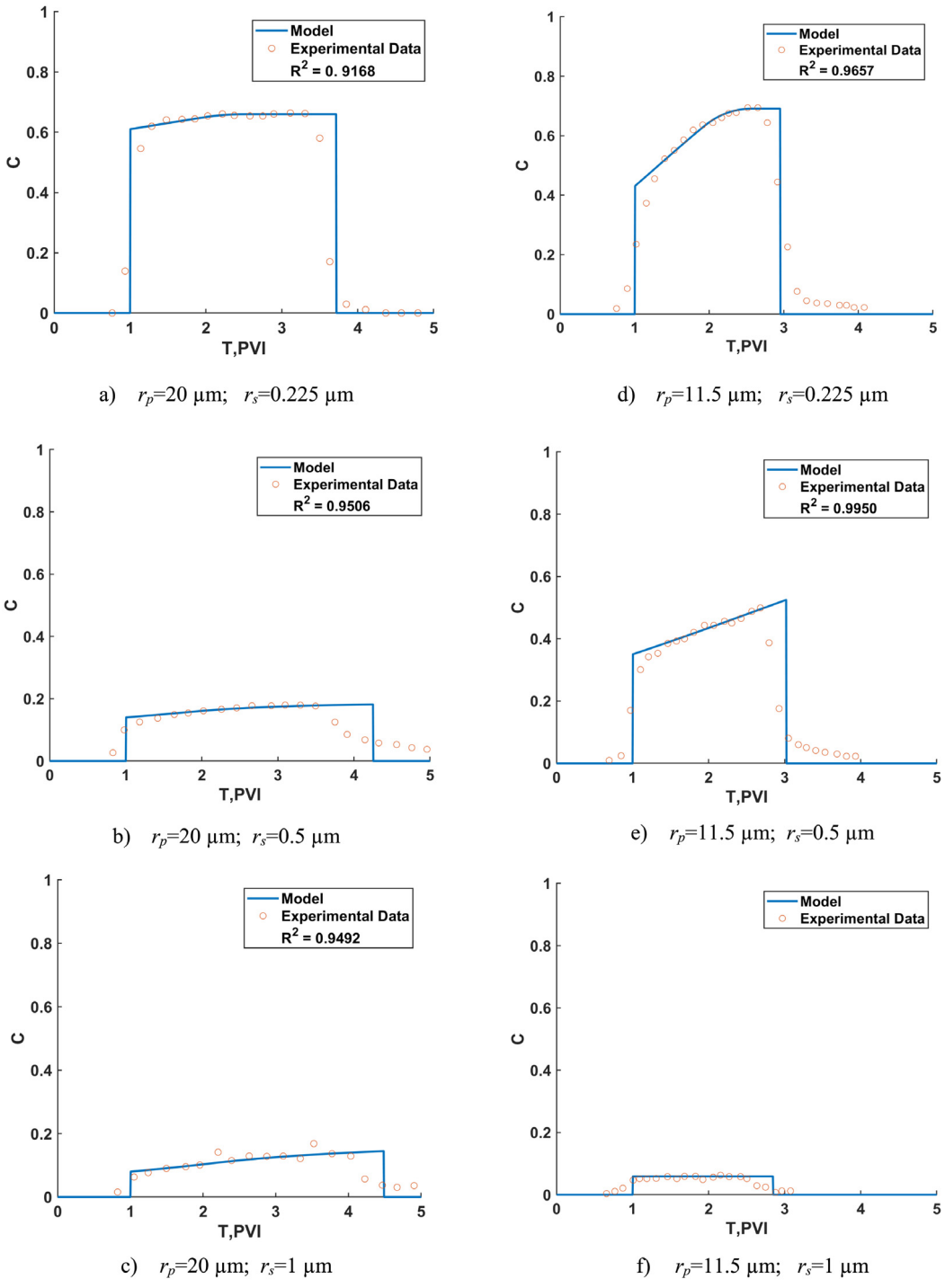

Fig. 9. Matching the breakthrough curves by the analytical model; the laboratory data are taken from paper [1].

sponding to two-capture deep be filtration. The solution process includes two developments:

1 – Introduction of a free variable, which is equal to the total retained concentration, instead of time, in n ODEs for capture kinetics (A.3) that yields the reduction of $(n+1) \times (n+1)$ classical advection–diffusion system (A.1)–(A.3) to 2×2 system (1), (2);

2 – Introduction of potential (17) that reduces 2×2 aggregated diffusion-free system (9), (10) to a scalar first order hyperbolic equation, where method of characteristics yields implicit solution (36) and explicit solution (57)–(63).

The first aggregation procedure is applied for a modified advection–diffusion system (1), (6), yielding its reduction to 2×2 system (1), (6).

The so-called aggregated procedure reduces system with n different particle capture mechanisms to a single-capture system. The binary filtration function is the approximation of the aggregated function, which is obtained for two capture mechanisms with constant and blocking (Langmuir) filtration functions.

In the case where of small retained concentrations and constant filtration functions, non-linear systems (A.1)–(A.3) and (A.1), (A.2), (B.1) degenerate into linear systems. The aggregation procedure degenerates

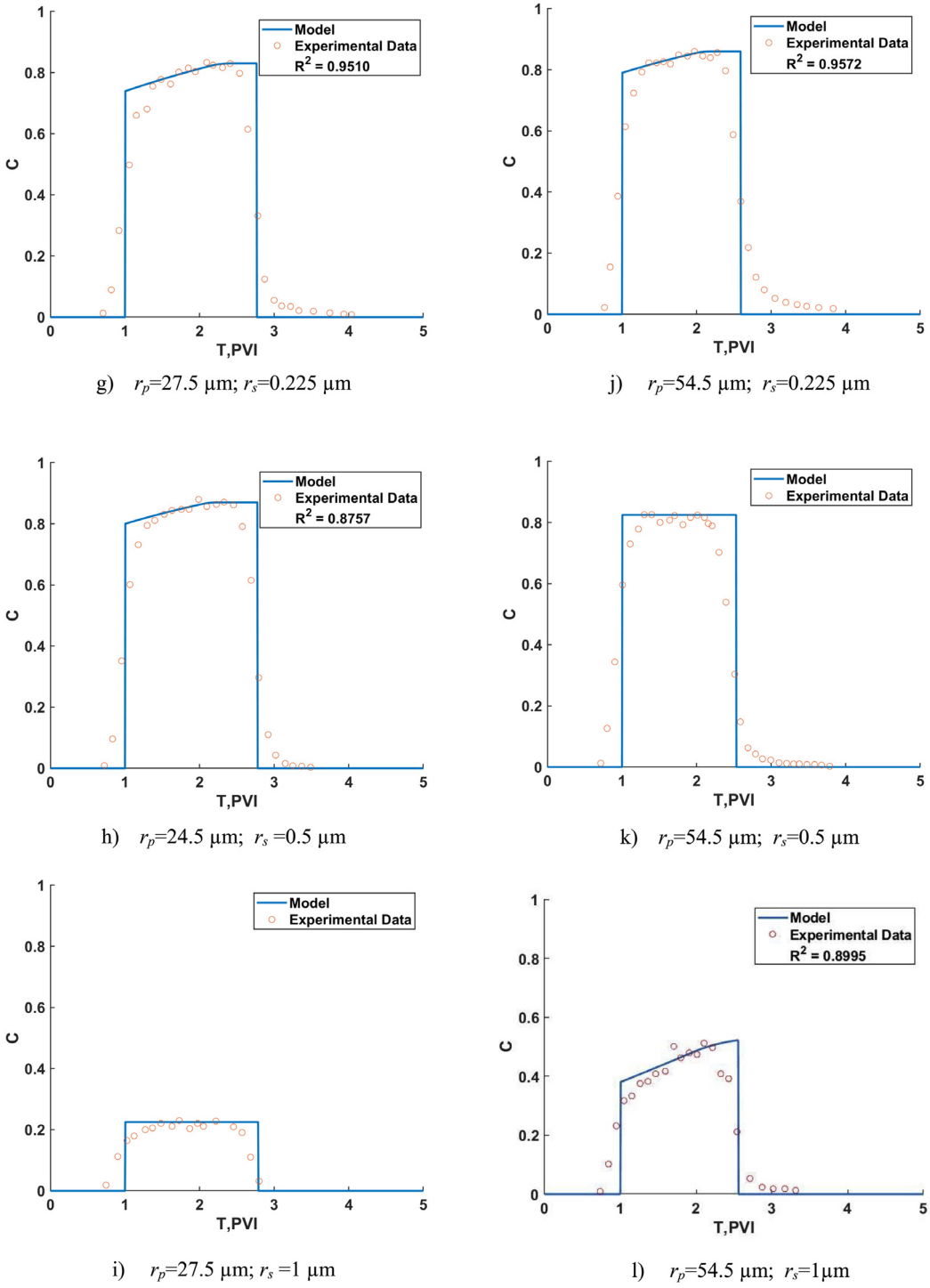

Fig. 9. (*continued*)

into the sum of individual filtration constants. The exact solutions of linear systems (1), (2), (A.1)–(A.3) and (A.1), (A.2), (B.1) exhibit steady state suspension concentration behind the front $T_1(X) = X$, and retained concentrations accumulating linearly with time. Even for two-capture system $n = 2$ with one varying filtration function, the system becomes non-linear, and the solution is significantly more complex.

Matching of BTCs with constant concentration by constant filtration function, and BTCs with concentration monotonically increasing up to the injected concentration, is widely applied in suspension-colloidal studies [1,4,10,46]. The exact solutions derived show that both aggregated and binary filtration functions exhibit BTCs where concentration monotonically increases up to the value that is lower than the injected concentrations; this type of BTCs is also widely spread for suspension-colloidal systems [1,13,22,46].

The exact solution for binary filtration function (Eqs. (57)–(63)) contains explicit formulae only, which is an advantage for tuning the

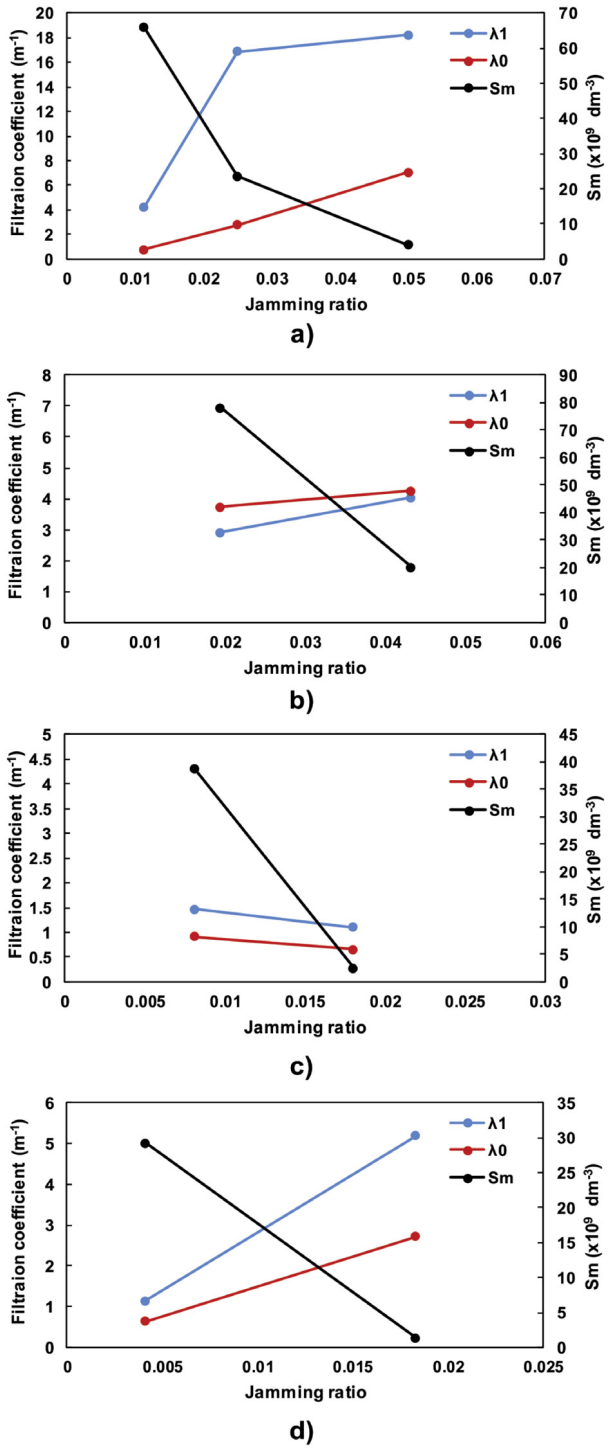

Fig. 10. Jamming-ratio dependency for the dimensional filtration coefficients and maximum retained particle concentration: (a) Glass breads (r_p = 20 μm); (b) Sand 70 110 (r_p = 11.5 μm); (c) Sand 3550 (r_p = 27.5 μm); (d) Sand 2030 (r_p = 54.5 μm) [1].

laboratory data, and also for 3D modelling using streamline simulators. The exact solution for aggregated filtration function contains implicit integral expressions.

Both binary and aggregated filtrations functions are fully determined by three constants: the initial attachment filtration coefficient Λ_0, maximum concentration for attachment vacancies S_m, and the filtration coefficient for size exclusion Λ_1. The total of Λ_0 and Λ_1 can be determined directly from the breakthrough concentration at the arrival time of 1PVI. The filtration coefficient for size exclusion Λ_1 can be determined directly from the stabilised breakthrough concentration with time tending to infinity. The maximum concentration for attachment vacancies must is determined by matching of the intermediate values of breakthrough concentrations.

The values Λ_0, Λ_1 and S_m as obtained from tuning the binary filtration function, can be used as initial value for tuning the exact aggregation function using minimisation least square iterative algorithm [43]. The overall calculations with minimisation using the exact aggregated function and software Shampaine is about 2 h, while the procedure using the piecewise-linear binary function takes about 1 min only. Moreover, sometimes the minimisation procedure after matching by the binary filtration function is not necessary. In the cases of r_s = 0.16 μm and γ = 30 mM, and r_s = 1.5 μm and γ = 100 mM, the minimisation provides only 7%–10% improvement, respectively, reducing coefficient of determination from R^2 = 0.9754 to R^2 = 0.8778, and R^2 = 0.9153 to R^2 = 0.8537.

The model validity Main purposes of matching the experimental results are prediction of the laboratory data for planning of the new tests, and the laboratory-based prediction of 3D reservoir behaviour. For both purposes, both aggregated and binary models match the laboratory data with high accuracy.

However, the aggregated model is derived from first principles, while the binary model is its approximation. The laboratory tests have been treated by both aggregated and binary models. The coefficient of determination R^2 is always higher for the aggregated model (Fig. 4b, c). This fact supports the validity of the aggregated model.

Applications The aggregation method (Lemma 1 in Section 2) and introduction of potential (18) yield exact solutions for numerous 1D suspension-colloidal transport processes in porous media.

Initial and boundary conditions (11), (12) correspond to injection of suspensions and colloids into clean bed. In exact solutions for non-zero initial retained concentration S_I, the value S_I adds to the clean-bed solution given by Eqs. (36) and (62).

Migration of natural reservoir fines corresponds to initial and boundary conditions

$$t = 0 : c_i = c_i^0,\ \sigma = 0, x = 0 : c_i = 0 \tag{77}$$

The aggregated Lemma 1 is fulfilled for the problem (1)–(3) and (77); the solution method is the same as that developed in Sections 3.3 and 4.

For the sake of simplicity, the Langmuir blocking function is attributed to attachment, and constant filtration function to straining. However, upscaling the transport of mono-sized suspensions in porous media with bimodal pore size distribution with straining yields the blocking Langmuir filtration function. Any of capture mechanisms with small retention corresponds to constant retention function [12] (Fig. 1).

Multiplying the flux U by the drift delay factor α in Eqs. (1), (2) and (A.1), (A.2) allows reflecting the phenomena of slow fines drift and rolling along the rock surface [39,47,48]. The translation $t \to \alpha t$ and rearranging dimensionless parameters reduces the problems to the original forms.

The aggregation method and introduction of the potential can be applied to suspension-colloidal flows of large particles with non-linear terms of changing porosity and flux in Eqs. (1), (2) and (A.1), (A.2) [7,22].

10. Conclusions

Derivation of exact solutions for non-linear 1D problems of suspension-colloidal transport in porous media with multiple capture

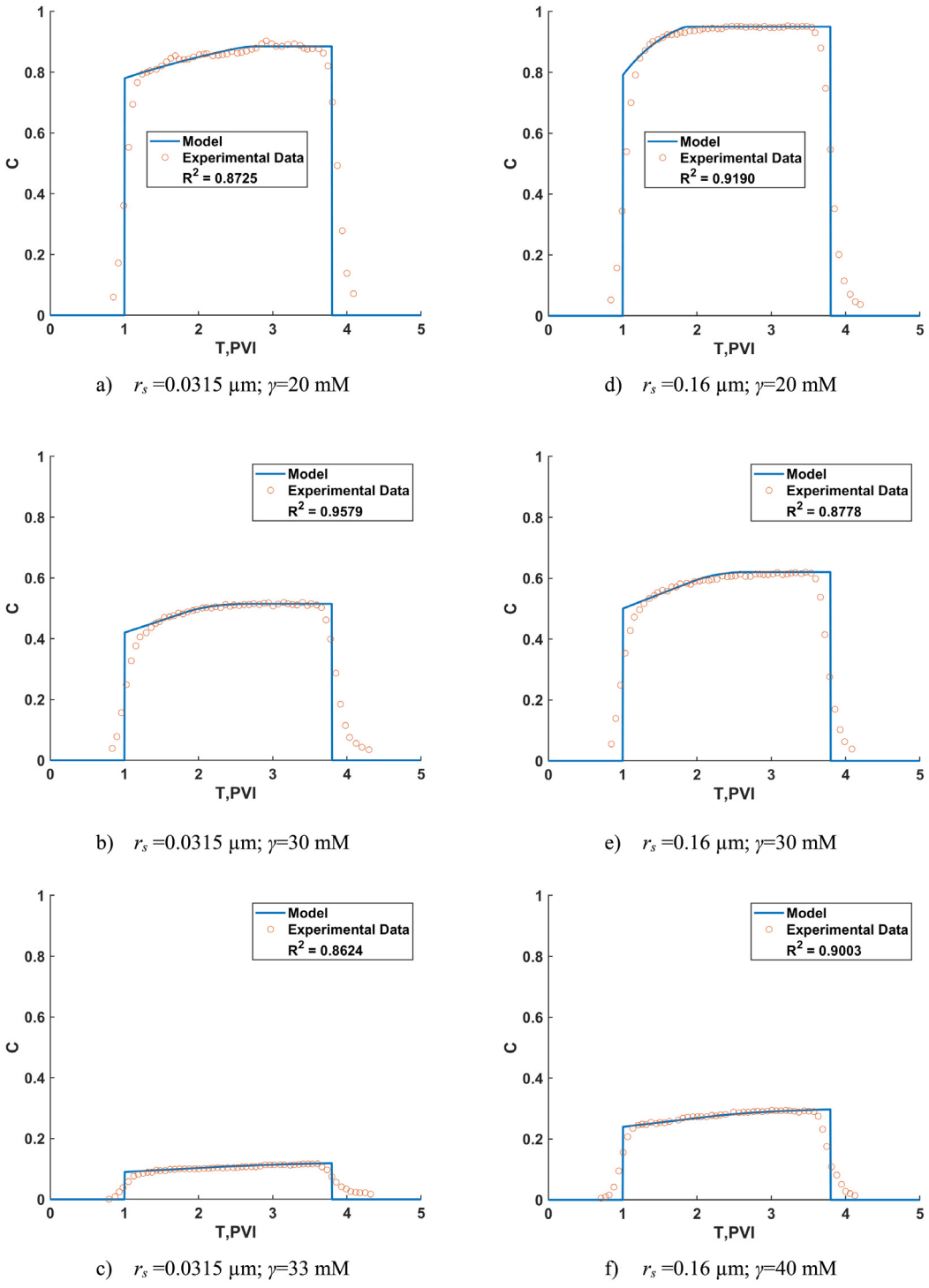

Fig. 11. Matching the breakthrough curves by the analytical model; the laboratory data are taken from paper [46].

mechanisms and development of the aggregation technique to reduce the multi-capture to single capture mechanism allow drawing the following conclusions:

System of $n+1$ PDEs for colloidal-suspension advective–diffusive transport with n particle capture mechanisms is equivalent to the 2×2 system with single capture. The aggregated filtration function is obtained by solution of n non-linear ODEs.

The exact solutions are obtained for both aggregated model and its piecewise-linear approximation (so-called binary model).

The solution for binary model is expressed by explicit formulae for suspended and retained concentrations, while that for aggregated model contains one transcendental equation with integral terms.

Both exact solutions exhibit BTCs with monotonic growth during several PVIs with further stabilisation at concentration that is lower than the injected concentration.

Both aggregated and binary models are determined by three constants – filtration coefficients Λ_0 and Λ_1, and maximum attachment

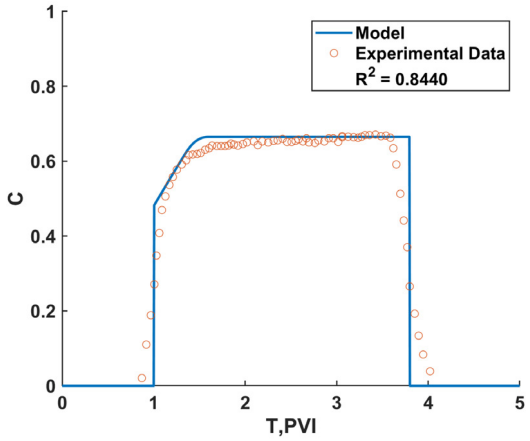

g) r_s =1.5 μm; γ=30 mM

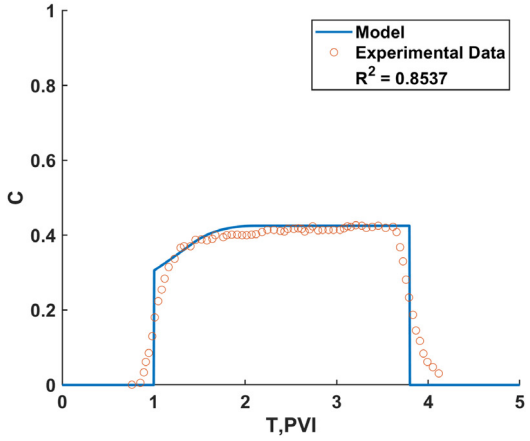

h) r_s =1.5 μm; γ=100 mM

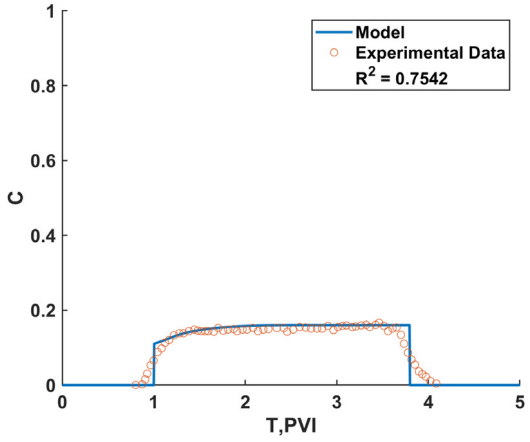

i) r_s =1.5 μm; γ=300 mM

Fig. 11. (*continued*)

capacity S_m. The filtration functions for both models take the same values at $S = 0$ and S tending to infinity. The corresponding BTCs also take the same values at the breakthrough moment $T = 1$ and at T tending to infinity. The aggregated function always exceeds the binary function, so BTC for aggregated function always lays below than that for the binary function.

The filtration coefficients Λ_0 and Λ_1 for both filtration functions are determined from stabilised BT concentration, and from the BT

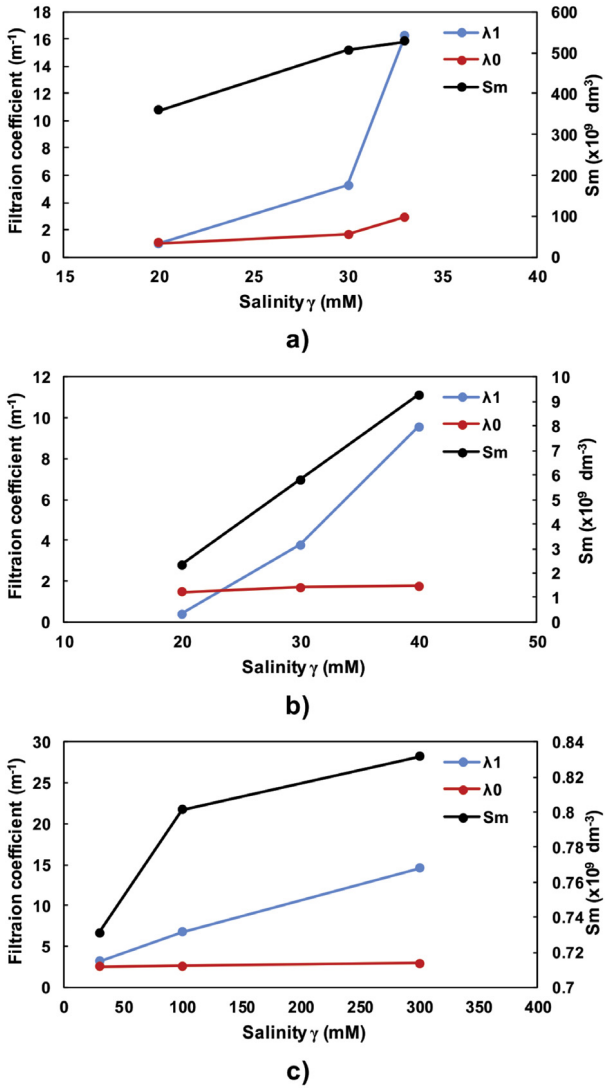

Fig. 12. Salinity dependency for the dimensional filtration coefficients and maximum retained particle concentration: (a) 0.0315 μm; (b) 0.16 μm; (c) 1.5 μm for Salinity vs. parameters [46].

concentration at the moment $T = 1$, leaving just one parameter S_m to be adjusted from the intermediate values of the BTC.

High accuracy of matching allows validating the interpretation of BTCs stabilising at lower value than injected concentration, by the model with binary filtration function.

Matching of numerous laboratory tests yields higher accuracy by the aggregated model than by the binary model.

The tuned model coefficients for different jamming ratios and salinities exhibit the same behaviour as that predicted by the theory of suspension-colloidal transport in porous media.

Appendix A. Proof of the aggregation lemma for multi-capture filtration with particle dispersion

This Appendix shows that colloidal-suspended system (1)–(3) of multiple-capture $(n+1) \times (n+1)$ can be reduced into the 2×2 system by a by the aggregation of n filtration coefficients into a single coefficient. The aggregated filtration coefficient can be expressed in term of the total retained concentration.

The $(n+1) \times (n+1)$ system of governing equation with advection and dispersion transport mechanisms consists of mass balance for suspended and retained particles [10,18,19]:

$$\frac{\partial}{\partial t}(c\phi + \sum_{i=1}^{n} \sigma_i) + \frac{\partial q}{\partial x} = 0 \tag{A.1}$$

$$q = cU - D\frac{\partial c}{\partial x} \tag{A.2}$$

and rate equations for n particle capture mechanisms

$$\frac{\partial \sigma_i}{\partial t} = \lambda_i\left(\sigma_1, \sigma_2 \cdots \sigma_n\right) cU, i = 1, 2 \cdots n \tag{A.3}$$

The sum of n kinetics (A.3) leads to the total particle capture rate,

$$\frac{\partial \sigma}{\partial t} = \sum_{i=1}^{n} \frac{\partial \sigma_i}{\partial t} = \left(\sum_{i=1}^{n} \lambda_i(\sigma_1, \sigma_2 \cdots \sigma_n)\right) cU \tag{A.4}$$

The total filtration coefficient is an algebraic sum of all filtration coefficients, which depends on all retained particle concentrations

$$\lambda(\sigma_1, \sigma_2 \cdots \sigma_n) = \sum_{i=1}^{n} \lambda_i(\sigma_1, \sigma_2 \cdots \sigma_n) \tag{A.5}$$

The total retained concentration is

$$\sigma = \sum_{i=1}^{n} \sigma_i \tag{A.6}$$

Fixing $x = x_0$ and assuming that $c\,(x, t)$ is already knows, yields a system of ordinary differential equations for retained concentrations

$$\frac{d\sigma_i}{dt} = \lambda_i(\sigma_1, \sigma_2 \cdots \sigma_n) cU \tag{A.7}$$

Time derivative of total retained concentration becomes

$$\frac{d\sigma}{dt} = \sum_{i=1}^{n} \frac{d\sigma_i}{dt} = \left(\sum_{i=1}^{n} \lambda_i(\sigma_1, \sigma_2 \cdots \sigma_n)\right) cU \tag{A.8}$$

Change independent variable in system (A.8) from t to σ:

$$\frac{d\sigma_i}{d\sigma} = \frac{d\sigma_i}{dt}\frac{dt}{d\sigma} = \frac{d\sigma_i}{dt} \Big/ \frac{d\sigma}{dt} = \frac{\lambda_i(\sigma_1, \sigma_2 \cdots \sigma_n)}{\left[\sum_{i=1}^{n} \lambda_i(\sigma_1, \sigma_2 \cdots \sigma_n)\right]} \tag{A.9}$$

Initial condition for system (A.9) follows from initial conditions (11) for each retained concentration:

$$\sigma = 0 : \sigma_i = 0, i = 1, 2 \ldots n \tag{A.10}$$

Substituting the solution of ODEs (A.9) subject to initial condition (A.10) into Eq. (A.5) allows expressing the aggregated filtration coefficient versus total retained concentration,

$$\lambda(\sigma) = \sum_{i=1}^{n} \lambda_i(\sigma_1(\sigma), \sigma_2(\sigma) \cdots \sigma_n(\sigma)) \tag{A.11}$$

Substituting Eq. (A.11) into (A.8) reduces system with n capture mechanisms (A.3) to a single capture system (1)–(3).

Appendix B. Proof of the aggregation lemma for multi-capture filtration in the modified dispersion model

This Appendix proves that the colloidal-suspension flow with n capture mechanisms can be reduced to a single-capture system (1), (3), (4) for the case of so-called modified system of DBF, where the capture rate is proportional to the overall particle flux [8,13,17]:

$$\frac{\partial \sigma_i}{\partial t} = \lambda_i\left(\sigma_1, \sigma_2 \cdots \sigma_n\right) q, i = 1, 2 \cdots n \tag{B.1}$$

Mass balance equation (A.1) and the total flux expression (A.2) close system for $n+1$ unknowns c, σ_1, $\sigma_2 \ldots \sigma_n$.

Eqs. (A.5), (A.6) hold for modified system (A.1), (A.2), (B.1).

Fixing $x = x_0$ and assuming that flux $q\,(x, t)$ is already knows, yields a system of ordinary differential equations for retained concentrations

$$\frac{d\sigma_i}{dt} = \lambda_i(\sigma_1, \sigma_2 \cdots \sigma_n) q \tag{B.2}$$

Time derivative of total retained concentration becomes

$$\frac{d\sigma}{dt} = \sum_{i=1}^{n} \frac{d\sigma_i}{dt} = \left(\sum_{i=1}^{n} \lambda_i(\sigma_1, \sigma_2 \cdots \sigma_n) \right) q \tag{B.3}$$

Change independent variable in system (B.3) from t to σ yields the same aggregated Eqs. (A.9) and (A.11).

Substituting Eqs. (A.6), (A.11) into system with n capture mechanisms (A.1), (A.2), (B.1) reduces this system to a single capture system (1), (4), (3).

References

[1] S.A. Bradford, S.R. Yates, M. Bettahar, J. Simunek, Physical factors affecting the transport and fate of colloids in saturated porous media, Water Resour. Res. 38 (2002).

[2] D. Mikhailov, V. Zhvick, N. Ryzhikov, V. Shako, Modeling of Rock Permeability Damage and Repairing Dynamics Due to Invasion and Removal of Particulate from Drilling Fluids, Transp. Porous Media 121 (2018) 37–67.

[3] N.P. Sotirelis, C.V. Chrysikopoulos, Heteroaggregation of graphene oxide nanoparticles and kaolinite colloids, Sci. Total Environ. 579 (2017) 736–744.

[4] S.A. Bradford, S. Torkzaban, A. Shapiro, A theoretical analysis of colloid attachment and straining in chemically heterogeneous porous media, Langmuir 29 (2013) 6944–6952.

[5] C.V. Chrysikopoulos, N.P. Sotirelis, N.G. Kallithrakas-Kontos, Cotransport of graphene oxide nanoparticles and kaolinite colloids in porous media, Transp. Porous Media 119 (2017) 181–204.

[6] V.E. Katzourakis, C.V. Chrysikopoulos, Modeling dense-colloid and virus cotransport in three-dimensional porous media, J. Contam. Hydrol. 181 (2015) 102–113.

[7] P. Bedrikovetsky, Upscaling of stochastic micro model for suspension transport in porous media, Transp. Porous Media 75 (2008) 335–369.

[8] X. Chen, B. Bai, Experimental investigation and modeling of particulate transportation and deposition in vertical and horizontal flows, Hydrogeol. J. 23 (2015) 365–375.

[9] L. Chequer, T. Russell, A. Behr, L. Genolet, P. Kowollik, A. Badalyan, A. Zeinijahromi, P. Bedrikovetsky, Non-monotonic permeability variation during colloidal transport: governing equations and analytical model, J. Hydrol. (2017).

[10] M. Elimelech, J. Gregory, X. Jia, Particle Deposition and Aggregation: Measurement, Modelling and Simulation, Butterworth-Heinemann, 2013.

[11] V.E. Katzourakis, C.V. Chrysikopoulos, Mathematical modeling of colloid and virus cotransport in porous media: Application to experimental data, Adv. Water Resour. 68 (2014) 62–73.

[12] R.G. Guedes, F.A. Al-Abduwani, P.G. Bedrikovetsky, P.K. Currie, Injectivity decline under multiple particle capture mechanisms, in: SPE International Symposium and Exhibition on Formation Damage Control, Society of Petroleum Engineers, 2006.

[13] B. Bai, T. Xu, H. Li, The semi-analytical solution of particle transport in porous media induced by seepage, Feb-Fresenius Environ. Bull. (2017) 6286.

[14] P. Bedrikovetsky, Mathematical Theory of Oil and Gas Recovery: With Applications to Ex-USSR Oil and Gas Fields, Springer Science & Business Media, 2013.

[15] A.D. Polyanin, A.V. Manzhirov, HandBook of Mathematics for Engineers and Scientists, CRC Press, 2006.

[16] A. Polyanin, V. Zaitsev, HandBook of Nonlinear Partial Differential Equations, Chapman & Hall/CRC Press, Boca Raton, 2012.

[17] P. Bedrikovetsky, A. Siqueira, A. de Souza, F. Shecaira, Correction of basic equations for deep bed filtration with dispersion, J. Pet. Sci. Eng. 51 (2006) 68–84.

[18] J. Herzig, D. Leclerc, P.L. Goff, Flow of suspensions through porous media—application to deep filtration, Ind. Eng. Chem. 62 (1970) 8–35.

[19] K.C. Khilar, H.S. Fogler, Migrations of Fines in Porous Media, Springer Science & Business Media, 1998.

[20] A.D. Polyanin, A.I. Zhurov, Non-linear instability and exact solutions to some delay reaction–diffusion systems, Int. J. Non-Linear Mech. 62 (2014) 33–40.

[21] M. Mirabolghasemi, M. Prodanović, D. DiCarlo, H. Ji, Prediction of empirical properties using direct pore-scale simulation of straining through 3D microtomography images of porous media, J. Hydrol. 529 (2015) 768–778.

[22] J.A. Araújo, A. Santos, Analytic model for DBF under multiple particle retention mechanisms, Transp. Porous Media 97 (2013) 135–145.

[23] L.I. Kuzmina, Y.V. Osipov, Particle transportation at the filter inlet, Int. J. Comput. Civil Struct. Eng. 10 (2014) 17–22.

[24] A.A. Shapiro, Elliptic equation for random walks. Application to transport in microporous media, Physica A 375 (2007) 81–96.

[25] H. Yuan, A. Shapiro, Colloid transport and retention: recent advances in colloids filtration theory, in: Colloids: Classification, Properties and Applications, Nova Science Publishers, Incorporated, 2012.

[26] A. Shapiro, J. Wesselingh, Gas transport in tight porous media: gas kinetic approach, Chem. Eng. J. 142 (2008) 14–22.

[27] H. Yuan, A.A. Shapiro, Modeling non-Fickian transport and hyperexponential deposition for deep bed filtration, Chem. Eng. J. 162 (2010) 974–988.

[28] M. Sharma, Y. Yortsos, Transport of particulate suspensions in porous media: model formulation, AIChE J. 33 (1987) 1636–1643.

[29] M. Sharma, Y. Yortsos, Fines migration in porous media, AIChE J. 33 (1987) 1654–1662.

[30] A. Santos, P. Bedrikovetsky, A stochastic model for particulate suspension flow in porous media, Transp. Porous Media 62 (2006) 23–53.

[31] A.C. Alvarez, G. Hime, D. Marchesin, P.G. Bedrikovetsky, The inverse problem of determining the filtration function and permeability reduction in flow of water with particles in porous media, Transp. Porous Media 70 (2007) 43–62.

[32] M. Hayek, G. Kosakowski, A. Jakob, S.V. Churakov, A class of analytical solutions for multidimensional multispecies diffusive transport coupled with precipitation-dissolution reactions and porosity changes, Water Resour. Res. 48 (2012).

[33] M. Hayek, Exact solutions for one-dimensional transient gas flow in porous media with gravity and Klinkenberg effects, Transp. Porous Media 107 (2015) 403–417.

[34] A.D. Polyanin, A.I. Zhurov, Exact solutions of linear and non-linear differential-difference heat and diffusion equations with finite relaxation time, Int. J. Non-Linear Mech. 54 (2013) 115–126.

[35] K. Sorbie, A. Stamatiou, Analytical solutions of a one-dimensional linear model describing scale inhibitor precipitation treatments, Transp. Porous Media (2018) 1–17.

[36] B. Yuan, R.G. Moghanloo, Analytical model of well injectivity improvement using nanofluid preflush, Fuel 202 (2017) 380–394.

[37] B. Yuan, W. Wang, Using nanofluids to control fines migration for oil recovery: Nanofluids co-injection or nanofluids pre-flush?-A comprehensive answer, Fuel 215 (2018) 474–483.

[38] L.I. Kuzmina, Y.V. Osipov, Asymptotic solution for deep bed filtration with small deposit, Procedia Eng. 111 (2015) 491–494.

[39] H. Yuan, A.A. Shapiro, A mathematical model for non-monotonic deposition profiles in deep bed filtration systems, Chem. Eng. J. 166 (2011) 105–115.

[40] L.I. Kuzmina, Y.V. Osipov, Y.P. Galaguz, A model of two-velocity particles transport in a porous medium, Internat. J. Non-Linear Mech. 93 (2017) 1–6.

[41] L.I. Kuzmina, Y.V. Osipov, Y.G. Zheglova, Analytical model for deep bed filtration with multiple mechanisms of particle capture, Int. J. Non-Linear Mech. (2018).

[42] A. Alvarez, P. Bedrikovetsky, G. Hime, A. Marchesin, D. Marchesin, J. Rodrigues, A fast inverse solver for the filtration function for flow of water with particles in porous media, Inverse Problems 22 (2005) 69.

[43] T.F. Coleman, Y. Li, An interior trust region approach for nonlinear minimization subject to bounds, SIAM J. Optim. 6 (1996) 418–445.

[44] L. Shampine, Solving hyperbolic PDEs in MATLAB, Appl. Numer. Anal. Comput. Math. 2 (2005) 346–358.

[45] L.F. Shampine, Two-step Lax–Friedrichs method, Appl. Math. Lett. 18 (2005) 1134–1136.

[46] N. Tufenkji, M. Elimelech, Breakdown of colloid filtration theory: Role of the secondary energy minimum and surface charge heterogeneities, Langmuir 21 (2005) 841–852.

[47] N. Sefrioui, A. Ahmadi, A. Omari, H. Bertin, Numerical simulation of retention and release of colloids in porous media at the pore scale, Colloids Surf. A 427 (2013) 33–40.

[48] Y. Yang, F.D. Siqueira, A.S. Vaz, Z. You, P. Bedrikovetsky, Slow migration of detached fine particles over rock surface in porous media, J. Nat. Gas Sci. Eng. 34 (2016) 1159–1173.

4 Cotransport of Suspended Colloids and Nanoparticles in Porous Media

G. Malgaresi, H. Zhang, C.V. Chrysikopoulos, and P. Bedrikovetsky

Statement of Authorship

Title of Paper	Cotransport of suspended colloids and nanoparticles in porous media
Publication Status	☐ Published ☐ Accepted for Publication ☑ Submitted for Publication ☐ Unpublished and Unsubmitted w ork w ritten in manuscript style
Publication Details	G. V. C. Malgaresi, H. Zhang, C.V. Chrysikopoulos, and P. Bedrikovetsky. Cotransport of suspended colloids and nanoparticles in porous media. Submitted to Transport in Porous Media.

Author Contributions

Name of Principal Author	Gabriel Malgaresi
Contribution to the Paper	Derivation of the mathematical model for co-transport, tuned laboratory data, finished DLVO calculations and gave an explanation for experiment result
Signature	Date 23/10/2018.

Name of Co-Author (Candidate)	Hao Zhang
Contribution to the Paper	Derivation of the mathematical model and exact solution for single population transport, tuned laboratory data. helped in interpretation for model result
Overall percentage (%)	40%
Signature	Date 22/10/2018

Name of Co-Author	Chrysikopoulos
Contribution to the Paper	Helped in explanations of laboratory tests and manuscript evaluation
Signature	Date 25/10/2018

Name of Co-Author	Pavel Bedrikovetsky
Contribution to the Paper	Supervised development of the whole work.
Signature	Date 23/10/2018

Statement of Authorship

Title of Paper	Cotransport of suspended colloids and nanoparticles in porous media
Publication Status	☐ Published ☐ Accepted for Publication ☑ Submitted for Publication ☐ Unpublished and Unsubmitted w ork w ritten in manuscript style
Publication Details	G. V. C. Malgaresi, H. Zhang, C.V. Chrysikopoulos, and P. Bedrikovetsky. Cotransport of suspended colloids and nanoparticles in porous media. Submitted to Transport in Porous Media.

Author Contributions

Name of Principal Author	Gabriel Malgaresi
Contribution to the Paper	Derivation of the mathematical model for co-transport, tuned laboratory data, finished DLVO calculations and gave an explanation for experiment result
Signature	Date 23/10/2018.

Name of Co-Author (Candidate)	Hao Zhang
Contribution to the Paper	Derivation of the mathematical model and exact solution for single population transport, tuned laboratory data. helped in interpretation for model result
Overall percentage (%)	40%
Signature	Date 22/10/2018

Name of Co-Author	Chrysikopoulos
Contribution to the Paper	Helped in explanations of laboratory tests and manuscript evaluation
Signature	Date 23/10/2018

Name of Co-Author	Pavel Bedrikovetsky
Contribution to the Paper	Supervised development of the whole work.
Signature	Date 23/10/2018

Cotransport of suspended colloids and nanoparticles in porous media

G. V. C. Malgaresi[1], H. Zhang[1], C.V. Chrysikopoulos[2], and P. Bedrikovetsky[1]

[1]Australian School of Petroleum, University of Adelaide, Australia

[2]School of Environmental Engineering, Technical University of Crete, Greece

Abstract The objective of this study is to develop a model for transport and cotransport of colloids and nanoparticles (NPs) in porous media. The particle capture rate is proportional to the capture probability, which is a function of retained concentration, called the filtration function. Laboratory bench scale experiments of individual transport of NPs and colloidal-size kaolinite-clay particles through packed columns produced breakthrough curves (BTCs) that monotonically increased with time and stabilized at some value lower than the injected concentration. We propose the filtration function that corresponds to breakthrough curves stabilising at the concentration lower than the injected value. This so-called binary filtration function incorporates two Langmuir and low-retention capture mechanisms. A novel, analytical model for one-dimensional (1D) transport with a binary filtration function was developed. The analytical transport model was capable to fit successfully BTCs obtained from individual transport experiments using kaolinite and NPs conducted by Chrysikopoulos et al. (2017). Assuming that the electrostatic particle-solid matrix interaction and the fraction of the solid matrix surface area occupied by a single attached particle (kaolinite or NP) are the same for individual transport of either kaolinite particles or NPs and for simultaneous cotransport of kaolinite particles and NPs, the proposed binary filtration function was extended for the cotransport case. Despite the breakthrough data from cotransport experiments with kaolinite particles and NPs have six degrees of freedom, the developed cotransport model successfully matches the BTCs by tuning two constants only. This validates the developed model for cotransport of two colloidal populations with different attachment and straining rates.

Index

c	Suspended concentration [ML^{-3}]
C	Normalized suspended concentration [-]
k	Permeability [L^2]
s	Retained concentration [ML^{-3}]
s_m	Maximum attached concentration [ML^{-3}]
S	Normalized retained concentration [-]

t	Time [T]
T	Dimensionless time [PVI]
U	Flow velocity [LT^{-1}]
x	Axial coordinate [L]
X	Dimensionless axial coordinate [-]

Greek letters

ϕ	Porosity [-]
λ_0	Initial attachment filtration coefficient [L^{-1}]
Λ_0	Dimensionless initial filtration coefficient [-]
λ_1	Size exclusion (straining) filtration coefficient [L^{-1}]
Λ_1	Dimensionless size exclusion filtration coefficient [-]
λ	Filtration coefficient [L^2M^{-1}]
μ	Viscosity [$ML^{-1}T^{-1}$]

Subscripts

K	Kaolinite
m	Maximum value
N	Nanoparticle

1. Introduction

Migration of suspended colloids predominately occurs in subsurface formations. However, flow of suspended colloids in porous media has also been observed in various processes of environmental, chemical, civil, and petroleum engineering (Civan 2015). Kaolinite clay particles are often present in numerous occasions of subterranean water contamination, plant irrigation, cold water injection into geothermal reservoirs, artificial recharge of aquifers, well drilling with filtrate invasion into formations, seawater intrusion into coastal aquifers, and low-salinity water injection into oilfields (You et al. 2015; Farajzadeh et al. 2017; Mirabolghasemi et al. 2015; Mikhailov et al. 2018). Kaolinite fines are detached from surfaces of sandstone rocks, yielding water contamination and permeability decline (Russell et al. 2017; Chequer et al. 2017).

Engineered nanoparticles have received considerable attention in a very large number of applications including the treatment of contaminated aquifers, fixing movable fines in oil and gas reservoirs for formation damage prevention (Arab et al. 2014; Yuan et al. 2016a; Yuan and Moghanloo 2017), and enhanced oil recovery by water flooding (Arab and Pourafshary 2013). The transport of NPs in porous media is relatively complicated, because it is affected by several

factors including: interstitial velocity, solution chemistry, temperature, and the presence of other suspended particles (Rottman et al. 2013; Syngouna et al. 2017; Yuan et al. 2016b).

Numerous stochastic and deterministic mathematical models are developed to describe particle transport, capture and the consequent rock alteration. The reviews by Shapiro, Yuan (2012) and Yuan et al. (2012) give a reasonably complete account of the available stochastic models, described by population balance equations (Sharma and Yortsos 1987; Santos and Bedrikovetsky 2006; Bedrikovetsky et al. 2017; Hayek et al. 2012), random walk models (Shapiro 2007; Yuan et al. 2012), deep-bed filtration equation with stochastically distributed filtration coefficient (Yuan and Shapiro 2010; Elimelech et al. 2013), and Boltzmann's equation (Shapiro and Wesselingh 2008). Population balance equations with probabilistic distribution of pore and particle sizes allow for exact upscaling for suspensions of uniform size, and the resulting system coincides with the classical filtration equations for the averaged values (Bedrikovetsky 2008; Hammadi et al. 2017).

Several mathematical models for deep bed filtration of individual (transport) as well as binary mixtures (cotransport) are available in the literature (Abdel-Salam and Chrysikopoulos 1995; Bekhit et al. 2009; Katzourakis and Chrysikopoulos 2014, 2015). The common assumption is proportionality between the particle capture rate and the advective particle flux; their ratio is called the filtration function. The non-linear deterministic deep-bed filtration model allows for an exact solution (Polyanin and Manzhirov 2006; Polyanin and Zaitsev 2012). Furthermore, exact solutions for direct problem yield regularisation of the corresponding inverse problems, which allow for determination of the associated model functions from the laboratory tests (Alvarez et al. 2005; Alvarez et al. 2007; Hayek 2015; Hayek et al. 2012). An analytical model for deep bed filtration of a binary mixture, where each species is captured by a separate capture mechanism, using constant and Langmuir's filtration functions, is proposed in Araújo, Santos (2013). However, recent studies have shown that for kaolinite and graphene oxide (GO) NP cotransport, the attachment processes can be simultaneous for both suspended particles (Chrysikopoulos et al. 2017; Sotirelis and Chrysikopoulos 2017). Because suspended particles near rough pore walls migrate with significantly smaller velocity than the mean interstitial velocity (Sefrioui et al. 2013), several investigators proposed mathematical models for two populations of particles with two different velocities (Yuan and Shapiro 2010; Bradford et al. 2009b; Kuzmina et al. 2017). Yuan, Moghanloo (2017) and Yuan et al. (2016a) proposed mathematical models for kaolinite and NPs cotransport with adsorption as a major capture

mechanism. However, a mathematical model for cotransport of colloids and NPs with simultaneous attachment and straining (size exclusion) of both species is not available.

The objective of the present work is to develop a mathematical model for the individual motion and cotransport of colloids and NPs in porous media using a novel filtration function capable of matching closely the experimental data collected by Chrysikopoulos et al. (2017) for kaolinite and NPs transport. The proposed novel filtration function incorporates two simultaneous capture mechanisms: Langmuir (blocking) and constant (low-retention) filtration.

2. Theoretical developments

This section proposes so-called binary filtration function that yields the BTCs with stabilised concentration lower than the injected concentration, and derived the exact solution for 1D transport of single colloidal population (section 2.1, Table 1). Then we extend the binary filtration function for two-population transport, and develop the transport equations (section 2.2).

2.1 Transport models

Assuming that the interstitial fluid is incompressible (water), the suspended particles are uniformly sized, particle concentration is low so that the carrier fluid density is not altered, particle dispersion (diffusion) is negligible compared to the interstitial velocity, particle capture by the solid matrix follows linear kinetics with capture rate proportional to the particle advective flux and occurs by size exclusion, straining, attachment, segregation, diffusion into dead-end pores, etc. (see Fig. 1a), permeability decline due to particle retention is adequately described Darcy's law, the governing equations for transport in porous media are as follows (Herzig et al. 1970; Alvarez et al. 2005; Alvarez et al. 2007):

$$\frac{\partial}{\partial t}\left(\phi c + s\right) + U\frac{\partial c}{\partial x} = 0 \tag{1}$$

$$\frac{\partial s}{\partial t} = \lambda\left(s\right)cU \tag{2}$$

$$U = -\frac{k\left(s\right)}{\mu\left(c\right)}\frac{\partial P}{\partial x} \tag{3}$$

where x [L] is the linear coordinate in the flow direction, t [T] is time, c [M/L^3] and s [M/M] are the suspended and attached concentrations, ϕ [-] is the porosity, U [L/T] is the fluid velocity, λ [L^2/M] is the filtration coefficient, k [L^2] is the permeability, μ [M/LT] is the viscosity, and P [M/LT^2] is the pressure. The suspended particle concentration c is determined as the number

of suspended particles in a unit volume of carrier fluid, while the retained particle concentration s is equal to the number of attached particles in a unit volume of the solid matrix. It should be noted that the effects of particle retention are in decreasing the suspended particle concentration and permeability. The suspended particle concentration decline due to retention is important for industrial waste disposal and aquifer contamination, while the permeability decline yields production and injection well impairment.

For constant particle concentration injection in a typical bench scale core or packed column, initially free of particles, the appropriate initial and boundary conditions are:

$$c(x,0) = s(x,0) = 0 \tag{4}$$

$$c(0,t) = c^0 \tag{5}$$

where c^0 [M/L^3] is the injected suspended particle concentration. The assumptions of a monolayer particle attachment (Langmuir type), where one attached particle occupies one vacancy, and of the small suspended and attached particle concentrations, yield the following "active-mass" law for the particle-vacancy "reaction" (Elimelech et al. 2013).

$$\lambda(s) = \begin{cases} \lambda_0\left(1-\dfrac{s}{s_m}\right), & s < s_m \\ 0, & s > s_m \end{cases} \tag{6}$$

where λ_0 is the initial filtration coefficient as determined by the solid matrix-particle attraction, and s_m is the maximum concentration of attached particles (Bedrikovetsky 2008). The maximum value s_m corresponds to complete occupation of the solid matrix surfaces by the attached particles, and $1/s_m$ relates to the solid matrix fraction occupied by a single particle. After the retained particle concentration reached its maximum value s_m, the particle attachment on the solid matrix surfaces stops. Note that the above-mentioned scenario corresponds to the case of solid matrix-particle attraction and particle-particle repulsion (Kuhnen et al. 2000; Bennacer et al. 2017). The Langmuir blocking filtration function (6) is usually used for monolayer electrostatic attachment of particles on solid matrix surfaces, but is also applicable for straining and size exclusion (Herzig et al. 1970; Kuhnen et al. 2000).

For a small retained particle concentration ($s<<s_m$), the filtration coefficient is assumed to be constant, $\lambda(s)=\lambda_1$. The probability of particle capture remains constant for low retention concentrations, because the particles do not compete for the same vacancy. For this case, the breakthrough concentration is expected to be initially equal zero and subsequently to jump up to some value that remains constant. It the present work, this low-retention mechanism is

referred to as size exclusion, whereas attachment corresponds to the Langmuir's blocking capture.

Note that BTCs, which are initially equal to zero, jump up to some value and then monotonically increase to a limit that is lower than the injected concentration as time tends to infinity, have been observed in laboratory breakthrough experiments with kaolinite colloid particles and graphene oxide nanoparticles conducted by Chrysikopoulos et al. (2017). In this study, it was assumed that such BTCs can be represented by a filtration function that consists of two simultaneous particle capture mechanisms as described by the following piecewise function:

$$\lambda(s) = \begin{cases} \lambda_0\left(1 - \dfrac{s}{s_m}\right) + \lambda_1, & s \le s_m \\ \lambda_1, & s \le s_m \end{cases} \tag{7}$$

where the filtration coefficient λ_0 corresponds to monolayer attachment where no particles were attached yet, and λ_1 corresponds to low-retention size exclusion. It should be noted that the filtration model (7) contains three parameters (λ_0, λ_1, and s_m) and can easily be modified to describe other combinations of particle retention mechanisms.

Further in the paper, the filtration coefficients are determined by tuning the experimental data. Theoretical calculations of straining filtration coefficient accounting for effects of attached particles can be performed from reconstruction of CT or NMR images using digital core techniques (Wang et al. 2018b; Wang et al. 2018a; Shikhov and Arns 2015). The approach is similar to calculation of permeability or electrical conductivity from rock geometry at pore scale (Yanici et al. 2013; Arns and Adler 2018).

Introducing the following dimensionless definitions for time, x-coordinate, filtration coefficients, suspended and attached concentrations:

$$T = \frac{Ut}{\phi L},\ X = \frac{x}{L},\ \Lambda_i = \lambda_i L,\ C = \frac{c}{c^0},\ S = \frac{s}{\phi c^0} \tag{8}$$

the governing model Eqs. (1, 2) become:

$$\frac{\partial C}{\partial T} + \frac{\partial C}{\partial X} = -\Lambda(S)C \tag{9}$$

$$\frac{\partial S}{\partial T} = \Lambda(S)C \tag{10}$$

the filtration function (7) is given by:

$$\Lambda(S)=\begin{cases}\Lambda_0\left(1-\dfrac{S}{S_m}\right)+\Lambda_1, & S\le S_m\\ \Lambda_1, & S\le S_m\end{cases} \tag{11}$$

and the initial and boundary conditions (4, 5) become:

$$C(X,0)=S(X,0)=0 \tag{12}$$

$$C(0,T)=1 \tag{13}$$

In view of the works Polyanin, Manzhirov (2006); Polyanin, Zaitsev (2012); Alvarez et al. (2005); Alvarez et al. (2007); Bedrikovetsky et al. (2017) an analytical solution to the model equations (9-13) describing the transport of suspended particles in one-dimensional, homogeneous, water saturated porous medium (see Fig. 2) can be obtained. Briefly, introducing the following integral potential from Eq. (10)

$$\Psi(S)=\int_0^S\frac{dy}{\Lambda(y)} \tag{14}$$

yields the following form for Eq. (10):

$$\frac{\partial\Psi(S)}{\partial T}=C \tag{15}$$

Substituting expression for *C(X,T)* (15) into Eq. (9), changing the order of differentiation by *X* and *T* in second derivative, and integrating in *T*, lead to the following expression:

$$\frac{\partial\Psi(S)}{\partial T}+S+\frac{\partial\Psi(S)}{\partial X}=\left.\frac{\partial\Psi(S)}{\partial T}\right|_{T=0}+S|_{T=0}+\left.\frac{\partial\Psi(S)}{\partial X}\right|_{T=0} \tag{16}$$

The constant of integration is situated in the right hand side of Eq. (16) and is calculated from initial conditions (12). In view of initial conditions (12) and rate equation (10), the right hand side of the previous equation is equal to zero. Consequently, Eq. (16) reduces to:

$$\frac{\partial\Psi(S)}{\partial T}+\frac{\partial\Psi(S)}{\partial X}=-S \tag{17}$$

The initial and boundary conditions (12), (13) for Eq. (17) become:

$$\Psi\left[S(X,0)\right]=0,\qquad \Psi\left[S(0,T)\right]=T \tag{18}$$

Along the characteristic lines $X = T–T_0$, $T_0>0$, equation (17) can be transformed as follows:

$$\frac{1}{\Lambda(S)}\frac{dS}{dX}=-S \tag{19}$$

Note that the characteristic lines $X = T - T_0$, $T_0>0$ cover the overall domain $T > X$. Integrating equation (19) over X and imposing boundary condition (18), yields:

$$\int_{S(0,T-X)}^{S(X,T)} \frac{dS}{S\Lambda(S)} = -X, \quad \Psi\left(S\left(0,T-X\right)\right) = T - X \tag{20}$$

Equations (15) and (20) determine the retained particle concentration $S(X,T)$ for $T>X$. For $T<X$, the integration along the characteristics gives: $S(X,T)=0$. As it follows from Eqs. (15) and (19), the value C/S is constant along the characteristic lines $X = T - T_0$, $T_0>0$, i.e. C/S is Riemann invariant. Accounting for boundary condition (13) yields

$$\frac{C\left(X,T\right)}{S\left(X,T\right)} = \frac{1}{S\left(0,T-X\right)} \tag{21}$$

The expression for the concentration of suspended particles $C(X,T)$ is obtained from Eq. (21) for known solution $S(X,T)$.

The concentration front $X=T$ moves along the porous medium with a velocity equal to unity. Ahead of this front, initial conditions (12) hold: $C(X,T)=S(X,T)=0$. Along the front, the concentration of deposited particles equals zero, $S(T,T)=0$. Therefore, as it follows from Eqs. (9, 10), the concentration of suspended particles along the front, $C(T,T)$, is expressed as:

$$C\left(T,T\right) = \exp\left(-\Lambda\left(0\right)T\right) \tag{22}$$

Equations (15) and (20) provide an exact solution in the form of two transcendental equations for unknowns $S(X,T)$ and $S(0,T)$. Using $S(0,T)$ as an independent variable allows for explicit calculation of T. The explicit formulae for suspended and retained particle concentrations are given in Table 1. Note that the analytical 1D model developed here can also be extended to three-dimensions by using streamline techniques (Oladyshkin and Panfilov 2007).

Fig. 3a presents breakthrough curves simulated by the analytical solutions listed in Table 1, for the three different filtration functions presented in Fig. 3b. The analytical solutions for the case of constant filtration coefficient are obtained by fixing $\lambda_0=0$ and $S_m\to\infty$, and for Langmuir blocking function by setting $\lambda_1=0$. The BTC corresponding to the constant filtration function is shown in Fig. 3a (curve 1), to the Langmuir filtration function is shown in Fig. 3a (curve 2), and to the case of combined constant and Langmuir filtration is shown in Fig. 3a (curve 3). The Langmuir mechanism exhibits blocking under conditions of substantial particle attachment. The Langmuir mechanism is usually applied for monolayer particle attachment onto the solid

matrix, where the attachment rate is proportional to number of vacant sites for retention on the surfaces of solid matrix.

Fig. 4a shows the plane (X,T), three concentration fronts, and the corresponding flow zones: 0, I, II, and III, as obtained by the exact analytical solutions listed in Table 1. The four different zones are separated by the trajectories of three concentration fronts: $T_I(X)$, $T_{II}(X)$, and $T_{III}(X)$. The corresponding domains separated by those fronts are presented in Table 1. The cotangents of the trajectory slopes $(dT_k(X)/dX)^{-1}$, $k=I, II, III$, are equal to the front speeds. Note that the method of characteristics was used for the derivation of the exact solutions presented in Table 1, and the characteristics are the particle trajectories. The initial conditions hold in zone 0 ahead of the concentration front $T_I(X)$ that moves with unitary speed. Zone I behind this front corresponds to flow with retained concentration $S(X,T)<S_m$, where the particles migrate subject to linear filtration function (6). Two capture mechanisms act in zone I. The filtration function is constant in zone III, where the suspended particles move from the inlet $X=0$ to the boundary between zones III and II, $T_{III}(X)$, where the retained particle concentration increases up to the maximum value S_m. Migration of suspended particles continues in zone II subject to linear filtration. Only straining occurs in zone III, while both retaining mechanisms act in zone II. The suspended particle concentration is at a steady state in zone III, so the capture rate is constant, and the retained particle concentration accumulates linearly with time. The structure of the flow pattern is as follows: (Zone 0) – initial conditions of no suspended and retained particles are held ahead of the first concentration front; (Zone I) – two simultaneous capture mechanisms act, front and rear boundaries of this zone move with unitary speed; (Zone II) – starts at the inlet at the moment T_m, when the maximum attached value S_m is reached by the retained particle concentration; subsequently, only straining occurs in zone III; and (Zone III) – steady-state suspended particle concentration decreases exponentially due to constant filtration. Figs. 4b,c present profiles of suspended and retained particles at three different points in time. At T_i, the particle front did not breakthrough yet. Both dimensionless particle concentrations C and S are zero ahead of this front. The suspended particle concentration jumps from zero at the front and increases behind the front, while the suspended particle concentration is continuous. At T_{ii}, after the front has breakthrough, the profiles of particle concentration decrease exponentially from the inlet in zone III, and continue to decrease in zones II and I. Suspended particle concentrations coincide at T_{ii} and T_{iii} in zone III.

Note that the first derivatives of the solution for piecewise-linear filtration function suffer discontinuity on the boundary between zones II and III, where $S(X,T)=S_m$, i.e. the derivative of the filtration function is also discontinuous. This phenomenon has been observed from the exact solution for flow with deposit dissolution, where the dissolution rate becomes zero when the deposit vanishes (Sorbie and Stamatiou 2018). Apart from the derivative discontinuity front, the system with deposit dissolution is linear, and the complete dissolution front propagates with constant speed. The problem (9), (10) is non-linear, so the front trajectory in Fig. 4a is curvilinear.

The governing equations (9), (10) and (11) subject to initial and boundary conditions (12), (13) were solved numerically using the computer code developed by Shampine (2005a). The algorithm implements a two-step Lax–Friedrichs finite-difference method (Shampine 2005b). The Matlab computer program, and pertinent supporting information are available from http://faculty.smu.edu/shampine/current.html. Fig. 5 presents a comparison of the analytical solution with the numerical solution for individual transport of NPs and kaolinite colloids at pH=7 and I_S=27 mM. The values of the parameters Λ_0, Λ_1, and S_m used are listed in Table 2, whereas space and time steps employed in the finite-difference method are ΔX=0.001, ΔT=0.0009. The exact analytical and numerical solutions are almost identical, suggesting that the numerical scheme exhibited very low numerical dispersion.

2.2 Cotransport model

For the case of cotransport of two different populations of suspended particles it was assumed that the concentration of each population of suspended particles was low, so that the suspended particles from one population do not compete for the same vacancies with suspended particles from the other population (Fig. 1b). Therefore, the maximum attached particles concentration and filtration coefficients of each population during cotransport are assumed to be identical to those during transport of each individual population. Consequently, for the case of kaolinite colloids and NPs cotransport the governing partial differential equations are (Bedrikovetsky 2013):

$$\frac{\partial C_i}{\partial T}+\frac{\partial C_i}{\partial X}=-\left[\Lambda_{0i}\left(1-\frac{S_N}{S_{mN}}-\frac{S_K}{S_{mK}}\right)+\Lambda_{1i}\right]C_i \tag{23}$$

$$\frac{\partial S_i}{\partial T}=\left[\lambda_{0i}\left(1-\frac{S_K}{S_{mK}}-\frac{S_N}{S_{mN}}\right)+\lambda_{1i}\right]C_i \tag{24}$$

where index $i=K, N$ for kaolinite colloids and NPs, respectively. It should be noted that S_{mN}, Λ_{0N}, S_{mK}, and Λ_{0K} are equal to those for the case of transport of each population of suspended particles, but Λ_{1N} and Λ_{1K} are different because particle onto the surfaces of the solid matrix can affect pore throat radii (Fig. 1b), which in turn can affect straining (Alem et al. 2015). Therefore, the filtration coefficients for straining during cotransport are assumed to be different from those corresponding to transport of each individual population (Fig. 1b). The cotransport model contains 6 independent parameters: S_{mN}, Λ_{0N}, S_{mK}, Λ_{0K}, Λ_{1N} and Λ_{1K}. Four parameters (S_{mN}, Λ_{0N}, S_{mK}, and Λ_{0K}) are determined from experimental breakthrough data of individual population transport, whereas two parameters (Λ_{1N} and Λ_{1K}) are obtained by fitting the cotransport experimental breakthrough curves.

3. Results and discussion

The new transport and cotransport mathematical models were used to match the experimental data reported by Chrysikopoulos et al. (2017) for transport and cotransport of graphene oxide (GO) NPs and kaolinite (KGa-1b) colloids in columns packed with glass beads and quartz sand under various water chemistry conditions (pH=4, 7, 10 and I_S=7, 12, 27 mM). The unknown parameters were determined with a nonlinear least squares method, which minimises the normalized deviation between the model and the experimental data (Coleman and Li 1996). Specifically, the Trust-Region-Reflective optimization algorithm of MATLAB was used for the solution of the resulting quadratic-deviation minimisation problem. Note that the steep continuous growth of a BTC around its breakthrough time (T=1) is treated in this work as a concentration jump from zero, before the breakthrough to continuously growing BTC after the breakthrough. The areas between the continuous and discontinuous BTCs before and after the breakthrough time are equal. This procedure used here for matching BTCs is analogous to matching of inner and outer asymptotic expansions when dispersion is small (Polyanin and Dil′man 1994; Polyanin 2004).

3.1 Matching of the transport experimental data

The experimental data for NPs and for kaolinite colloids individual transport in a column packed with glass beads at 5 different sets of water chemistry conditions reported by Chrysikopoulos et al. (2017) are presented in Fig. 6, together with the corresponding fitted analytical model simulations. Furthermore, the experimental data for NPs and for kaolinite colloids individual transport in a column packed with quartz sand for just one set of water chemistry conditions are presented in Fig. 9a, together with the corresponding fitted analytical

model simulations. All fitted parameters for the individual transport experiments were listed in Table 2. Based on the R^2 values listed in Table 2, the analytical model fitted adequately the experimental data for both NPs and kaolinite colloids. This validates the proposed binary model given by Eq. (7).

For all cases presented in Fig. 6 (except the NP case in Fig. 6c), the experimental data were fitted with the analytical model utilizing the filtration piecewise function (7). The unfavourable attachment conditions (high pH and low I_S) in Fig. 6c lead to large solid matrix-particle repulsion, as suggested by (Derjaguin-Landau-Verwey-Overbeek) DLVO theory (Chrysikopoulos et al. 2017). Consequently, suspended particles are mobile and unstable (Bennacer et al. 2017). Furthermore, attachment onto the solid matrix under unfavourable attachment conditions can be better represented by the Langmuir filtration function.

The fitted parameters listed in Table 2 are also presented graphically in Fig. 7 as a function of pH and I_S. Parameter values corresponding to transport experiments in columns packed with glass beads and quartz sand, are represented by circles and squares, respectively. Figs. 7a and 4d show the initial filtration coefficient variability with pH, at I_S= 7 mM for NPs and kaolinite colloids, respectively. The higher is the pH, the lower is the electrostatic solid matrix-particle attraction, and the lower is the Λ_0 as well as the straining Λ_1 (Bradford et al. 2009a). Figs. 7b and 7e show the initial filtration coefficient variability with I_S, at pH= 7 for NPs and kaolinite colloids, respectively. The higher is the I_S, the larger is the expected electrostatic attraction between the suspended particles and the solid matrix, and in turn the higher the expected value for both filtration coefficients (Λ_0 and Λ_1). The Λ_0 fitted values for both NPs and kaolinite colloids do not exhibit a clear increasing trend with increasing I_S. However, the fitted values for Λ_1 for both NPs and kaolinite colloids generally fulfil this tendency. Figs. 7c and 7f show the maximum retention concentration variability with I_S and pH for both NPs and kaolinite colloids, respectively. For increasing pH and decreasing I_S, both the electrostatic attraction between the suspended particles and the solid matrix and S_m are expected to decrease. This is clearly the case for NPs, but it is somewhat less pronounced for kaolinite colloids.

The mean radius of the glass beads employed in this study was 1 mm, while the mean radius of quartz sand grain was 0.3 mm. So, the sand grains were smaller than the glass-beads, thus the solid matrix surface area was larger in the columns packed with quartz sand. Furthermore, sand grain shapes are irregular, so the surface area was larger than that for the glass-beads. Consequently, Λ_0 must be greater for quartz sand. This is clearly the case for both NPs and

kaolinite colloids (see Figs. 7a,b,d,e) (Bradford et al. 2009a; Bradford et al. 2003). The pore throats in columns packed with quartz sand are smaller than those packed with glass beads. Also, sand has rougher surface than glass beads, which facilitates size exclusion. The average radii for nanoparticles and kaolinite colloids were 0.4 μm and 0.6 μm, respectively, i.e. they are almost the same. Therefore, size exclusion filtration coefficient Λ_1 must be higher for sand than for glass beads. This is the case for NPs (see Figs. 7a and 7b), but not for kaolinite colloids (see Figs. 7d and 7e). The maximum retention concentration for columns packed with quartz sand is higher due to the larger solid matrix surface area of the smaller irregular grains. Therefore, S_m must be higher for columns packed with quartz. This is the case for NPs (see Fig. 7c), but not for kaolinite colloids (see Fig. 7f). The deviation of kaolinite colloids from expected behaviour is attributed to kaolinite particle aggregation. It should be noted that based on DLVO theory kaolinite aggregation is significant (Chrysikopoulos et al. 2017).

3.2 Matching of the cotransport experimental data

The experimental data for NPs and for kaolinite colloids cotransport in a column packed with glass beads at 5 different sets of water chemistry conditions reported by Chrysikopoulos et al. (2017) are presented in Fig. 8, together with the corresponding fitted numerical model simulations. Furthermore, the experimental data for NPs and for kaolinite colloids cotransport in a column packed with quartz sand for just one set of water chemistry conditions are presented in Fig. 9b, together with the corresponding fitted numerical model simulations. All fitted parameters for the cotransport experiments were listed in Table 3. Based on the R^2 values listed in Table 3, the numerical model (Eqs. 23 and 24) fitted adequately the experimental data for both NPs and kaolinite colloids. It should be noted that for individual suspended particle transport the BTCs have an exponential form, so the number of degrees of freedom for each BTC is three. Therefore, three coefficients (Λ_0, Λ_1 and S_m) are determined from experimental BTC. However, for the case of cotransport (Eqs. 23 and 24), there are two breakthrough curves with 6 degrees of freedom, and the number of fitted parameters is only two (Λ_{1N} and Λ_{1K}).

The fitted parameters listed in Table 3 are also presented graphically in Fig. 10 as a function of pH and I_S. Both Λ_{1N} and Λ_{1K} correspond to NPs and kaolinite colloids, respectively, decrease with increasing pH, at I_S=7 mM (see Fig. 10a). Whereas, both Λ_{1N} and Λ_{1K} at pH=7, are not strongly affected by I_S (see Fig. 10b). The unexpected behaviour of kaolinite colloids (Fig. 10b) is attributed to kaolinite-kaolinite particle aggregation, which is far more significant than that of kaolinite-NP and NP-NP (Chrysikopoulos et al. 2017). It should be noted that based on

DLVO theory kaolinite aggregation is significant (Chrysikopoulos et al. 2017). However, particle aggregation was beyond the scope of this study and has not been accounted for by the proposed transport and cotransport models.

4. Conclusions

The fate and transport of nanoparticles and clays in subterranean waters is highly affected by the nanoparticle-clay interactions, cotransport and their capture by the porous matrix. In this study, a novel 1D transport model with binary filtration functions was developed to simulate the transport of suspended colloidal particles as well as the cotransport of colloids and NPs. The proposed cotransport model assumes that the different types of suspended particles have electrostatic interactions with the solid matrix, which are similar under both transport and cotransport conditions. Also, the initial attachment filtration coefficient for each particle type in the mixture is equal to that for transport of each individual particle type, which implies that the maximum retention concentration for attachment for each particle type is the same under both transport and cotransport conditions. The model fitted successfully the transport and cotransport experimental data collected by Chrysikopoulos et al. (2017). Six-dimensional laboratory data set for co-transport was fitted by two model parameters only, which validates the model developed. The explicit analytical solution provided in Table 1 allows for direct numerical implementation without going through complicated mathematical derivations. The derived analytical model for binary particle capture mechanisms is preferred over computationally expensive numerical solutions, and can be used as a benchmark for numerical models. The analytical 1D model can be implemented in quasi 3D streamline model to interpret field studies. The proposed cotransport model with two capture mechanisms can be also used for prediction of simultaneous flows of bacteria, viruses, clays, NPs, etc.

References

Abdel-Salam, A., Chrysikopoulos, C.V.: Modeling of colloid and colloid-facilitated contaminant transport in a two-dimensional fracture with spatially variable aperture. Transp. Porous Med. **20**(3), 197-221 (1995)

Alem, A., Ahfir, N.-D., Elkawafi, A., Wang, H.: Hydraulic operating conditions and particle concentration effects on physical clogging of a porous medium. Transp. Porous Med. **106**(2), 303-321 (2015)

Alvarez, A., Bedrikovetsky, P., Hime, G., Marchesin, A., Marchesin, D., Rodrigues, J.: A fast inverse solver for the filtration function for flow of water with particles in porous media. Inverse Probl. **22**(1), 69 (2005)

Alvarez, A.C., Hime, G., Marchesin, D., Bedrikovetsky, P.G.: The inverse problem of determining the filtration function and permeability reduction in flow of water with particles in porous media. Transp. Porous Med. **70**(1), 43-62 (2007)

Arab, D., Pourafshary, P.: Nanoparticles-assisted surface charge modification of the porous medium to treat colloidal particles migration induced by low salinity water flooding. Colloids and Surfaces A: Physicochemical Eng. Aspects **436**, 803-814 (2013)

Arab, D., Pourafshary, P., Ayatollahi, S.: Mathematical modeling of colloidal particles transport in the medium treated by nanofluids: deep bed filtration approach. Transp. Porous Med. **103**(3), 401-419 (2014)

Araújo, J.A., Santos, A.: Analytic model for DBF under multiple particle retention mechanisms. Transp. Porous Med. **97**(2), 135-145 (2013)

Arns, C., Adler, P.: Fast Laplace solver approach to pore-scale permeability. Physical Review E **97**(2), 023303 (2018)

Bedrikovetsky, P.: Upscaling of stochastic micro model for suspension transport in porous media. Transp. Porous Med. **75**(3), 335-369 (2008)

Bedrikovetsky, P.: Mathematical theory of oil and gas recovery: with applications to ex-USSR oil and gas fields, vol. 4. Springer Science & Business Media, (2013)

Bedrikovetsky, P., You, Z., Badalyan, A., Osipov, Y., Kuzmina, L.: Analytical model for straining-dominant large-retention depth filtration. Chem. Eng. J. **330**, 1148-1159 (2017)

Bekhit, H.M., El-Kordy, M.A., Hassan, A.E.: Contaminant transport in groundwater in the presence of colloids and bacteria: Model development and verification. J. Contam. Hydrol. **108**(3-4), 152-167 (2009)

Bennacer, L., Ahfir, N.-D., Alem, A., Wang, H.: Coupled effects of ionic strength, particle size, and flow velocity on transport and deposition of suspended particles in saturated porous media. Transp. Porous Med. **118**(2), 251-269 (2017)

Bradford, S.A., Kim, H.N., Haznedaroglu, B.Z., Torkzaban, S., Walker, S.L.: Coupled factors influencing concentration-dependent colloid transport and retention in saturated porous media. Environ. Sci. Technol. **43**(18), 6996-7002 (2009a)

Bradford, S.A., Simunek, J., Bettahar, M., van Genuchten, M.T., Yates, S.R.: Modeling colloid attachment, straining, and exclusion in saturated porous media. Environ. Sci. Technol. **37**(10), 2242-2250 (2003)

Bradford, S.A., Torkzaban, S., Leij, F., Šimůnek, J., van Genuchten, M.T.: Modeling the coupled effects of pore space geometry and velocity on colloid transport and retention. Water Resour. Res. **45**(2) (2009b)

Chequer, L., Russell, T., Behr, A., Genolet, L., Kowollik, P., Badalyan, A., Zeinijahromi, A., Bedrikovetsky, P.: Non-monotonic permeability variation during colloidal transport: governing equations and analytical model. J. Hydrology (2017)

Chrysikopoulos, C.V., Sotirelis, N.P., Kallithrakas-Kontos, N.G.: Cotransport of Graphene Oxide Nanoparticles and Kaolinite Colloids in Porous Media. Transp. Porous Med. **119**(1), 181-204 (2017)

Civan, F.: Reservoir formation damage. Gulf Professional Publishing, (2015)

Coleman, T.F., Li, Y.: An interior trust region approach for nonlinear minimization subject to bounds. SIAM J. Optim. **6**(2), 418-445 (1996)

Elimelech, M., Gregory, J., Jia, X.: Particle deposition and aggregation: measurement, modelling and simulation. Butterworth-Heinemann, (2013)
Farajzadeh, R., Guo, H., van Winden, J., Bruining, J.: Cation exchange in the presence of oil in porous media. ACS Earth Space Chem. **1**(2), 101-112 (2017)
Hammadi, A., Ahfir, N.-D., Alem, A., Wang, H.: Effects of particle size non-uniformity on transport and retention in saturated porous media. Transp. Porous Med. **118**(1), 85-98 (2017)
Hayek, M.: Exact solutions for one-dimensional transient gas flow in porous media with gravity and Klinkenberg effects. Transp. Porous Med. **107**(2), 403-417 (2015)
Hayek, M., Kosakowski, G., Jakob, A., Churakov, S.V.: A class of analytical solutions for multidimensional multispecies diffusive transport coupled with precipitation-dissolution reactions and porosity changes. Water Resour. Res. **48**(3) (2012)
Herzig, J., Leclerc, D., Goff, P.L.: Flow of suspensions through porous media—application to deep filtration. Ind. Eng. Chem. **62**(5), 8-35 (1970)
Katzourakis, V.E., Chrysikopoulos, C.V.: Mathematical modeling of colloid and virus cotransport in porous media: Application to experimental data. Adv. Water Resour. **68**, 62-73 (2014)
Katzourakis, V.E., Chrysikopoulos, C.V.: Modeling dense-colloid and virus cotransport in three-dimensional porous media. J. Contam. Hydrol. **181**, 102-113 (2015)
Kuhnen, F., Barmettler, K., Bhattacharjee, S., Elimelech, M., Kretzschmar, R.: Transport of iron oxide colloids in packed quartz sand media: monolayer and multilayer deposition. J. Colloid Interface Sci. **231**(1), 32-41 (2000)
Kuzmina, L.I., Osipov, Y.V., Galaguz, Y.P.: A model of two-velocity particles transport in a porous medium. Int J. Non-linear Mech. **93**, 1-6 (2017)
Mikhailov, D., Zhvick, V., Ryzhikov, N., Shako, V.: Modeling of Rock Permeability Damage and Repairing Dynamics Due to Invasion and Removal of Particulate from Drilling Fluids. Transp. Porous Med. **121**(1), 37-67 (2018)
Mirabolghasemi, M., Prodanović, M., DiCarlo, D., Ji, H.: Prediction of empirical properties using direct pore-scale simulation of straining through 3D microtomography images of porous media. J. Hydrology **529**, 768-778 (2015)
Oladyshkin, S., Panfilov, M.: Streamline splitting between thermodynamics and hydrodynamics in a compositional gas–liquid flow through porous media. Comptes Rend. Mécan. **335**(1), 7-12 (2007)
Polyanin, A.: EqWorld, The World of Mathematical Equations. http://eqworld.ipmnet.ru/ (2004). Accessed 01/06/2018
Polyanin, A., Zaitsev, V.: Handbook of nonlinear partial differential equations. Chapman & Hall/CRC Press, Boca Raton. (2012)
Polyanin, A.D., Dil′man, V.V.: Methods of modeling equations and analogies in chemical engineering. CRC Press, Boca Raton, (1994)
Polyanin, A.D., Manzhirov, A.V.: Handbook of mathematics for engineers and scientists. CRC Press, Boca Raton, (2006)
Rottman, J., Sierra-Alvarez, R., Shadman, F.: Real-time monitoring of nanoparticle retention in porous media. Environ. Chem. Lett. **11**(1), 71-76 (2013)
Russell, T., Pham, D., Neishaboor, M.T., Badalyan, A., Behr, A., Genolet, L., Kowollik, P., Zeinijahromi, A., Bedrikovetsky, P.: Effects of kaolinite in rocks on fines migration. J. Natural Gas Sci. Eng. **45**, 243-255 (2017)
Santos, A., Bedrikovetsky, P.: A stochastic model for particulate suspension flow in porous media. Transp. Porous Med. **62**(1), 23-53 (2006)
Sefrioui, N., Ahmadi, A., Omari, A., Bertin, H.: Numerical simulation of retention and release of colloids in porous media at the pore scale. Colloids and Surfaces A: Physicochemical Eng. Aspects **427**, 33-40 (2013)
Shampine, L.: Solving hyperbolic PDEs in MATLAB. Appl. Num. Anal. Comp. Math. **2**(3), 346-358 (2005a)
Shampine, L.F.: Two-step Lax–Friedrichs method. Appl. Math. Lett. **18**(10), 1134-1136 (2005b)
Shapiro, A., Wesselingh, J.: Gas transport in tight porous media: gas kinetic approach. Chem. Eng. J. **142**(1), 14-22 (2008)

Shapiro, A., Yuan, H.: Application of stochastic approaches to modelling suspension flow in porous media. In: Statistical Mechanics and Random Walks: Principles, Processes and Applications. pp. 1-36. Nova Science Publishers, Incorporated, (2012)
Shapiro, A.A.: Elliptic equation for random walks. Application to transport in microporous media. Physica A: Statistical Mech. its Applic. **375**(1), 81-96 (2007)
Sharma, M., Yortsos, Y.: Transport of particulate suspensions in porous media: model formulation. AlChE J. **33**(10), 1636-1643 (1987)
Shikhov, I., Arns, C.H.: Evaluation of capillary pressure methods via digital rock simulations. Transp. Porous Med. **107**(2), 623-640 (2015)
Sorbie, K., Stamatiou, A.: Analytical Solutions of a One-Dimensional Linear Model Describing Scale Inhibitor Precipitation Treatments. Transp. Porous Med., 1-17 (2018)
Sotirelis, N.P., Chrysikopoulos, C.V.: Heteroaggregation of graphene oxide nanoparticles and kaolinite colloids. Sci. Total Environ. **579**, 736-744 (2017)
Syngouna, V.I., Chrysikopoulos, C.V., Kokkinos, P., Tselepi, M.A., Vantarakis, A.: Cotransport of human adenoviruses with clay colloids and TiO2 nanoparticles in saturated porous media: Effect of flow velocity. Sci. Total Environ. **598**, 160-167 (2017)
Wang, Y., Arns, C.H., Rahman, S.S., Arns, J.-Y.: Porous Structure Reconstruction Using Convolutional Neural Networks. Mathematical Geosciences, 1-19 (2018a)
Wang, Y., Rahman, S.S., Arns, C.H.: Super resolution reconstruction of μ-CT image of rock sample using neighbour embedding algorithm. Physica A: Statistical Mech. its Applic. **493**, 177-188 (2018b)
Yanici, S., Arns, J.-Y., Cinar, Y., Pinczewski, W., Arns, C.: Percolation effects of grain contacts in partially saturated sandstones: Deviations from Archie's law. Transp. Porous Med. **96**(3), 457-467 (2013)
You, Z., Bedrikovetsky, P., Badalyan, A., Hand, M.: Particle mobilization in porous media: temperature effects on competing electrostatic and drag forces. Geophysical Res. Lett. **42**(8), 2852-2860 (2015)
Yuan, B., Moghanloo, R.G.: Analytical model of well injectivity improvement using nanofluid preflush. Fuel **202**, 380-394 (2017). doi:10.1016/j.fuel.2017.04.004
Yuan, B., Moghanloo, R.G., Zheng, D.: Analytical evaluation of nanoparticle application to mitigate fines migration in porous media. SPE Journal **21**(06), 2,317-312,332 (2016a)
Yuan, B., Wang, W., Moghanloo, R.G., Su, Y., Wang, K., Jiang, M.: Permeability reduction of berea cores owing to nanoparticle adsorption onto the pore surface: mechanistic modeling and experimental work. Energy & Fuels **31**(1), 795-804 (2016b)
Yuan, H., Shapiro, A., You, Z., Badalyan, A.: Estimating filtration coefficients for straining from percolation and random walk theories. Chem. Eng. J. **210**, 63-73 (2012)
Yuan, H., Shapiro, A.A.: Modeling non-Fickian transport and hyperexponential deposition for deep bed filtration. Chem. Eng. J. **162**(3), 974-988 (2010)

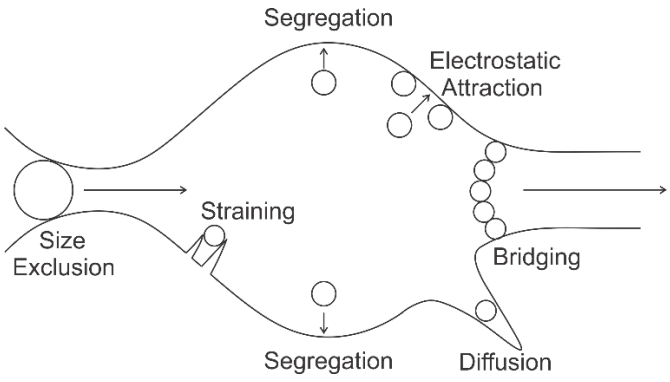

a)

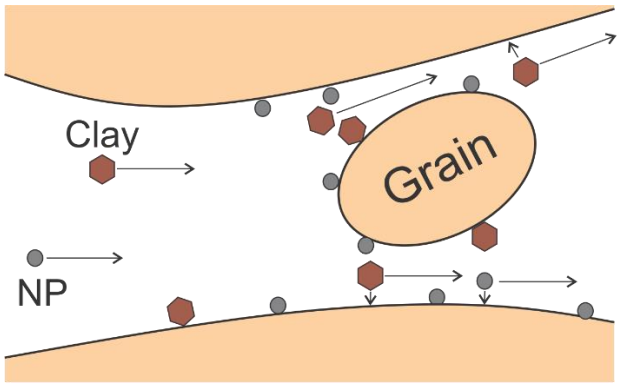

b)

Fig. 1. Multiple particle capture mechanisms: (a) various mechanisms at the pore scale; (b) attachment and straining of nano- and clay particles.

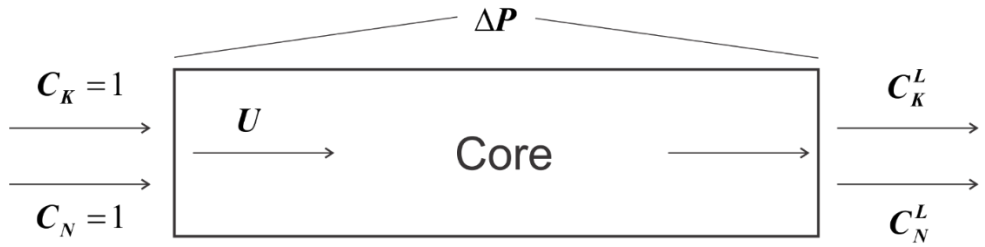

Fig. 2. Schematic illustration of a bench-scale porous medium. Kaolinite clay particles (C_K) and nanoparticles (C_N) are injected simultaneously. The dimensionless inlet concentrations are equal to one ($C_K = C_N = 1$).

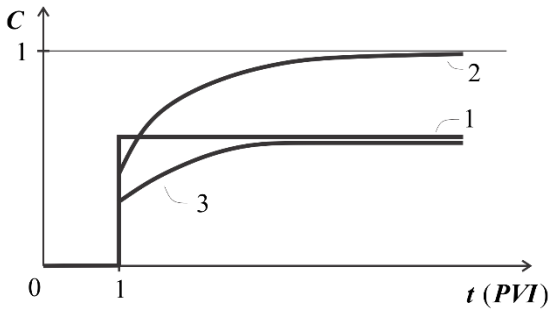

a)

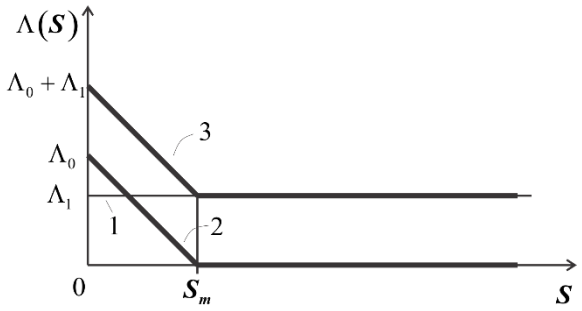

b)

Fig. 3. Illustration of three different shapes of the filtration function: (a) Breakthrough curves BTCs, and (b) Shapes of filtration functions. Curves 1, 2, and 3 correspond to constant filtration coefficient, Langmuir blocking, and combined filtration function for two simultaneous mechanisms, respectively.

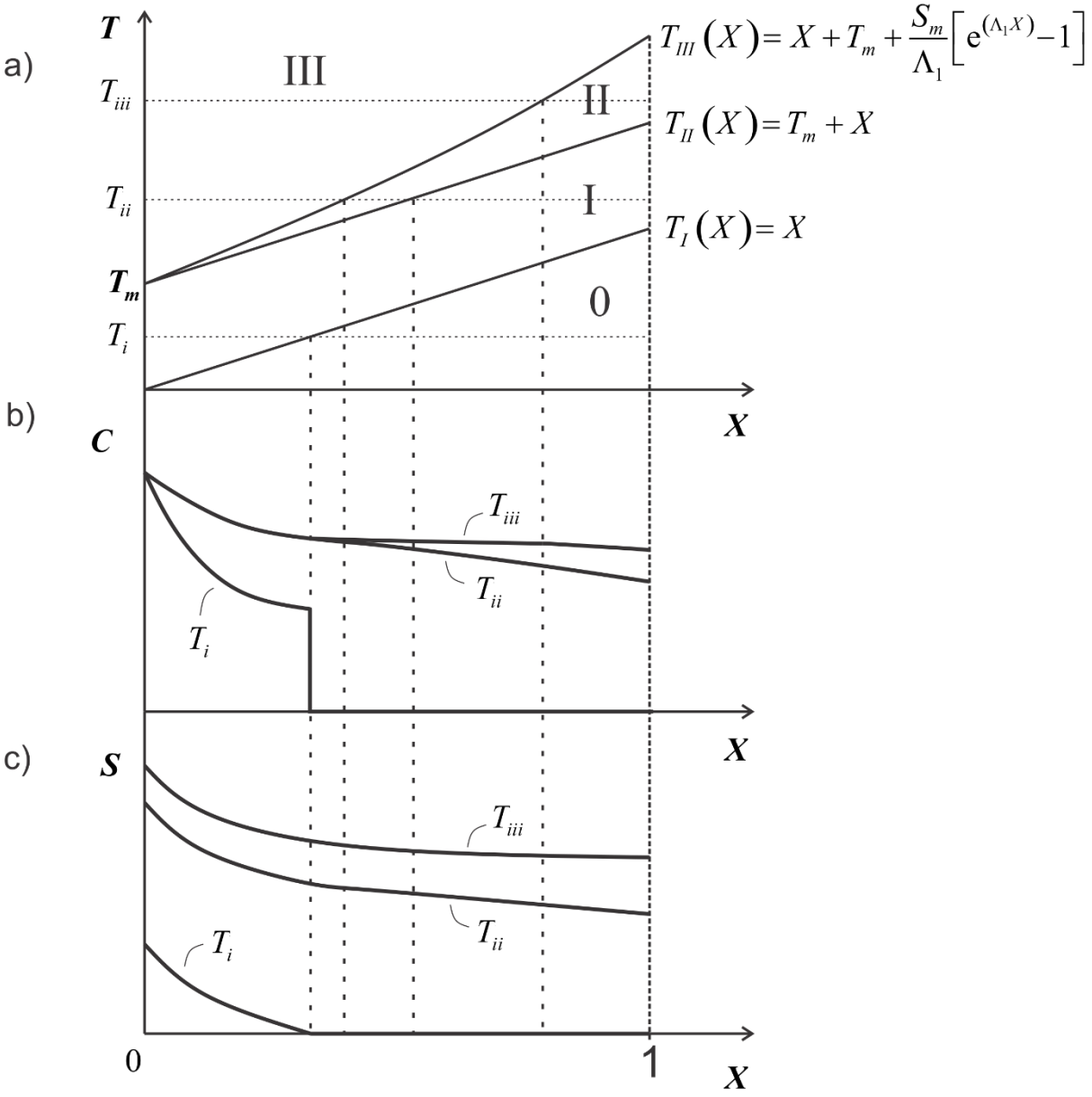

Fig. 4. Exact solution for particle transport in porous media with piecewise linear filtration function: (a) structure of flow zone, (b) suspended particle concentration profiles at various times, and (c) retained particle concentration profiles at various times.

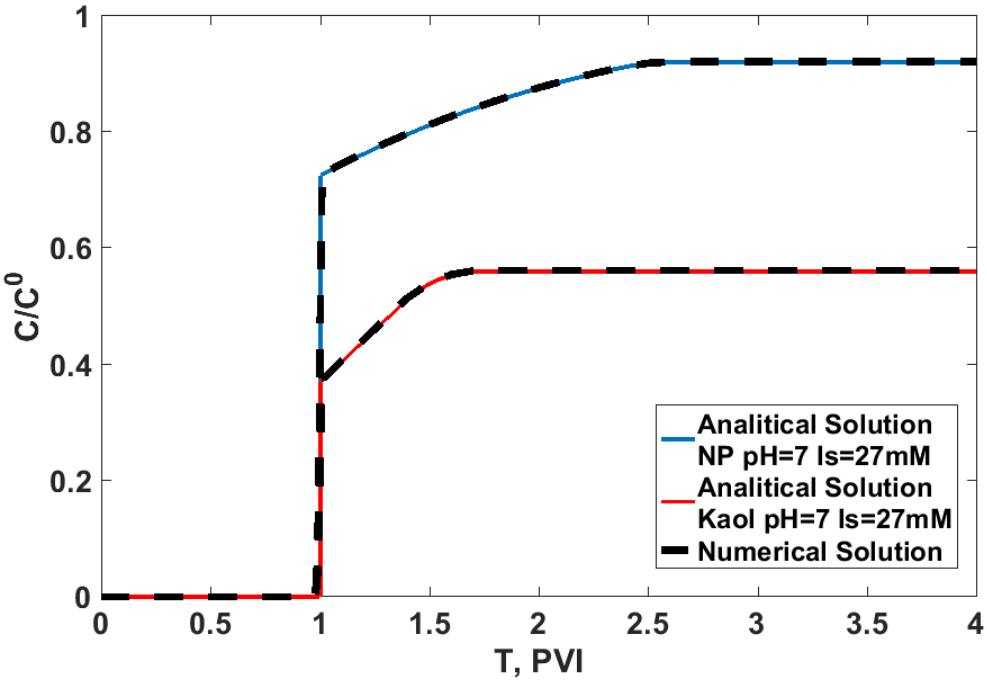

Fig. 5. Comparison between the analytical and numerical modelling for individual suspended particle transport

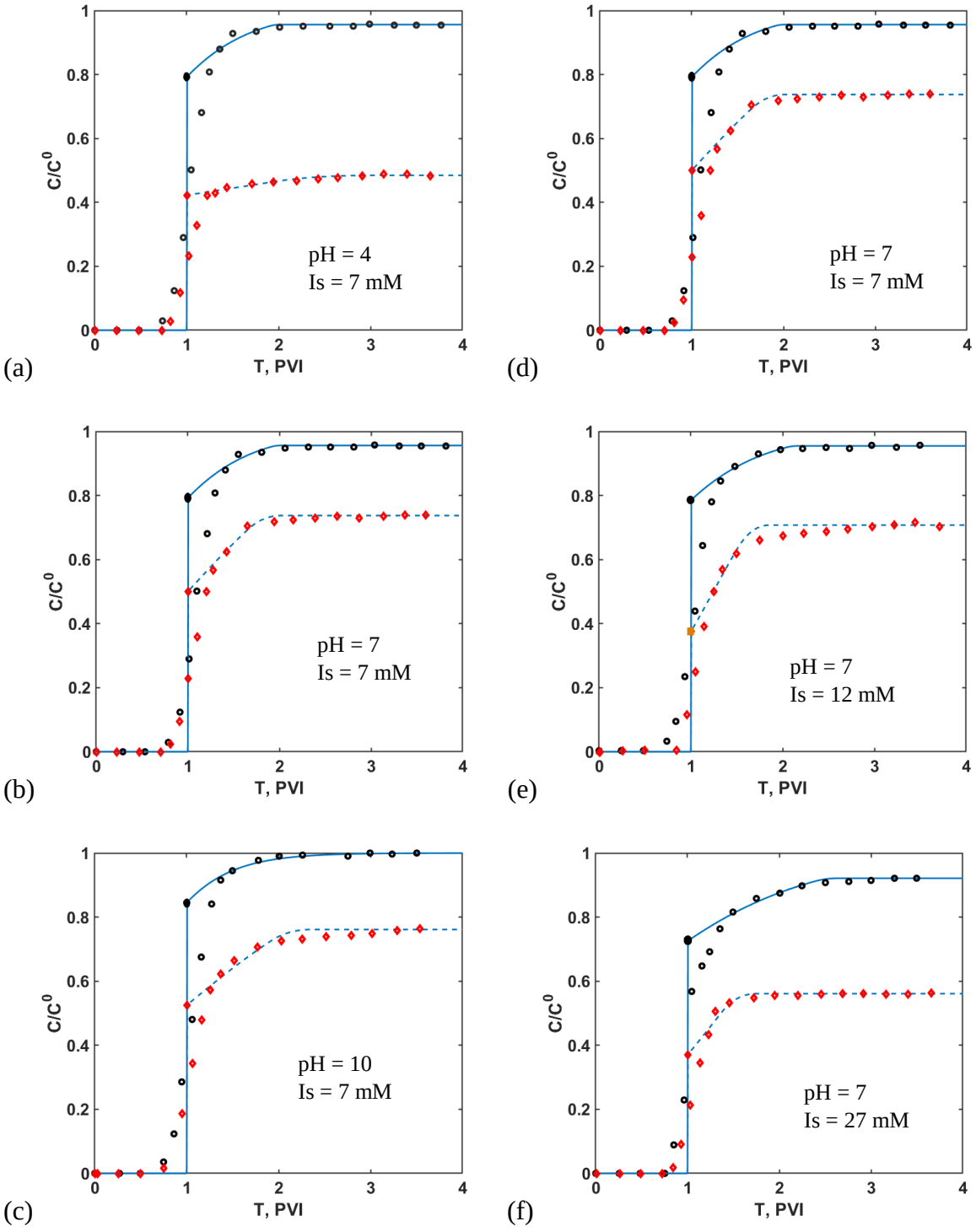

Fig. 6. Fitted breakthrough data reported by Chrysikopoulos et al.[1] for individual transport experiments of GO NPs (open black circles) and kaolinite colloids (red diamonds) in columns packed with glass beads at different conditions: (a) pH=4, *Is* =7 mM, (b) and (d) pH=7, I_S =7 mM, (c) pH=10, I_S=7 mM, (e) pH=7, I_S =12 mM, and (f) pH=7, I_S =27 mM. BTC tending to unity is fitted with a Langmuir function (solid curves in figure c), while those tending to the limit below unity are fitted with a piecewise filtration function.

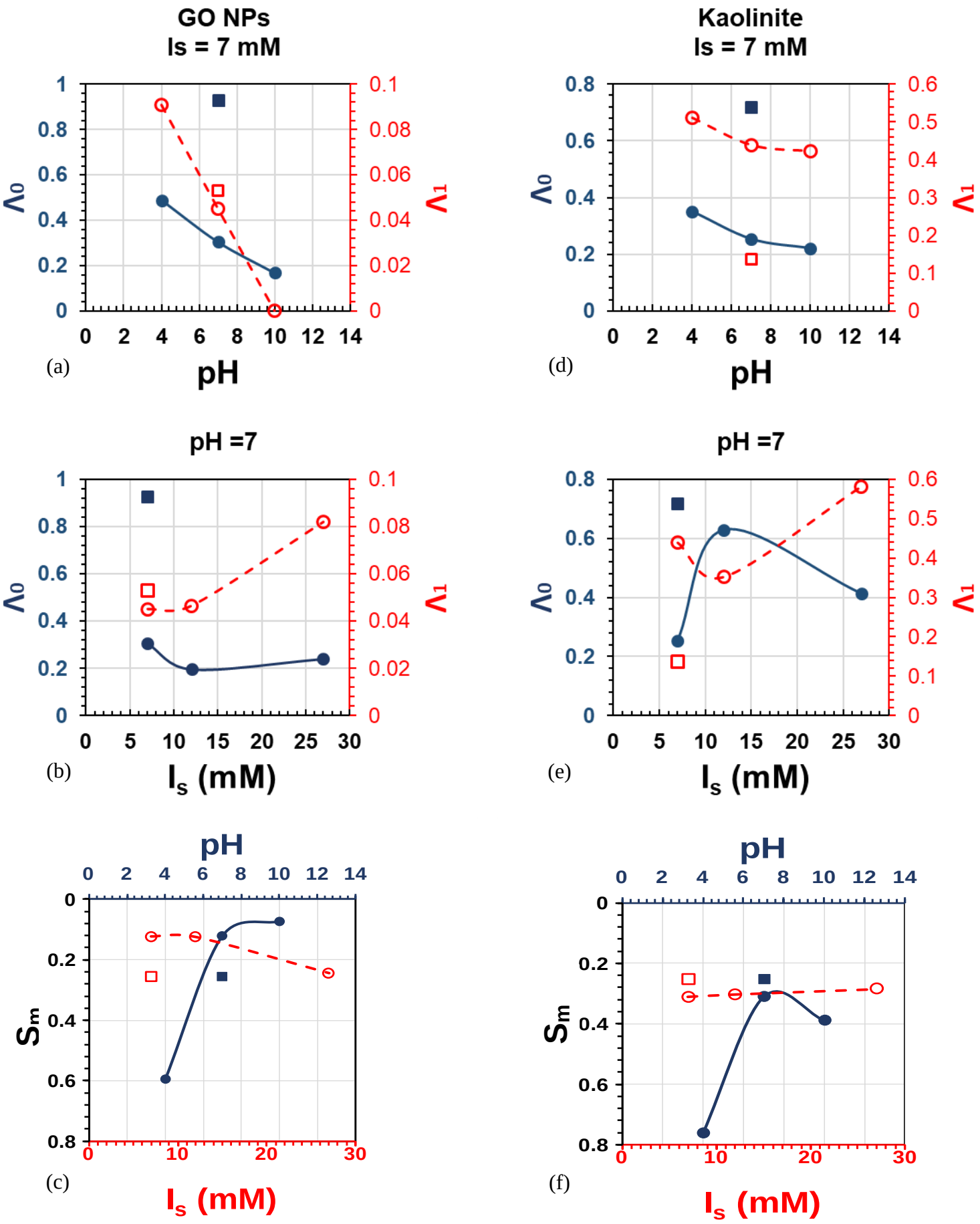

Fig. 7. Behaviour of fitted parameters for individual transport experiments of: (a-c) GO NPs and (d-e) kaolinite colloids as a function of pH and I_S. Circles and squares correspond to columns packed with glass beads and quartz sand, respectively. Solid and open symbols in (a,b,d,e) correspond to parameters Λ_0 and Λ_1, respectively. Solid and open symbols in (c,f) correspond to parameter variation with pH and I_S, respectively.

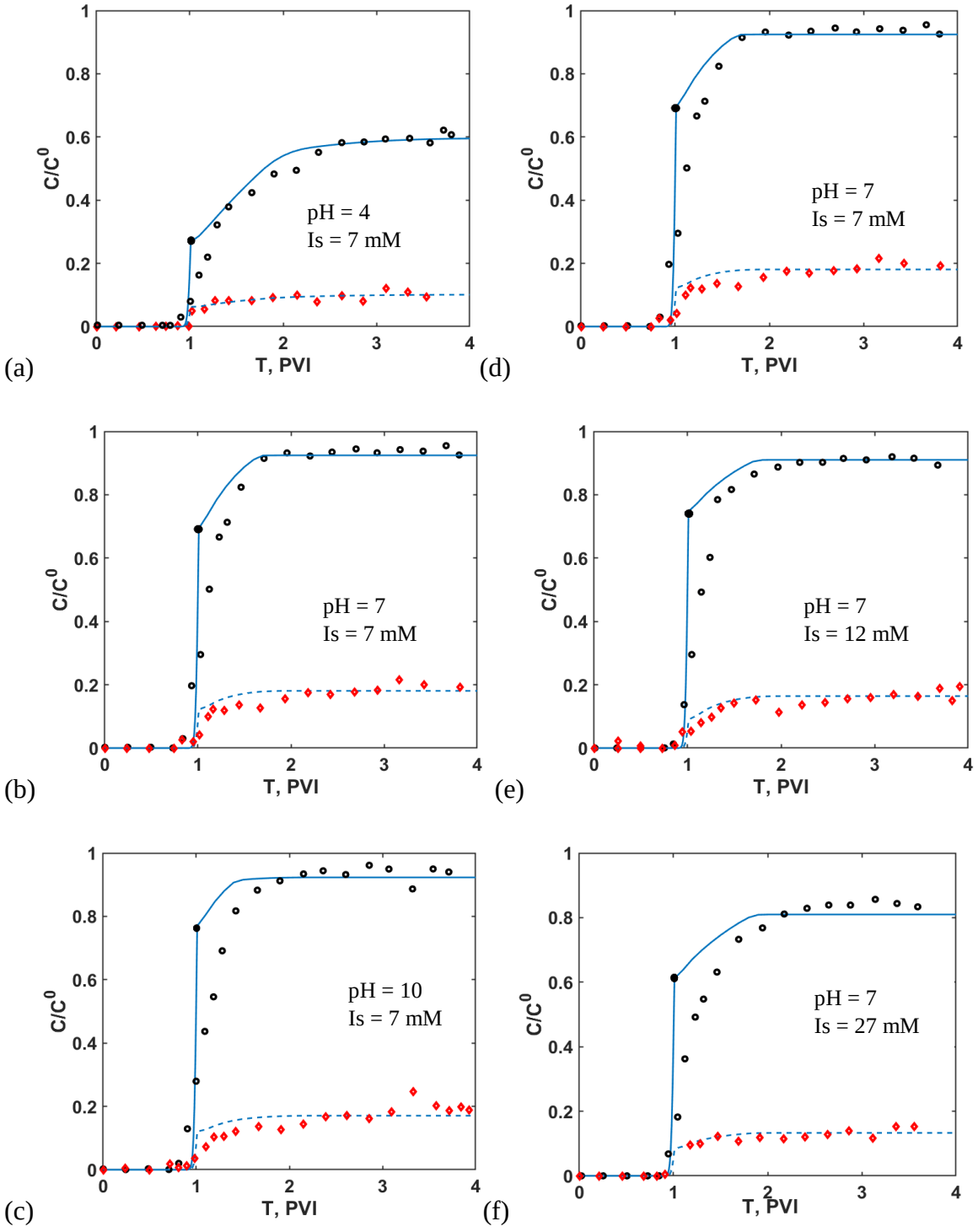

Fig. 8. Fitted breakthrough data reported by Chrysikopoulos et al.[1] for cotransport experiments of GO NPs (open black circles) and kaolinite colloids (red diamonds) in columns packed with glass beads at different conditions: (a) pH=4, *Is* =7 mM, (b) and (d) pH=7, I_S =7 mM, (c) pH=10, I_S=7 mM, (e) pH=7, I_S =12 mM, and (f) pH=7, I_S =27 mM. The matched modelling data are given by continuous curves.

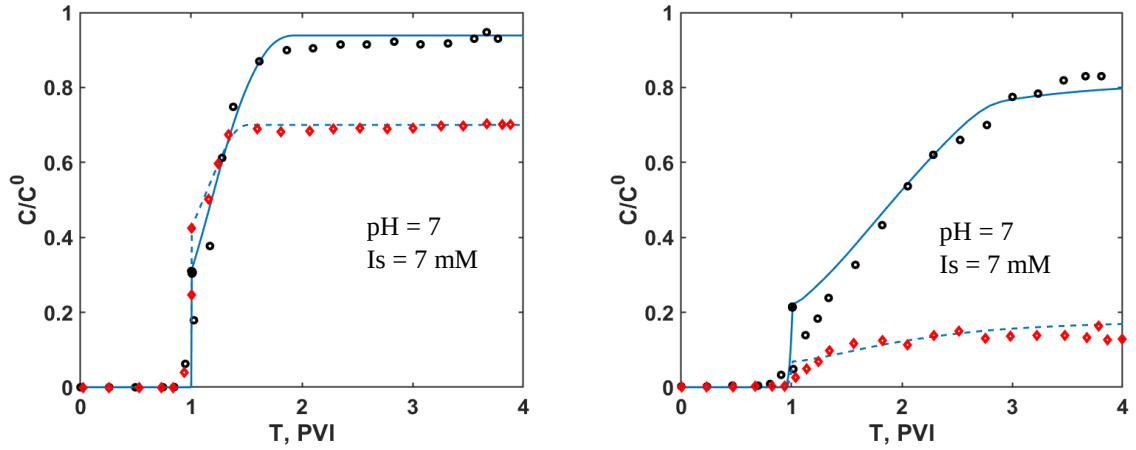

(a) (b)

Figure 9: Fitted breakthrough data reported by Chrysikopoulos et al.[1] for (a) individual transport experiments of NPs (open black circles) and kaolinite colloids (red diamonds), and (b) cotransport experiments of GO NPs (open black circles) and kaolinite colloids (red diamonds) in columns packed with sand at pH=7 and *Is*=7 mM. The matched modelling data are given by continuous curves.

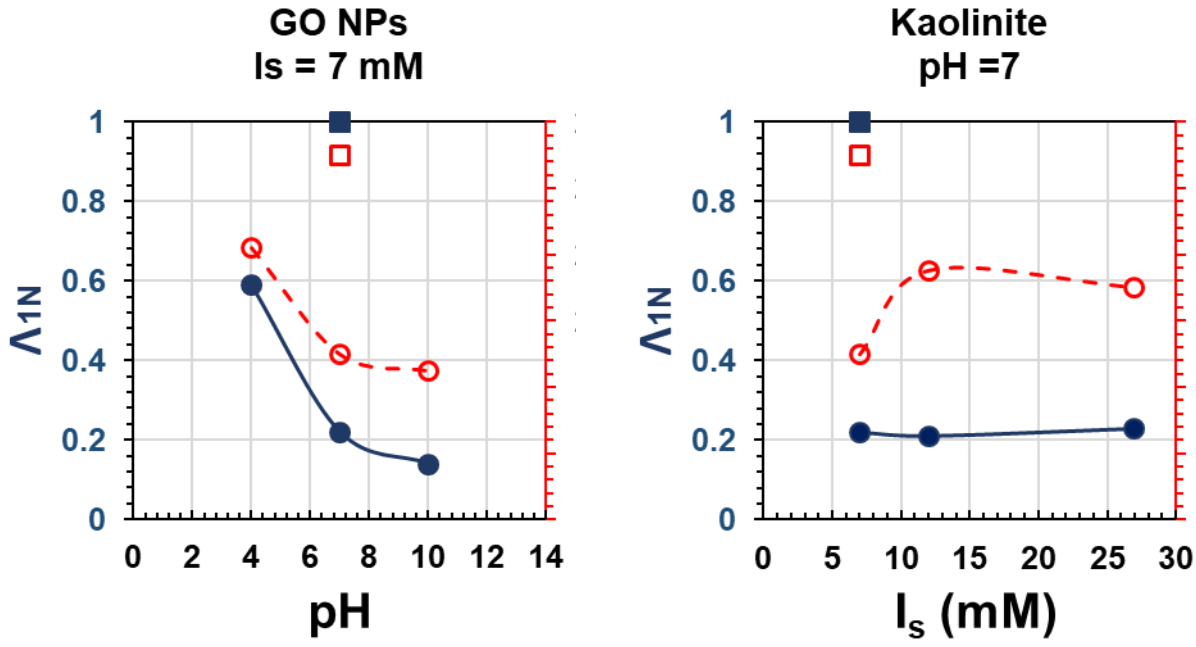

(a) (b)

Figure 10: Behaviour of fitted parameters associated with the cotransport experiments of GO NPs and kaolinite colloids as a function of: (a) pH and (b) I_S. Circles and squares correspond to columns packed with glass beads and quartz sand, respectively. Solid and open symbols in (a, b) correspond to parameters Λ_{1N} (for GO NPs) and Λ_{1K} (for kaolinite), respectively.

Table 1. Explicit dimensionless expressions for suspended and attached particle concentrations

Zone	Domains	$C(X,T)$	$S(X,T)$
0	$T(X) \le X$	0	0
I	$X < T(X) \le X + T_m$	$\dfrac{1}{\left[1-\exp\left[-\dfrac{\Lambda_0}{S_m}(T-X)\right]+\exp\left[(\Lambda_0+\Lambda_1)X-\dfrac{\Lambda_0}{S_m}(T-X)\right]\right]}$	$\dfrac{S_m\dfrac{(\Lambda_0+\Lambda_1)}{\Lambda_0}\left(1-\exp\left[-\dfrac{\Lambda_0}{S_m}(T-X)\right]\right)}{\left[1-\exp\left[-\dfrac{\Lambda_0}{S_m}(T-X)\right]+\exp\left[(\Lambda_0+\Lambda_1)X-\dfrac{\Lambda_0}{S_m}(T-X)\right]\right]}$
II	$X+T_m < T(X) < \dfrac{S_m}{\Lambda_1}\left(\exp(\Lambda_1 X)-1\right)+X+T_m$	$\dfrac{S_m\left(\dfrac{\Lambda_0+\Lambda_1}{\Lambda_0}\right)}{\left[\Lambda_1(T-X-T_{cr})+S_m\right]\left\{\dfrac{\Lambda_1}{\Lambda_0}\exp\left[(\Lambda_0+\Lambda_1)\left(X-\dfrac{1}{\Lambda_1}\ln\left[\dfrac{\Lambda_1}{S_m}(T-X-T_{cr})+1\right]\right)\right]+1\right\}}$	$\dfrac{S_m\left(\dfrac{\Lambda_0+\Lambda_1}{\Lambda_0}\right)}{\dfrac{\Lambda_1}{\Lambda_0}\exp\left[(\Lambda_0+\Lambda_1)\left(X-\dfrac{1}{\Lambda_1}\ln\left[\dfrac{\Lambda_1}{S_m}(T-X-T_m)+1\right]\right)\right]+1}$
III	$T(X) \ge \dfrac{S_m}{\Lambda_1}\left(\exp(\Lambda_1 X)-1\right)+X+T_m$	$\exp(-\Lambda_1 X)$	$\left[\Lambda_1(T-X-T_m)+S_m\right]\exp(-\Lambda_1 X)$

Table 2. Fitted parameters for GO NPs and kaolinite colloids individual transport experimental data.

Porous medium	Glass Beads									
Particle	GO NPs					Kaolinite colloids				
Model parameter	Λ_0	Λ_1	S_M	T_m	R^2	Λ_0	Λ_1	S_M	T_m	R^2
(a) pH =4 I_S =7 mM	0.4888	0.0910	0.5953	2.2555	0.9536	0.3506	0.5110	0.7629	1.1368	0.8815
(b) pH =7 I_S =7 mM	0.3045	0.0451	0.1216	0.8180	0.9598	0.2536	0.4395	0.3113	0.5592	0.9754
(c) pH =10 I_S =7 mM	0.1684	-	0.0731	-	0.9863	0.2211	0.4233	0.3898	0.7409	0.9751
(e) pH =7 I_S =12 mM	0.1956	0.0465	0.1233	1.0402	0.9851	0.6283	0.3526	0.3032	0.4938	0.9841
(f) pH =7 I_S =27mM	0.2395	0.0821	0.2433	1.3870	0.9807	0.4130	0.5813	0.2847	0.3700	0.9276
Column	Sand									
Particle	Nanoparticles					Kaolinite				
Model parameter	Λ_0	Λ_1	S_M	T_m	R^2	Λ_0	Λ_1	S_M	T_m	R^2
pH=7 I_S =7 mM	0.9279	0.0529	0.2542	0.7998	0.9396	0.7186	0.1371	0.2542	0.6478	0.9597

Table 3. Fitted parameters for GO NPs and kaolinite colloids cotransport experimental data.

Porous medium	Glass Beads			
Particle	GO NPs		Kaolinite colloids	
Model parameter	$\Lambda_{N,coinj}$	R^2	$\Lambda_{k,coinj}$	R^2
(a) pH =4 I_S =7 mM	0.59	0.9142	2.32	0.9263
(b) pH =7 I_S=7 mM	0.22	0.9426	2.00	0.9296
(c) pH =10 Is=7 mM	0.14	0.8925	1.95	0.8805
(e) pH =7 I_S =12 mM	0.21	0.9144	2.25	0.8968
(f) pH =7 I_S =27 mM	0.23	0.8770	2.20	0.8992
Porous medium	Quartz Sand			
Particle	GO NPs		Kaolinite colloids	
Model parameter	$\Lambda_{N,coinj}$	R^2	$\Lambda_{k,coinj}$	R^2
pH=7 I_S =7 mM	1.00	0.9710	2.60	0.9381

5 Conclusions

The thesis develops a series of novel mathematical models based on the discussions of multiple particle capture mechanisms during suspension-colloidal transport in porous media. Exact solutions and numerical solutions are derived for 1D quasi-linear and non-linear advection-dispersion-reaction governing systems, which can be used in the wider range of particulate flow problems and supplemented to classical colloids filtration theory. It allows drawing the following conclusions:

The model considering simultaneous multiple capture mechanisms allows for exact solutions by two procedures: the “aggregation” and the potential non-linear transformation.

The “aggregation” technique is developed to reduce the multi-capture to single capture mechanism (or reduce n kinetics to one aggregated kinetics), where $(n+1)\times(n+1)$ system for n particle capture mechanisms is equal to the 2×2 system for a single capture mechanism.

The “potential” non-linear transformation allows for reduction to one scalar quasi-linear hyperbolic equation.

The two capture model contains the filtration function both in the aggregated (exact) and binary (approximated) forms, which can be widely applied in the monodisperse colloid filtration problems.

The cotransport model provides an insight into the new area not only for mono-dispersion single population but also for multiple sizes and various particle populations.

The co-transport phenomena of natural clays and nanoparticles helps to nanoparticle injection into reservoirs in which rock surfaces are usually coated by clays (fines).

The analytical model is preferred over computationally numerical solutions, and can be used as a benchmark for numerical models.

The 1D analytical model can be implemented in quasi 3D streamline model for interpretation field data.